



**NTNU – Trondheim**  
Norwegian University of  
Science and Technology

# Dynamic Simulation of Module Installation on Deep Water

**Joar Pedersen**

Marine Technology

Submission date: June 2015

Supervisor: Carl Martin Larsen, IMT

Norwegian University of Science and Technology  
Department of Marine Technology





## **M.Sc. thesis 2015**

**for**

**Joar Pedersen**

### **DYNAMIC SIMULATION OF MODULE INSTALLATION ON DEEP WATER**

Floating production systems must be linked to a variety of installations on the sea floor. These include anchors, pipelines and manifolds for linking production pipes to marine risers, and structures for connections between export risers and pipelines to shore or offloading systems. Installation of such modules requires control of dynamic response during all phases of the operation (lift-off from deck or barge, through splash-zone, during lowering and set-down on bottom).

The Aasta Hansteen field outside Norway is at present under planning. The floater will be the first Spar platform, and the water depth will be the largest for floating production in Norwegian waters. Installation of bottom modules must obviously be well planned in order to minimise costs but still be safe. The present project is a continuation of the pre-project from fall 2014, and should include a set of simulations in order to identify criteria for acceptable sea states for a specific module installation.

The work may be carried out in steps as follows:

1. Literature study that should concentrate on equipment and procedures for installation of modules that are planned for the Aasta Hansteen field. Part of this work has already been carried out in the pre-project from last year, but the study might be extended to cover hydrodynamic damping of complex structures in water, and optionally also identification of needed weather window for the operation and statistics of weather windows.
2. Identify eigenfrequencies for heave motions of the module for varying position of the module between sea surface and bottom, and also the transfer function for vertical crane tip motions and wire tension at varying water depth.
3. Calculate the dynamic response in the lifting wire for a set of positions by simulation and by use of the transfer function, and compare the results.
4. If time allows, use known data for sea state duration, and evaluate the total operation time and probability of success for varying starting date during the year.

The work may show to be more extensive than anticipated. Some topics may therefore be left out after discussion with the supervisor without any negative influence on the grading.

The candidate should in her/his report give a personal contribution to the solution of the problem formulated in this text. All assumptions and conclusions must be supported by mathematical models and/or references to physical effects in a logical manner.

The candidate should apply all available sources to find relevant literature and information on the actual problem.

The report should be well organised and give a clear presentation of the work and all conclusions. It is important that the text is well written and that tables and figures are used to support the verbal presentation. The report should be complete, but still as short as possible.

The final report must contain this text, an acknowledgement, summary, main body, conclusions and suggestions for further work, symbol list, references and appendices. All figures, tables and equations must be identified by numbers. References should be given by author name and year in the text, and presented alphabetically by name in the reference list. The report must be submitted in two copies unless otherwise has been agreed with the supervisor.

The supervisor may require that the candidate should give a written plan that describes the progress of the work after having received this text. The plan may contain a table of content for the report and also assumed use of computer resources.

From the report it should be possible to identify the work carried out by the candidate and what has been found in the available literature. It is important to give references to the original source for theories and experimental results.

The report must be signed by the candidate, include this text, appear as a paperback, and - if needed - have a separate enclosure (memory stick or DVD/ CD) with additional material.

Supervisor at NTNU is professor Carl M. Larsen

Trondheim, February 2015

Carl M. Larsen

Deadline:           10 June 2015

## Preface

This is the master's thesis which completes my master's degree in Marine Technology at NTNU. It has been five fine, but hard years at the University. Working with the thesis has been interesting and has, besides a few technical issues, offered few problems. It has been rewarding both in a technical point of view, as well as the fact that it is related to activity in Northern Norway where yours truly is born and raised.

I would like to thank professor Carl Martin Larsen for help and guidance during my work with this thesis, and for always having an open door. I also would like to thank Tore Jacobsen at Subsea 7 for providing me with the data needed for this project and for coming up with the idea for my thesis. Always answering e-mails and questions on demand, he has been of great help. And to my dear Malin, for putting up with me through these years.

Last, but not least, I would like to thank my parents for their everlasting support and love. I owe them everything in life. Thank you.

Trondheim, June 10, 2015

A handwritten signature in black ink that reads "Joar Pedersen". The signature is written in a cursive style and is positioned above a horizontal dotted line.

Joar Pedersen



## Summary

The Aasta Hansteen field is a gas field outside the coast of Northern Norway. Production is planned to start in 2017. The gas field is situated at 1300m water depth – the deepest on the Norwegian continental shelf. During the summer of 2015, subsea manifolds are going to be installed by Subsea 7 by use of a crane vessel.

Installing the 191 tonnes heavy modules is done by use of a single lifting wire. In order for such an installation to be safe and cost effective, it has to be well planned. Part of this planning is a dynamic analysis of the lowering operation. A structural model with certain hydrodynamic properties is created in RIFLEX. The hydrodynamic properties are taken from DNV's RP-H103 and a report by Øritsland (1989) containing findings from model tests with subsea modules. Subsea 7 has provided the structural properties of the lifting wire and slings, as well as RAOs for the crane vessel.

Eigenperiods, RAOs for crane tip motion and RAOs for wire tension are found through time-domain simulations in RIFLEX. The eigenperiods are found by use of response spectra from irregular analyses. RAOs are found by regular wave analysis with different wave periods. Crane tip responses are largest for periods around 7s, with a minor peak at 10s. Eigenperiods for the manifold response are from approximately 2s to 6s, depending on the vertical position of the module. In addition to the RIFLEX model, a separate MATLAB model has been created. The MATLAB model is a simplified version of the one in RIFLEX, only calculating responses in vertical direction using Newmark- $\beta$  for solving the equation of motion in time-domain. Responses are calculated based on regular waves and RAOs for crane tip motion gathered from RIFLEX.

Results from MATLAB and RIFLEX have been compared, and are in general similar in magnitude. For certain combinations of depth and wave periods the difference is however significant. The reason for this might be the difference in response calculations, where RIFLEX is a non-linear FEM-program and my MATLAB code is linear.





## Sammendrag

Aasta Hansteen-feltet er et gassfelt utenfor kysten av Nord-Norge. Produksjonen er planlagt å starte i 2017. Gassfeltet ligger på 1300m vandyp - det dypeste på norsk sokkel. I løpet av sommeren 2015, skal undervannsmanifolder installeres av Subsea 7 ved bruk av et kranfartøy.

Installering av 191 tonn tunge moduler gjøres ved bruk av en enkel løftevaier. For at en slik installasjon skal være trygg og kostnadseffektiv, må den være godt planlagt. En del av denne planleggingen er en dynamisk analyse av nedsenkningsprosessen. En strukturell modell med gitte hydrodynamiske egenskaper er laget i RIFLEX. De hydrodynamiske egenskapene er hentet fra DNVs Recommended Practice H103 og en rapport fra Øritsland (1989) som inneholder resultatene fra modellforsøk med undervannsmoduler. Subsea 7 har gitt de strukturelle egenskapene for løftevaier og løftestropper, samt RAOer for kranfartøyet.

Egenperioder, RAOer for krantippbevegelse og RAOer for vaierspenningen er funnet gjennom tidsdomenesimuleringer i RIFLEX. Egenperiodene er funnet ved bruk av responsspektra fra uregelmessige analyser. RAOer finnes ved regulær bølgeanalyse med forskjellige bølgeperioder. Resultatene viser at responsen for krantippbevegelse er størst rundt 7s, med en mindre topp på 10s. Egenperioder for manifoldens respons er fra ca. 2s til 6s, avhengig av vandyp. I tillegg til RIFLEX-modellen, har en separat MATLAB-modell blitt laget. MATLAB-modellen er en forenklet versjon av den i RIFLEX, og inkluderer bare beregning av responser i vertikalretning. Ved hjelp av Newmark- $\beta$  blir bevegelsesligningen løst i tidsdomenet. Svarene er beregnet basert på regulære bølger og RAOer for krantippbevegelse hentet fra RIFLEX-simuleringer.

Resultater fra MATLAB og RIFLEX har blitt sammenlignet og er stort sett like i størrelse. For visse kombinasjoner av dybde og bølgeperiode er forskjellen imidlertid betydelig. Grunnen til dette kan være forskjellen i hvordan responsen beregnes. Mens RIFLEX en ikke-lineær FEM program, er MATLAB-koden lineær.



# Contents

Summary . . . . .	v
Sammendrag . . . . .	vii
<b>1 Introduction</b>	<b>1</b>
1.1 Aasta Hansteen Field . . . . .	1
1.2 Subsea manifold to be installed . . . . .	4
1.3 Installation of subsea equipment . . . . .	4
1.4 Defining the problem . . . . .	5
<b>2 Background theory</b>	<b>8</b>
2.1 Equation of motion . . . . .	8
2.2 Dynamic effects . . . . .	11
2.3 Wave spectra . . . . .	12
2.4 Frequency response function . . . . .	15
2.5 Stiffness calculations . . . . .	18
2.5.1 Axial stiffness for slings . . . . .	18
2.5.2 Geometric stiffness . . . . .	20
2.6 Horizontal offset due to current . . . . .	22
<b>3 Modeling in RIFLEX</b>	<b>24</b>
3.1 Main dimensions . . . . .	24
3.2 Modeling of the manifold . . . . .	27
3.3 Modeling of wires and spreader bar . . . . .	28
3.4 Hydrodynamic modeling . . . . .	31

3.4.1	Damping . . . . .	32
3.4.2	Added mass . . . . .	34
3.5	Crane and vessel . . . . .	35
<b>4</b>	<b>Matlab model</b>	<b>37</b>
4.1	Numerical solution of the equation of motion . . . . .	38
<b>5</b>	<b>Results from simulations</b>	<b>41</b>
5.1	Static offset due to current . . . . .	41
5.2	Static elongation due to own weight . . . . .	44
5.3	RAO for crane tip motion . . . . .	45
5.4	Eigenperiods from hand calculations . . . . .	48
5.5	Results from MATLAB model . . . . .	49
5.5.1	Wire tension in head sea . . . . .	49
5.5.2	Wire tension for $\pm 15^\circ$ wave direction. . . . .	51
5.6	RIFLEX results . . . . .	53
5.6.1	Identification of eigenperiods . . . . .	53
5.6.2	RAO for wire tension . . . . .	58
5.7	Comparison of MATLAB and RIFLEX results for wire tension RAOs . . . . .	60
5.8	Effect of changing damping . . . . .	64
<b>6</b>	<b>Discussion and Recommendations for Further Work</b>	<b>66</b>
6.1	Discussion . . . . .	66
6.1.1	Identification of eigenperiods . . . . .	66
6.2	Calculation of damping . . . . .	67
6.3	Force responses . . . . .	68
	<b>Bibliography</b>	<b>70</b>
	<b>Appendices</b>	<b>I</b>
A	Sling configuration . . . . .	I
B	Spreader bar . . . . .	II
C	Excel spreadsheet from Tore Jacobsen . . . . .	III

D	Matlab script for RAO conversion . . . . .	V
E	Matlab script for calculation of dynamic response . . . . .	XIII
F	Matlab script for computing RAO . . . . .	XIX
G	Matlab script for plot of RAOs. . . . .	XXI
H	Response spectra for lifting wire tension from RIFLEX. . . . .	XXII
I	RAOs from MATLAB for different vertical positions. . . . .	XXVIII
J	RAOs from RIFLEX for different vertical positions. . . . .	XXXII



# List of Figures

1.1	Map showing location of Aasta Hansteen and the Polarled gas pipe (dotted line). (Image: Statoil.com) . . . . .	2
1.2	The Aasta Hansteen Spar platform will be the tallest in the world. (Image: Statoil.com) . . . . .	3
1.3	Layout of the Aasta Hansteen Field (Image: Statoil.com) . . . . .	3
1.4	The 191Te manifold to be installed, including sling configuration. (Subsea 7/Aker Solutions) . . . . .	4
1.5	Principle sketch of a crane operation showing definitions and DOFs (2D). . . . .	5
2.1	Simplified model to describe manifold motion. . . . .	9
2.2	Dynamic load factor for different damping ratios. . . . .	12
2.3	Matlab plot of Pierson-Moskowitz spectrum for $H_s = 5m$ , $T_p = 10s$ . . . . .	14
2.4	Definitions of the six degrees of freedom for a floating structure. (Faltinsen, 1990). . . . .	18
2.5	Vertical load acting on cable with an angle relative to the horizon. . . . .	19
2.6	Geometrical stiffness as an effect of normal force. (Adopted by Larsen, 2014) . . . . .	21
3.1	Port view of the manifold showing total length. . . . .	25
3.2	Port view of the manifold showing height. . . . .	25
3.3	Aft view of the manifold showing total width. . . . .	25
3.4	Placement of slender elements in SIMO-model. (Adopted by Tore Jacobsen) . . . . .	26
3.5	A beam element showing all six degrees of freedom per node. (MARINTEK, 2011) . . . . .	27
3.6	Model of the manifold. Screenshot from RIFLEX . . . . .	28

3.7 Sling configurations. Front/aft view to the left. Side view to the right. (Adopted by Tore Jacobsen) . . . . .	29
3.8 A bar element showing the three degrees of freedom per node. (MARINTEK, 2011)	30
3.9 Lifting wire specifications . . . . .	31
3.10 Drag coefficients for a rectangular plate (DNV, 2014b) . . . . .	32
3.11 The idealized subsea structure used for estimation of hydrodynamic properties. (Reproduced from Øritsland, 1989). . . . .	34
3.12 Added mass coefficients for a rectangular plate (DNV, 2014b) . . . . .	34
3.13 Illustration of RIFLEX coordinate system vs. RAO coordinate system. . . . .	36
5.1 Static offset of module for mean current velocity. . . . .	43
5.2 Static offset of module for max current velocity. . . . .	44
5.3 RAO for vertical crane tip motion at heading $0^\circ$ . . . . .	46
5.4 RAO for vertical crane tip motion at heading $15^\circ$ . . . . .	47
5.5 RAO for vertical crane tip motion at heading $-15^\circ$ . . . . .	47
5.6 Dynamic amplification in axial force in lifting wire as a fraction of static load. Wave height 1m. . . . .	50
5.7 RAO for axial force in lifting wire. . . . .	51
5.8 Maximum axial force in lifting wire as a fraction of static load. Wave height 1m, $15^\circ$ incoming angle. . . . .	52
5.9 Maximum axial force in lifting wire as a fraction of static load. Wave height 1m, $-15^\circ$ incoming angle. . . . .	53
5.10 Response spectrum for axial force in the lifting wire. $T_p=15s$ , $H_s=1.5m$ , $d=900m$ . . . . .	54
5.11 Response spectrum for axial force in the lifting wire. $T_p=15s$ , $H_s=1.5m$ , $d=1200m$ . . . . .	56
5.12 Spectrum for vertical crane tip motion . . . . .	57
5.13 Spectrum for vertical module motion at a depth of 600m . . . . .	57
5.14 Spectrum for vertical module motion at a depth of 200m . . . . .	58
5.15 Linearity check for a depth of 1200m and wave period 4s. $R^2$ value and interpolated equation included. . . . .	59



5.16 Linearity check for a depth of 1000m and wave period 6s.  $R^2$  value and interpolated equation included. . . . . 59

5.17 Wire tension amplitude per meter wave amplitude for wire tension in head sea. . . 60

5.18 Ratio between maximum responses for reduced and full damping. Period to the left, depth at the top. . . . . 65

# Nomenclature

$\alpha$	Parameter in Pierson-Moskowitz spectrum
$\beta$	Parameter in Pierson-Moskowitz spectrum
$\eta_{x,c}$	Translatory motion of crane in x-direction
$\eta_{x,m}$	Translatory motion of manifold in x-direction
$\eta_{z,c}$	Translatory motion of crane in y-direction
$\eta_{z,m}$	Translatory motion of manifold in y-direction
$\gamma$	Peakedness parameter
$\lambda$	Damping ratio
$\omega_n$	Natural frequency [rad/s]
$\omega_p$	Peak frequency, $\omega_p = \frac{2\pi}{T_p}$
$\rho$	Sea water density
$\Theta$	Adjustment factor for wire mass
$\zeta$	Wave elevation
$A_\gamma$	Normalizing factor in JONSWAP spectrum
$c$	Damping coefficient
$c_{cr}$	Critical damping

$C_{DS}$	Drag coefficient for three dimensional objects
$c_{eq}$	Equivalent damping coefficient
$EA$	Product of Young's modulus and cross sectional area
$g$	Acceleration of gravity
$H(\omega)$	Frequency response function
$H_S$	Significant wave height
$i$	Imaginary number, $\sqrt{-1}$
$k$	Stiffness
$M$	Mass included added mass
$RAO$	Response Amplitude Operator
$S$	Projected area normal to flow direction
$S(\omega)$	Wave spectrum
$S_x(\omega)$	Response spectrum
$S_J(\omega)$	JONSWAP spectrum
$S_{PM}(\omega)$	Pierson-Moskowitz spectrum
$T_n$	Eigenperiod
$T_p$	Peak period
$U$	Wind speed at 19.5m



# Chapter 1

## Introduction

### 1.1 Aasta Hansteen Field

The Aasta Hansteen field, formerly Luva, is a gas field outside the coast of Norway. It is located in the Norwegian Sea 320km west of Bodø at a water depth of 1300m. Production is planned to start in 2017. As of today this is the oil/gas field situated at the greatest water depth on the Norwegian continental shelf. The Aasta Hansteen field was discovered by British Petroleum in 1997, but has since 2006 been operated by Statoil. Gas reserves are estimated to 47 billions standard cubic meters, in addition to some condensate. Produced gas is to be sent to Nyhamna, a processing plant in the county of Møre og Romsdal, through a 480km long gas pipe - *Polarled*. Laying of the Polarled gas pipe represent the first gas infrastructure north of the Arctic circle in Norway.



Figure 1.1: Map showing location of Aasta Hansteen and the Polarled gas pipe (dotted line). (Image: Statoil.com)

The choice of development for Aasta Hansteen is a Spar platform (Statoil, 2015). It will be the first Spar platform on Norwegian continental shelf and the tallest Spar platform in the world so far, with a total hull length of 195 meters (Technip, 2015). It will also be the first in Norway to have steel catenary risers. The Spar will in addition contain storage tanks for condensate. Sub-sea templates will be connected to the platform by pipelines and risers.

Sandnessjøen is chosen as the supply base for the Aasta Hansteen field. It is also the harbor from which the subsea manifolds discussed in this thesis are going to be transported offshore. Installation is planned to begin sometime during the summer of 2015. As of today, the manifolds are already onshore in Sandnessjøen.

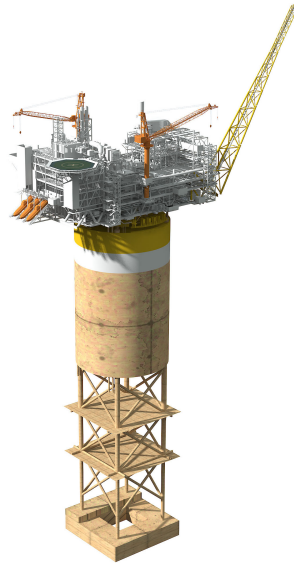


Figure 1.2: The Aasta Hansteen Spar platform will be the tallest in the world. (Image: Statoil.com)

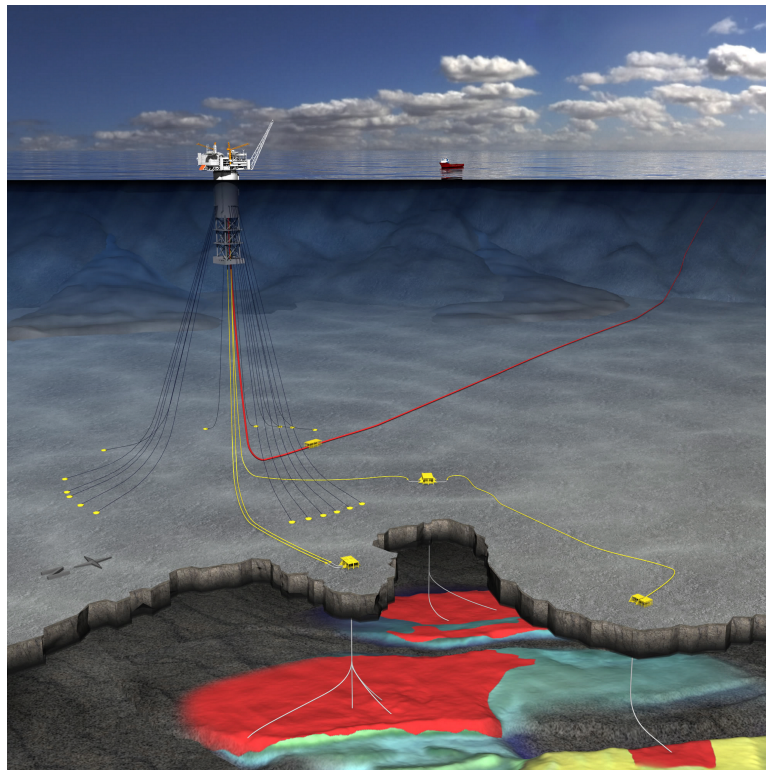


Figure 1.3: Layout of the Aasta Hansteen Field (Image: Statoil.com)

## 1.2 Subsea manifold to be installed

The module subject to analysis in this thesis is a 191Te manifold. It is to be installed using a single lifting wire and slings connecting the lifting wire to the load. The slings are separated by a spreader bar. Figure 1.4 shows the manifold with slings attached, as well as the spreader bar. The module, or manifold, consists of a truss work, contents (not shown in figure 1.4) and a flat plate on top. Further specifications are given in section 3.1.

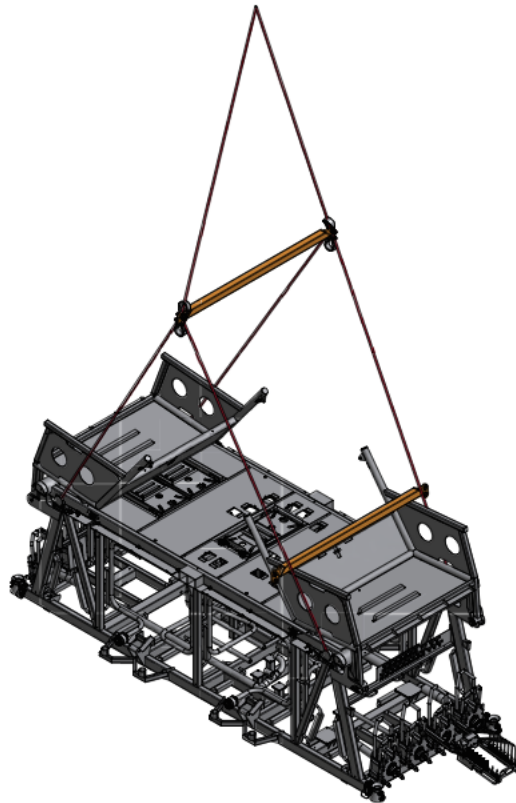


Figure 1.4: The 191Te manifold to be installed, including sling configuration. (Subsea 7/Aker Solutions)

## 1.3 Installation of subsea equipment

With increasing water depths comes the need for more subsea equipment. Installation of such equipment has to be well planned to ensure safe installation. Installation of the manifold is done by use of a crane vessel where single lifting wire is to be used. The manifold is connected to the lifting wire by use of slings which are separated by a spreader bar (see figure 1.4).



To prevent damage to equipment and installed objects, marine operations are executed when the weather allows it. Depending on the operation different weather windows are needed. A weather window is a window in time where the weather is "better" than a certain threshold (Nielsen, 2007). Significant wave height and spectral peak period are often chosen as limiting factors. These criteria are set based on the dynamic effects in the installation vessel and lowered object caused by waves. Certain wave periods cause greater responses and hence forces, and are therefore to be avoided.

## 1.4 Defining the problem

A lowering operation using a crane vessel can in a simplified way be expressed as in figure 1.5. The figure shows the crane tip modeled as a point with prescribed motion where the module is attached to the crane tip through a lifting wire. This model is for a given vertical position of the module and does not include vertical velocity due to lowering.

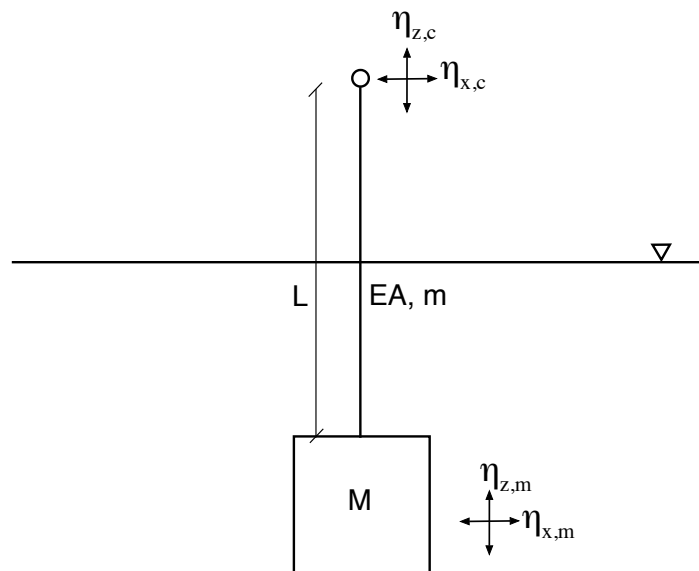


Figure 1.5: Principle sketch of a crane operation showing definitions and DOFs (2D).

$\eta_{x,m}$  and  $\eta_{z,m}$  are the translatory motions of the manifold in x- and y-direction respectively.

While  $\eta_{x,c}$  and  $\eta_{z,c}$  are the corresponding degrees of freedom for the crane tip.  $EA$  is the wire stiffness and  $m$  is the mass per unit length.  $M$  is the total mass of the manifold including structural and added mass.

As the crane tip is set in motion, forces acting through the wire will set the manifold in motion. Since the manifold is fully submerged during lowering, hydrodynamic as well as buoyancy forces will act on it. This will affect the dynamic of the problem. Depending on the amplitude and period of the crane tip motion, module responses will vary. Calculating these motions is done by solving the equation of motion in time domain. In order to do so, essential parameters such as added mass and damping has to be determined. It shows that this might be challenging, but by use of empirical data, reasonable estimates of these parameters may be found.

## Literature Survey

This thesis is the continued work of my project thesis from the autumn of 2014. While working with my project and master's thesis, I have gone through data provided to me by Subsea 7 as well as looked into the relevant codes from Det Norske Veritas (DNV). Important literature regarding dynamics are the Compendium in Marine Dynamics by Carl M. Larsen and the book *Dynamic Analysis of Structures* by Sigbjørnsen and Langen. Theory related to waves, spectra and sea loads in general is taken from *Sea Loads on Ships and Offshore Structures* by Odd M. Faltinsen. The background theory in this thesis is based on my project work. Some parts are kept in its original form, but changes have been made and additional material has been included.

DNV has gathered the four effects that should be considered in their *Recommended Practice DNV-RP-H103, February 2014, Sec.5 Deepwater lowering operations*:

*For lifting operations in deep water the following effects should be considered,*

- *stretched length of cable due to cable own weight and weight of lifted object*
- *horizontal offset due to current where the current velocity may be time-dependent and its magnitude and direction may vary with water depth*
- *dynamics of lifted object due to wave induced motion of crane tip on vessel*

- *methods for controlling vertical motion of lifted object.*

Among the above mentioned points the first three points create the basis of this thesis, and are investigated by use of the MARINTEK software RIFLEX in addition to a self made MATLAB code. The three first effects mentioned by DNV create the basis for my thesis. Although important for analyses of marine operations, I have not evaluated the weather aspect of the operation. I.e. sea state durations, weather windows, total expected operation time and probability of a successful operation.

# Chapter 2

## Background theory

A dynamic analysis is based on solving the equation of motion, a differential equation describing a dynamic force equilibrium in time domain. Three basic parameters characterize a system in motion: its mass, damping and stiffness. These parameters are related to acceleration, velocity and displacement respectively, i.e. inertia, kinetic and potential energy. For the solution to be as close to nature as possible, these three parameters has to be as well modeled as possible.

In this chapter I will present theory related to establishing the dynamic equilibrium, as well as ways to calculate the vertical stiffness of the system. The exciting force in this case is a prescribed motion of a point connected to the system. I will present theory related to finding this as well. This chapter summarizes my work related to background theory which is needed for approaching the dynamic analysis. Some static analyses are also performed; static elongation of the lifting wire and static offset due to current. Static elongation is found by use of the same theory as needed for finding vertical stiffness of the system.

### 2.1 Equation of motion

With the motion of the crane tip regarded as a single degree of freedom, the lifting wire and manifold can be modeled as shown in figure 2.1. This simplified model shows the manifold connected to the crane tip through a lifting wire. The manifold is modeled as a mass,  $m$ . Mass

included added mass is denoted  $M$ . The wire is modeled as a spring with stiffness  $k$  while drag forces acting on the module are modeled as a viscous damper,  $c$ .

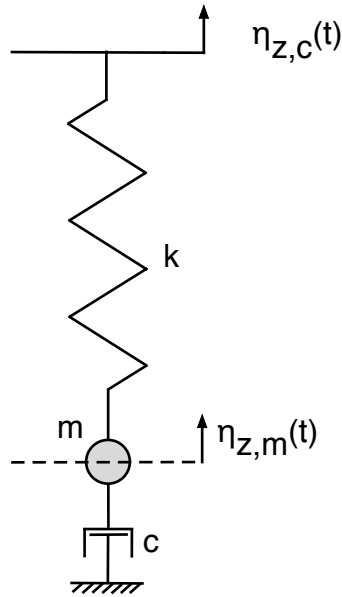


Figure 2.1: Simplified model to describe manifold motion.

Excitation is made through the motion of the crane tip,  $\eta_{z,c}$ . Due to this excitation the mass is set in motion. When set in motion forces from the spring and damper will act on the mass. The dynamic equilibrium is determined based on Newton's 2<sup>nd</sup> law as shown by Larsen (2012):

$$M\ddot{\eta}_{z,m}(t) = F_S + F_D \quad (2.1)$$

where  $F_S$  is the spring force and it is determined from the relative displacement between the crane tip and module.

$$F_S = k[\eta_{z,m}(t) - \eta_{z,c}(t)] \quad (2.2)$$

$F_D$  is the damping force, and this is determined from the velocity of the module. The damping term may be linear or nonlinear. In this case the damping is nonlinear, since drag forces are proportional to the square of the velocity.

$$F_D = c \dot{\eta}_{z,m}(t) |\dot{\eta}_{z,m}(t)| \quad (2.3)$$

Since the spring force depends on the relative motion between crane and module, it is practical to introduce

$$\eta_{rel}(t) = \eta_{z,m}(t) - \eta_{z,c}(t) \quad (2.4)$$

Then equation 2.1 can be written as

$$M\ddot{\eta}_{z,m}(t) = k\eta_{rel}(t) - c\dot{\eta}_{z,m}(t)|\dot{\eta}_{z,m}(t)| \quad (2.5)$$

which again can be written as

$$\begin{aligned} M\ddot{\eta}_{z,m}(t) - M\ddot{\eta}_{z,c}(t) + M\dot{\eta}_{z,c}(t) - k\eta_{rel}(t) + c\dot{\eta}_{z,m}(t)|\dot{\eta}_{z,m}(t)| &= 0 \\ M\ddot{\eta}_{rel}(t) + k\eta_{rel}(t) = -M\ddot{\eta}_{z,c}(t) + c\dot{\eta}_{z,m}(t)|\dot{\eta}_{z,m}(t)| &= P(t) \end{aligned} \quad (2.6)$$

Further simplifications can be made if the damping is linearized using an equivalent damping coefficient,  $c_{eq}$ . How this is found is described further in chapter 4. Linearization of the damping simplifies equation 2.6 to

$$M\ddot{\eta}_{rel}(t) + k\eta_{rel}(t) = -M\ddot{\eta}_{z,c}(t) + c_{eq}\dot{\eta}_{z,m}(t) = P(t) \quad (2.7)$$

Subtracting  $c_{eq}\dot{\eta}_{z,c}(t)$  on each side of the equality sign gives the following final expression:

$$M\ddot{\eta}_{rel}(t) - c_{eq}\dot{\eta}_{z,m}(t) + k\eta_{rel}(t) = -M\ddot{\eta}_{z,c}(t) + c_{eq}\dot{\eta}_{z,c}(t) = P(t) \quad (2.8)$$

It is seen that the external force consists of an inertia term and a damping term. The damping force related to the crane tip velocity is expressed as an external force since the equation is solved for the relative motion, and the damping is solely dependent on the actual motion of the module and not the relative motion between the module and crane tip. The inertia term is a result of the prescribed motion from the crane tip.

## 2.2 Dynamic effects

During installation one has to consider the danger of resonance. With increasing length of the lifting wire, its axial stiffness reduces (see eq. 2.32). Reduced stiffness means reduced eigenfrequency (or increased eigenperiod), as seen in eq 2.9. When planning lowering operations one has to make sure that the eigenperiod of the system is sufficiently far away from the dominating wave periods.

$$\omega_n = \sqrt{\frac{k}{M}} \quad (2.9)$$

where

$\omega_n$  is natural frequency in rad/s

$k$  is axial stiffness

$M$  is mass included added mass

Calculating the eigenperiod for a system as shown in figure 1.5 can be done according to equation 2.10, where the mass includes structural mass, added mass and wire mass (DNV, 2014b).

$$T_n = \frac{2\pi}{\omega_n} = 2\pi \sqrt{\frac{M + A_{33} + \Theta \cdot mL}{k}} \quad (2.10)$$

where

$m$  is wire mass per meter

$\Theta$  is an adjustment factor to account for cable mass.

If the eigenperiod is close to the wave period, the oscillations of the system may have large dynamic amplifications. How large these are depends on the damping of the system. This effect can be seen from the dynamic amplification factor (DAF), or the dynamic load factor (DLF). The DAF is the ratio between maximum dynamic displacement and the static displacement. It is also used for ratio between static and dynamic load. Figure 2.2 shows this factor for different damping ratios,  $\lambda = \frac{c}{c_{cr}}$ . Where  $c_{cr}$  is the critical damping expressed by  $c_{cr} = 2M\omega_n$  (Larsen,

2012). For a frequency ratio  $\frac{\omega}{\omega_n} = 1$  the system is in resonance.

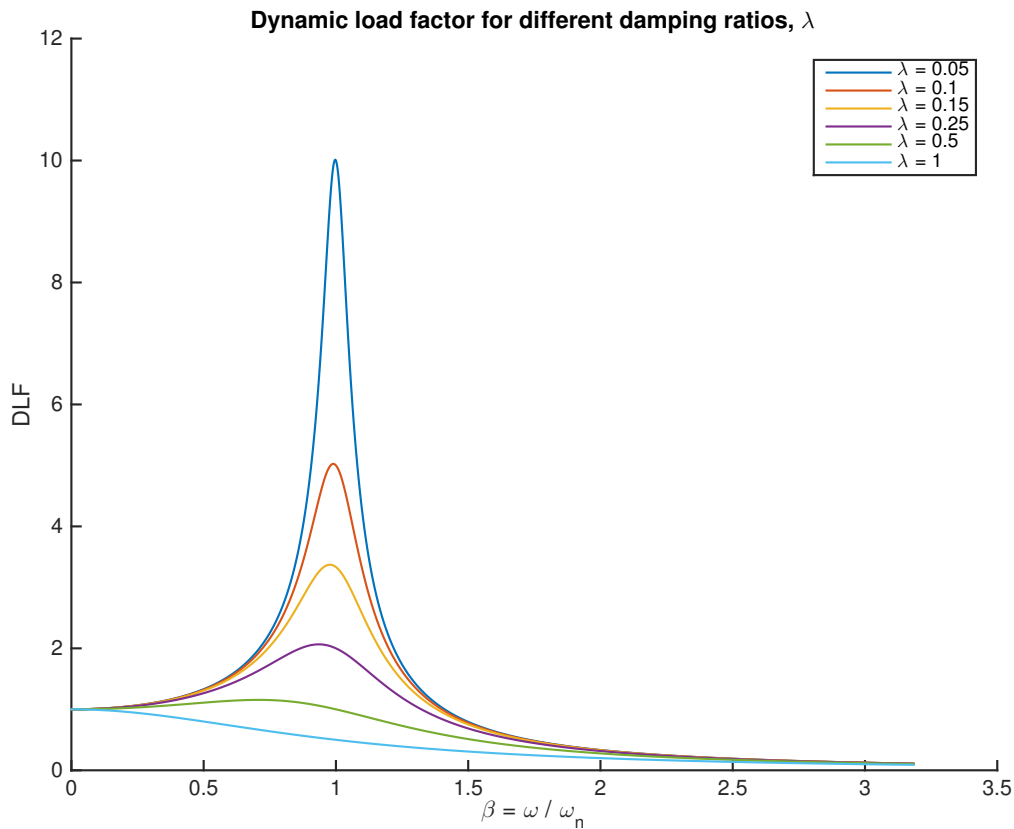


Figure 2.2: Dynamic load factor for different damping ratios.

## 2.3 Wave spectra

The motion of the crane tip is based on an incoming wave, or an irregular sea state, and corresponding motion of the crane vessel. The sea elevation,  $\zeta(t)$  is characterized by a wave spectrum,  $S_\zeta(\omega)$  as a function of wave frequency in rad/s. A wave spectrum is a statistical representation of random process, and is often referred to as spectral density or mean square spectral density. If the random process is the wave elevation on a certain location, the wave spectrum expresses the distribution of energy for different wave frequencies. This is seen from the integral of a wave spectrum (Newland, 1993).



$$E[\zeta^2] = \int_{-\infty}^{\infty} S_{\zeta}(\omega) d\omega \quad (2.11)$$

I.e. the integral of a wave spectrum corresponds to the mean square value. The unit of  $S_{\zeta}(\omega)$  is thus  $\frac{m^2}{rad/s}$ . The energy per unit of area contained in a wavelength of a wave with amplitude  $\zeta_a$  is proportional to  $\zeta_a^2$  as shown below (Pettersen, 2007).

$$E = \frac{1}{2} \rho g \zeta_a^2 \quad (2.12)$$

There are different types of spectra, one being the Pierson-Moskowitz (PM) wave spectrum for wind sea. The spectrum is valid for a fully developed sea state and is on the form as shown in equation 2.13. (Pierson and Moskowitz, 1964).

$$S_{PM}(\omega) d\omega = \frac{\alpha g^2}{\omega^5} e^{-\beta(\omega_0/\omega)^4} d\omega \quad (2.13)$$

where

$\alpha = 0.0081$  and  $\beta = 0.74$  are dimensionless parameters

$$\omega_0 = \frac{g}{U}$$

$g$  is the acceleration of gravity

$U$  is the wind speed at 19.5m height

The PM spectrum as presented in equation 2.13 gives the spectrum as a function of wind speed. In some cases it is more practical to use significant wave height and peak periods,  $H_S$  and  $T_p$  respectively, as parameters. In that case the PM spectrum is as shown in equation 2.14 (DNV, 2014a).

$$S_{PM}(\omega) = \frac{5}{16} H_S^2 \omega_p \omega^{-5} \exp\left(-\frac{5}{4} \left(\frac{\omega}{\omega_p}\right)^{-4}\right) \quad (2.14)$$

where

$$\omega_p = \frac{2\pi}{T_p} \text{ is the peak frequency}$$

An example of the PM spectrum for a significant wave height of 5m and a peak period of 10s is shown in figure 2.3.

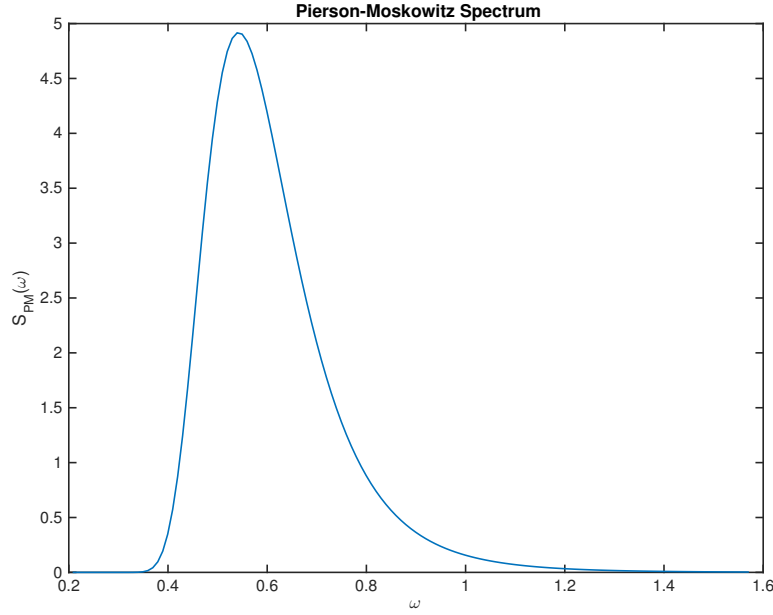


Figure 2.3: Matlab plot of Pierson-Moskowitz spectrum for  $H_s = 5m$ ,  $T_p = 10s$ .

Wave spectra can be established based on measurements, or simply by using standardized spectra such as the PM spectrum with the desired parameters. A modified version of the PM spectrum is the JONSWAP (Joint North Sea Wave Project) spectrum. It is similar to the PM spectrum, but is modified to fit a developing sea state rather than a fully developed sea state. The JONSWAP spectrum is expressed as follows (Hasselmann et al., 1973):

$$S_J(\omega) = A_\gamma S_{PM}(\omega) \gamma \exp\left(-0.5\left(\frac{\omega - \omega_p}{\sigma \omega_p}\right)^2\right) \quad (2.15)$$

Where  $A_\gamma$  is a normalizing factor,  $S_{PM}$  is the PM spectrum,  $\gamma$  is a non-dimensional peak shape parameter and  $\sigma$  is the spectral width parameter.

When conducting simulations, the wave elevation,  $\zeta$  can be generated as a sum of regular wave components with different frequencies, wavelengths and phases as shown in equation 2.16 (Faltinsen, 1990).

$$\zeta(t) = \sum_{j=1}^N A_j \sin(\omega_j t - k_j x + \epsilon_j) \quad (2.16)$$

$\omega_j$ ,  $k_j$  and  $\epsilon_j$  represent the frequency, wavenumber and phase respectively of wave component  $j$ .

If the wave spectrum is divided into  $n$  frequency intervals with width  $\Delta\omega$ , the amplitude,  $A_j$  can be found from the spectral value corresponding to frequency component  $\omega_j$  from

$$A_j = \sqrt{2S_\zeta(\omega_j)\Delta\omega} \quad (2.17)$$

## 2.4 Frequency response function

When the environment is described by a wave spectrum, and the equation of motion is established, the excitation of the system has to be determined. This is done by use of a frequency response function, also known as transfer function. A structure or vessel subjected to waves will respond differently for different wave amplitudes and periods. The dynamic characteristics of a system can be defined by the frequency response function,  $H(\omega)$ . It can be defined from the equation of motion when the load, and hence the response,  $u$  is harmonic. Langen and Sigbjørnsen (1979) show this for a single degree-of-freedom system as follows:

The load  $Q(t)$  is harmonic and written using complex numbers.  $X$  is generally a complex number describing the load in the frequency domain.

$$Q(t) = X e^{i\omega t} \quad (2.18)$$

Although complex numbers are used, the real part is the one of interest for responses. The imaginary part contains information on the phase between load and response. Inserting the expression for  $Q(t)$  into the general equation of motion gives

$$M\ddot{u} + c\dot{u} + ku = X e^{i\omega t} \quad (2.19)$$

where the particular solution to equation 2.19,  $u$  also is harmonic:

$$u = xe^{i\omega t} = H(\omega)Q(t) = H(\omega)Xe^{i\omega t} \quad (2.20)$$

Here  $x$  also generally is a complex number. Inserting this in equation 2.19 and solving for  $H(\omega)$  gives:

$$H(\omega) = \frac{1}{-M\omega^2 + i\omega c + k} \quad (2.21)$$

The frequency response function is here expressed by use of the characteristic parameters of the equation of motion.  $\beta = \frac{\omega}{\omega_n}$  and  $\lambda = \frac{c}{c_{cr}}$ , where  $c_{cr}$  is critical damping (eq. 2.22). This allows me to express  $c$  as:

$$c_{cr} = 2\omega_n M \implies c = 2\lambda\omega_n M \quad (2.22)$$

Furthermore the relation between mass, stiffness and eigenfrequency allows me to express  $k$  as shown in equation 2.23

$$\omega_n = \sqrt{\frac{k}{M}} \implies k = \omega_n^2 M \quad (2.23)$$

$H(\omega)$  can now be written by use of  $k$ ,  $\beta$  and  $\lambda$ :

$$H(\omega) = \frac{1}{k(1 - \beta^2 + i2\lambda\beta)} \quad (2.24)$$

The phase information contained in  $H(\omega)$  can be found by realizing that the phase angle between load and response is the same as the angle between the real and imaginary part of  $H(\omega)$  in the imaginary plane. Hence

$$\theta = \tan^{-1} \left( \frac{\text{Im}[H(\omega)]}{\text{Re}[H(\omega)]} \right) = \tan^{-1} \left( \frac{2\lambda\beta}{1 - \beta^2} \right) \quad (2.25)$$

The way of expressing the frequency response function as it is done in equation 2.24, requires that one knows the parameters of the equation of motion defining the dynamics of the system. If these are not established, another approach is by measurements. Rewriting equation 2.20 gives  $H(\omega)$  as the ratio between response and load:

$$H(\omega) = \frac{x}{X} \quad (2.26)$$

The absolute value of this expression is commonly referred to as the Response Amplitude Operator, or RAO. The RAO contains information on how the system responds to loads in the frequency domain, and has dimension [response/load]. For ships this might be e.g. roll angle per meter wave amplitude.

$$RAO = |H(\omega)| = \frac{|x|}{|X|} \quad (2.27)$$

Once the wave spectrum and frequency response function are known, the response spectrum  $S_x(\omega)$  can be found from the relation (Newland, 1993)

$$S_x(\omega) = |H(\omega)|^2 S_\zeta(\omega) \quad (2.28)$$

Knowing the motion of the vessel the motion of any point rigidly connected to the vessel, e.g. the crane tip, can be expressed as a vector  $\mathbf{s}$ , as stated by Faltinsen (1990):

$$\mathbf{s} = (\eta_1 + z\eta_5 - y\eta_6)\mathbf{i} + (\eta_2 - z\eta_4 + x\eta_6)\mathbf{j} + (\eta_3 + y\eta_4 - x\eta_5)\mathbf{k} \quad (2.29)$$

where  $\mathbf{i}$ ,  $\mathbf{j}$  and  $\mathbf{k}$  refer to the unit vectors in x-, y- and z-direction respectively and  $\eta_i$  ( $i = 1 - 6$ ) as shown in figure 2.4

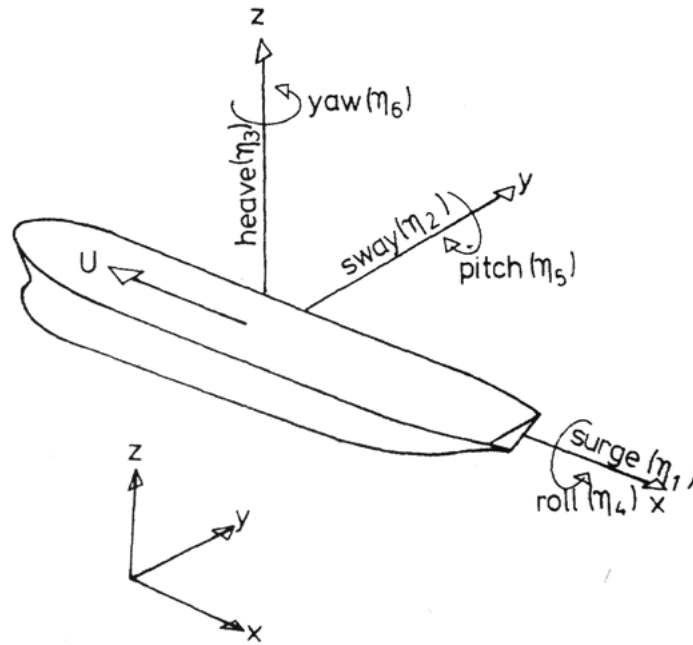


Figure 2.4: Definitions of the six degrees of freedom for a floating structure. (Faltinsen, 1990).

## 2.5 Stiffness calculations

### 2.5.1 Axial stiffness for slings

The equivalent vertical stiffness of a geometric system consisting of a wire with axial stiffness  $EA$  and length  $L$ , creating an angle  $\Theta$  with the horizontal plane can be calculated by geometrical considerations. Figure 2.5 represent two slings attached to a load, contributing with a vertical force  $P$  in each end. One end is considered for illustrative purposes.

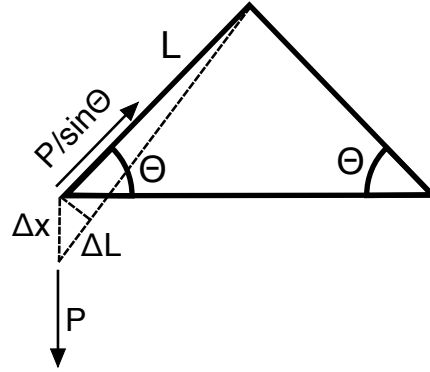


Figure 2.5: Vertical load acting on cable with an angle relative to the horizon.

The downward force will elongate the sling a distance  $\Delta L$ . The vertical component of this elongation is  $\Delta x$ . By geometrical considerations, one can see that  $\sin\Theta = \frac{\Delta L}{\Delta x}$ . In order to reach force equilibrium, the force parallel to the sling has to be greater than the vertical force. The force parallel to the sling can be expressed as  $\frac{P}{\sin\Theta}$ . This is the axial force acting on the sling. By use of Hooke's law  $\Delta L$  is found (Larsen, 2015):

$$\Delta L = \frac{\frac{P}{\sin\Theta}}{\frac{EA}{L}} \quad (2.30)$$

By using the fact that

$$\Delta L = \Delta x \sin\Theta \quad (2.31)$$

and combining this with equation 2.30 I get

$$k = \frac{EA}{L} \sin^2(\Theta) \quad (2.32)$$

As the module is set in motion, sling forces will vary in time. This leads to a time varying angle, and hence a time varying vertical stiffness. This gives rise to nonlinearities and solving this problem correctly in time domain will thus take a nonlinear FEM analysis, where the stiffness is continuously updated.

From the crane tip to the manifold, the lifting wire and slings make out a system of springs

in series and parallel. Looking at figure 3.6, one can see that the four lowermost slings are in parallel. So are the two upper slings. These "groups" are in series with the lifting wire, creating a system of three springs in series. Equations 2.33 and 2.34 show how the stiffness of  $n$  springs in parallel and series can be calculated.

$$k_{tot,parallel} = \sum_{i=1}^n k_i \quad (2.33)$$

$$k_{tot,series} = \frac{1}{\sum_{j=1}^n \frac{1}{k_j}} \quad (2.34)$$

### 2.5.2 Geometric stiffness

Another source of non-linearities is geometric stiffness. Figure 2.6 shows a tensioned rope subjected to a normal force. In an ocean environment both waves, wind and current can be present. Current forces may cause geometrical changes in the lifting wire by exerting horizontal forces. A vertical wire in tension will have, in addition to axial stiffness, a geometric stiffness. As the force acts on the rope, the rope will change shape, and so will the directions of the forces. This will lead to a horizontal force component counteracting the applied force until equilibrium is obtained. This force gives rise to geometric stiffness. The geometric stiffness for a system as in figure 2.6 can be found as explained by Larsen (2014).



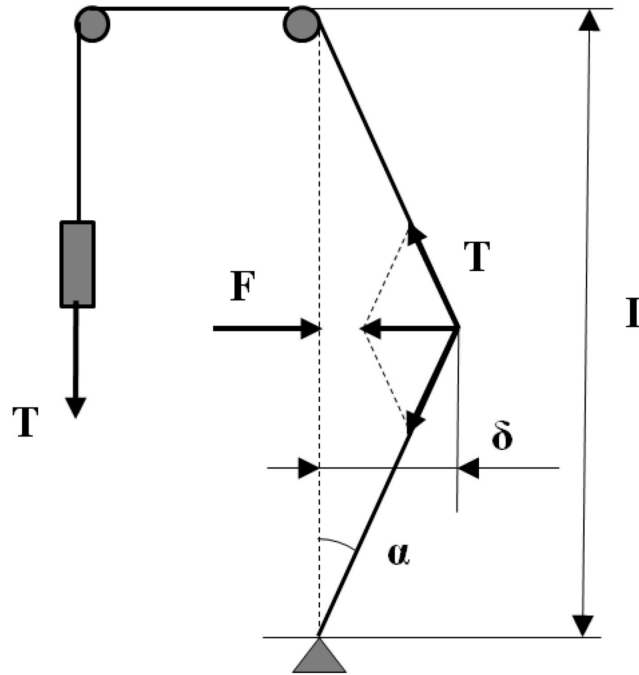


Figure 2.6: Geometrical stiffness as an effect of normal force. (Adopted by Larsen, 2014)

Equilibrium in horizontal direction is obtained when the horizontal component of the tension,  $T$  balances the applied force,  $F$ :

$$F = 2T \cdot \sin\alpha \quad (2.35)$$

If small deformations are assumed, the sine value of the angle can be expressed as

$$\sin\alpha = \frac{2\delta}{L} \quad (2.36)$$

This gives an expression for the horizontal force,  $F$  by inserting for  $\sin\alpha$ .

$$F = \frac{4T\delta}{L} \quad (2.37)$$

Which means the geometrical stiffness can be expressed as

$$K_G = \frac{4T}{L} \quad (2.38)$$

Equation 2.38 shows how the tension affects the geometrical stiffness. During a lowering operation the tension in the lifting wire and slings may vary significantly. Hence the geometrical stiffness will vary in time, and cause non-linearities.

## 2.6 Horizontal offset due to current

In addition to the dynamic analysis, I am going to do a short evaluation of the effect of horizontal offset of the manifold during installation due to current.

The submerged part of the hoisting wire is at most almost 1300m long. If this part is exposed to current, this will give a contribution to the drift off of the module. The total current force on the wire can be written as Faltinsen (1990) shows:

$$F_d = \frac{1}{2} \rho C_{D,w} D_w \int_z^0 U_C(z_1)^2 dz_1 \quad (2.39)$$

where  $\rho$  is the density of seawater,  $C_{D,w}$  is the drag coefficient of the wire,  $U_C$  is the current velocity as a function of depth,  $D_w$  is the diameter of the wire and  $z_1$  is a dummy integration variable. Both  $\rho$ ,  $C_{D,w}$  and  $D_w$  are assumed to be constant with depth.

This net horizontal force from the wire causes the lowered module to drift off. In addition drag forces will act on the module itself. Finding this is somewhat more complicated. Based on equation 2.39 the general expression for drag force can be written approximately as follows:

$$F_d = \frac{1}{2} \rho C_{D,m} U_C(-d)^2 A_m \quad (2.40)$$

where  $C_{D,m}$  is the drag coefficient of the manifold and  $A_m$  is the projected area of the manifold facing the current.  $U_C(-d)$  is the velocity of the current at the water depth where the module is located.

The challenge is finding  $C_{D,m}$  and  $A_m$ .  $C_{D,m}$  can be found from e.g. CFD-analysis or experi-

ments, while  $A_m$  can be found by geometrical considerations. However, if these parameters are known, the total drag force acting on the system can be written as:

$$F_{d,tot} = \frac{1}{2} \rho \left( C_{D,m} U_C (-L)^2 A_m + C_{D,w} D_w \int_z^0 U_C(z_1)^2 dz_1 \right) \quad (2.41)$$

For practical cases formulas in e.g. DNV's recommended practice H103, appendix B can be used. Drag forces are typically calculated in two ways; either based on projected area normal to flow direction,  $S$  or characteristic diameter,  $D$ . When using characteristic diameter, forces per unit length are calculated. Both ways include a drag coefficient,  $C_D$ , water density,  $\rho$  and flow velocity squared,  $u^2$ . (DNV, 2014b)

$$F_D = \frac{1}{2} \rho C_D S u^2 \quad (2.42)$$

$$f = \frac{1}{2} \rho C_D D u^2 \quad (2.43)$$

Similar to the deduction of geometric stiffness in section 2.5.2, a horizontal equilibrium has to be reached here as well. A horizontal force will act on the manifold and has to be balanced by the tension in the wire. Compared to the situation for calculating geometric stiffness the module is now hanging freely, and there is only one tension component, acting upwards. This gives a static offset,  $\delta = \frac{F_D L}{2T}$ .

# Chapter 3

## Modeling in RIFLEX

RIFLEX is a computer program for analysis of flexible risers and other slender structures, and is the program I am using for my dynamic analysis. RIFLEX uses a non-linear finite element method to calculate responses in the modeled structure. The theory manual included in RIFLEX gives an overview over the basic finite element formulation. I will not go into details here, only present some relevant theory.

The main dimensions of the manifold is taken from the data specified by Tore Jacobsen at Subsea 7 (Appendix C). The data is used in a SIMO-model, not a RIFLEX model. SIMO is another software for calculating dynamics related to marine operations, but the same hydrodynamic forces are calculated. I have adopted the main dimensions from the SIMO-model, not from the general arrangement (GA), also provided by Jacobsen. Dimensions from the GA can be seen from figure 3.1- 3.3. I have also been given the configuration of the slings attached to the manifold as well as wire data. (See appendix A - C)

### 3.1 Main dimensions

The following figures give an impression of the size and design of the manifold. As previously stated, I do not use these dimensions directly. The purpose of this project is not to dimension the module, and the length of the beams are thus not of interest per se. More interesting is the hydrodynamic forces acting on the structure. Hence it is desirable to model mass, added mass,

damping and drag forces correctly, rather than structural properties.

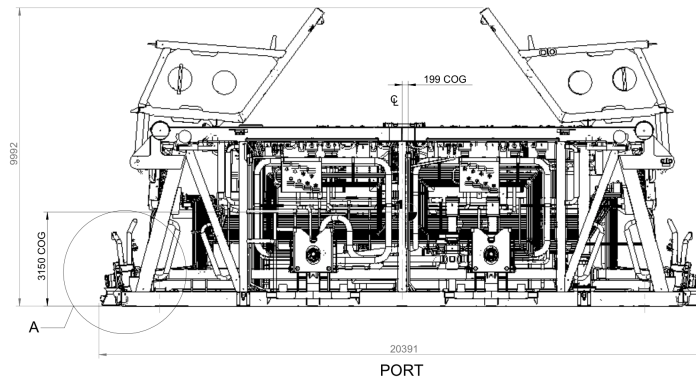


Figure 3.1: Port view of the manifold showing total length.

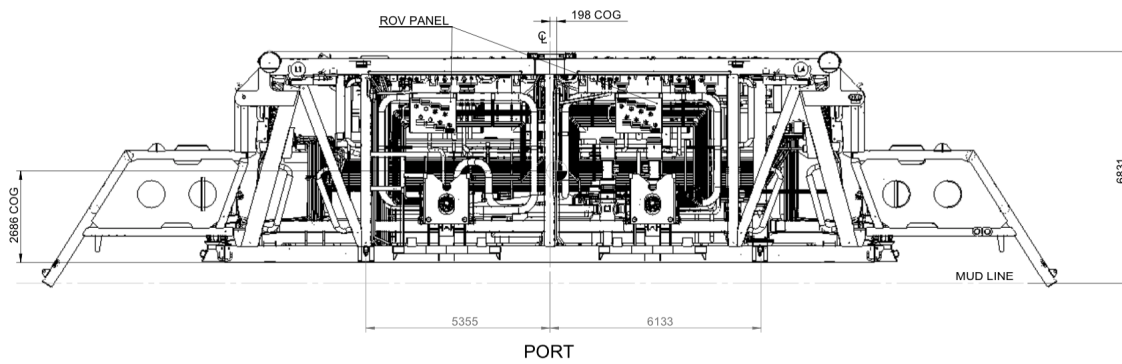


Figure 3.2: Port view of the manifold showing height.

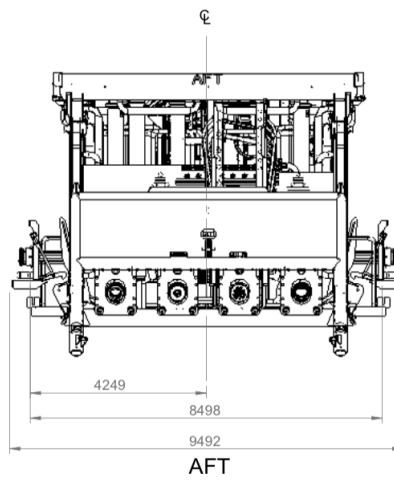


Figure 3.3: Aft view of the manifold showing total width.

From the SIMO-model I was given I could find the main dimensions of the hydrodynamic model. The model consists of three slender elements with dimensions as given in table 3.1. Figure 3.4 shows the layout of this model.

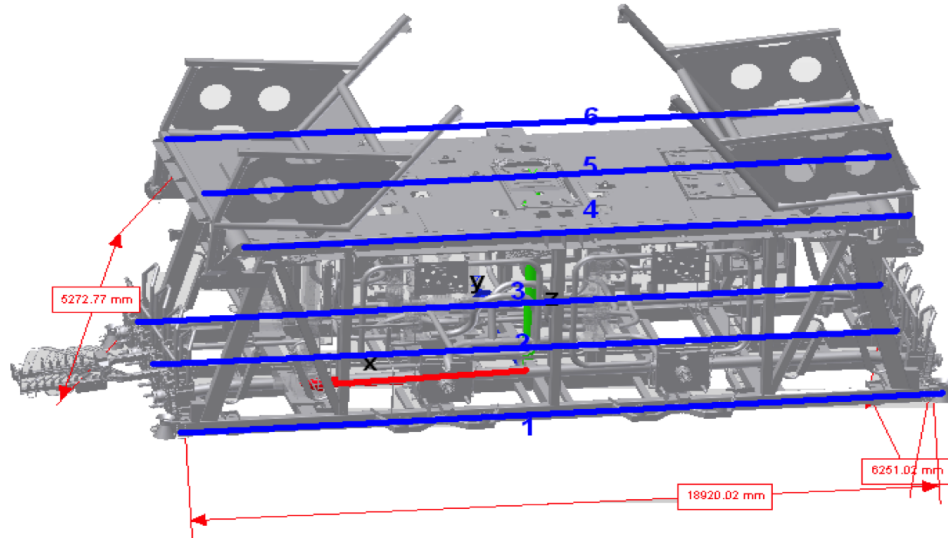


Figure 3.4: Placement of slender elements in SIMO-model. (Adopted by Tore Jacobsen)

	Top Assembly	Bottom Assembly
Length [ $m$ ]	16.3	18.9
Width [ $m$ ]	6.3	6.3
z-coordinate (local) [ $m$ ]	0	5.2
Mass per meter [ $tons$ ]	2.46	1.28
Volume per meter [ $m^3$ ]	0.73	0.34

Table 3.1: Main dimensions from SIMO-model

Summing up mass and volume gives a total mass of 191 tonnes and a volume of  $55m^3$ . The volume of  $55m^3$  is based on the assumption that there is no air filling in the structure. In addition, the mass distributed over the elements is based on the mass matrix exported from a 3D model of the manifold. This gives correct kinematics when conduction dynamic simulations (Jacobsen, 2015).

### 3.2 Modeling of the manifold

The manifold is modeled in RIFLEX by use of beam elements, where "supernodes" are used for each connection point. The beams are seen in figure 3.6 as green cylinders. The supernodes are seen as dark spheres. It is in these points restrains in degrees of freedom are set. All supernodes are free to move in any degree of freedom relative to the global coordinate system.

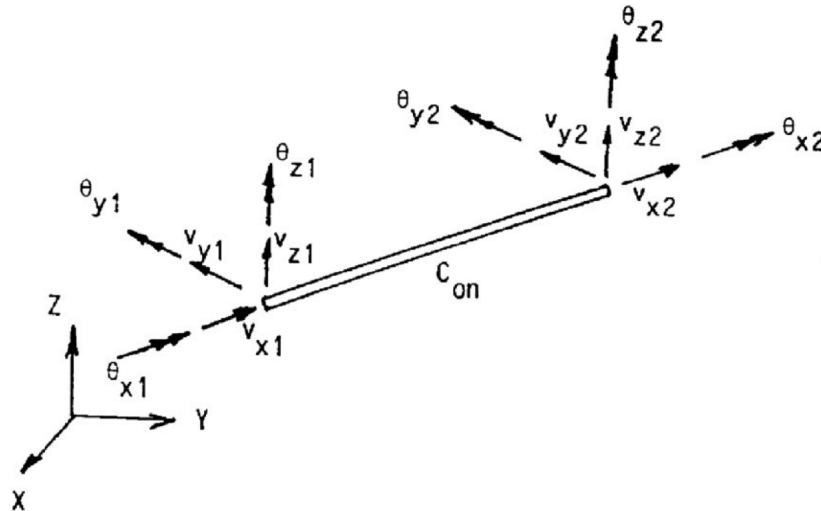


Figure 3.5: A beam element showing all six degrees of freedom per node. (MARINTEK, 2011)

A beam has six DOFs per node.  $\Theta_{xi}$ ,  $\Theta_{yi}$  and  $\Theta_{zi}$  denote the rotations around the respective axis at node  $i$ . While  $v_{xi}$ ,  $v_{yi}$  and  $v_{zi}$  denote the translations along the respective axis at node  $i$ .

The beams used in my RIFLEX model are circular cylinders with different diameters. According to the specifications provided to me (see appendix C), the total submerged volume of the manifold is  $55 \text{ m}^3$ . It is important to make sure this is the case also for my model, such that the wet weight of the manifold is correct. I have done this by adjusting the diameter of the beams. There are two different beam diameters; the top part consists of beams with a diameter of 0.682m while the bottom part, vertical and diagonal beams have a diameter of 0.465m.

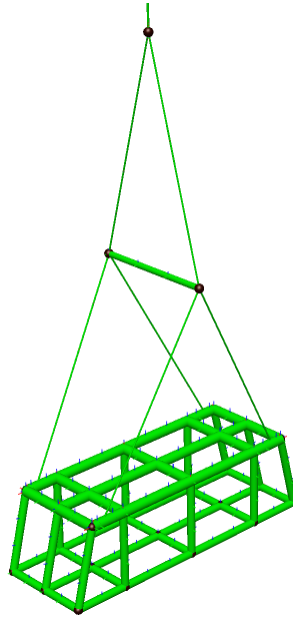


Figure 3.6: Model of the manifold. Screenshot from RIFLEX

When studying figure 1.4 it is clear that the beams which I have made circular are not so; they are in fact rectangular. Circular beams will have different structural properties than rectangular ones. This is however not of importance for this analysis, since the structural properties of the module it self is not of interest. What is interesting is the forces acting *on* and not *inside* the structure.

### 3.3 Modeling of wires and spreader bar

Modeling of the wires is done with basis in figure 3.7, which shows the configuration of the slings attached to the manifold. The spreader bar separating the slings can also be seen. Figure 1.4 shows a three dimensional view of the same slings and manifold. The drawing is taken from a technical drawing provided to me by Jacobsen. The drawing can be seen in its entirety in appendix A.



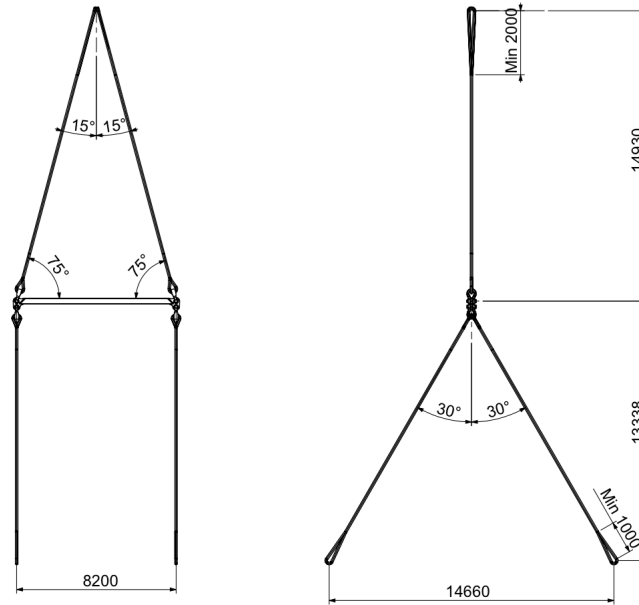


Figure 3.7: Sling configurations. Front/aft view to the left. Side view to the right. (Adopted by Tore Jacobsen)

The wires are modeled as bar elements, meaning they can only take up axial forces, not bending moment. Using bar elements leads to issues related to the connection between the wires and the manifold it self. A beam element has six DOFs in each end - three translational and three rotational. A bar element on the other hand has only three translational DOFs in each end as seen from figure 3.8. This problem is solved by adding a beam element at the end of the wires. If the wires are modeled solely by bar elements, they will also lack torsional stiffness, such that the smallest amount of torsion will lead to large rotations. This is also solved by adding beam elements at the ends.

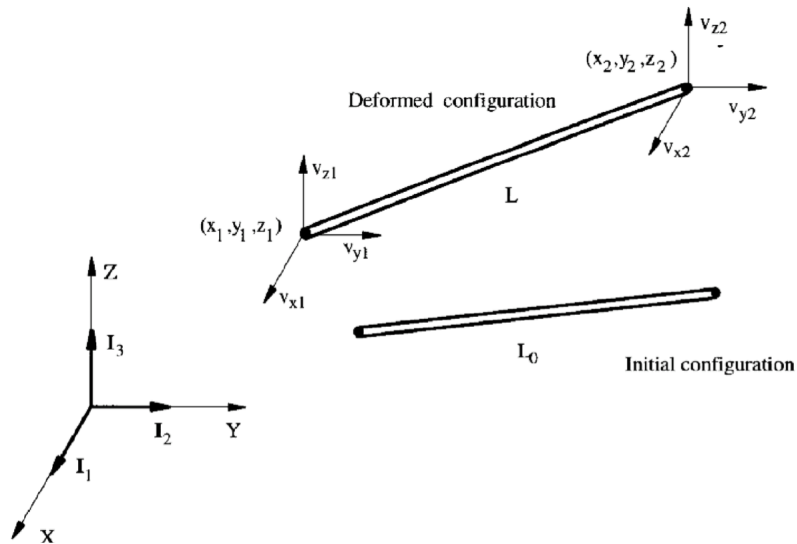


Figure 3.8: A bar element showing the three degrees of freedom per node. (MARINTEK, 2011)

When modeling a bar element, the only structural properties specified is the axial stiffness,  $EA$ , i.e. the product of Young's modulus and the cross sectional area. The axial stiffness of the slings and lifting wire is set to be the value given in the SIMO-model. In addition the dry weight,  $m$  [kg/m], is specified.

The main lifting wire is a wire from Bridon, more specifically *Big Hydra*. The wire has a diameter of 128mm, its the specifications can be seen from figure 3.9.

## Big Hydra (Dyform)

Low rotation, Dyformed multi-stand ropes with optimised strength to weight ratio.



Rope diameter	Approximate mass		Minimum breaking force (F <sub>min</sub> )		Axial stiffness @20% load	Torque generated @20% load	Metallic cross section
	In air	Submerged	kN	Tonnes		Lang's lay	
mm	kg/m	kg/m					MN
76	27.4	24.3	5003	510	335	2281	3049
77	28.8	25.5	5140	524	354	2375	3220
80	29.9	26.5	5199	530	366	2496	3329
83	32.4	28.7	5572	550	396	2687	3600
88.9	37.5	33.2	6180	630	459	3297	4170
96	44.1	39.2	7455	760	548	4294	4978
106	52.3	46.3	8829	900	641	5615	5826
109	55.5	49.1	9613	980	680	6287	6185
120	66.1	58.5	11036	1125	810	7946	7366
122	70.8	62.7	12262	1250	865	8976	7864
128	78.3	69.3	13145	1340	958	10096	8705

Figure 3.9: Lifting wire specifications

Modeling of the spreader bar is done based on the drawing in appendix B. An 8.2m long beam is placed in the transition between the top and bottom slings. In order to avoid buckling, the spreader bar has to have sufficient buckling capacity. I will not go into detail, but the beam used to model the spreader bar is given a bending stiffness based on a square steel cross section with 300mm sides.

### 3.4 Hydrodynamic modeling

For the response of the module to be as realistic as possible, it is important that its hydrodynamic properties are described as well as possible. When submerged, the hydrodynamic forces acting on the system will arise from two different contributions.

Firstly the induced motion of the model due to crane tip motion will cause a flow around the model. This is due to the relative motion between the system and the surrounding water. Forces from this motion will mainly be vertical and introduce damping to the system. Secondly there is a horizontal force acting on the system due to the current on site. This will cause the module to drift off and has to be taken into account when planning installation.

### 3.4.1 Damping

One of the parameters defining the dynamics of the manifold's motion is its damping through drag forces. Accurately modeling the damping of such a complex structure is difficult without using model tests. However there are ways of estimating damping coefficients for different geometries. Figure 3.4 shows the manifold to be installed. For modeling purposes it can be divided into two parts – a top and a bottom part. The top part is a flat plate measuring 16.3m x 6.3m. The bottom part is the rest of the structure, consisting of truss work and the components making the manifold. The latter part is the most complex, and hence the most difficult to model.

Modeling the flat plate of the manifold can be done by using drag coefficients taken from DNV's recommended practice H103, Modeling and Analysis of Marine Operations (DNV, 2014b). Drag coefficients for a rectangular plate normal to flow direction are found in table B-2 in the same standard. A screenshot from this table is shown in figure 3.10. It is worth noticing that the drag coefficients used in this analysis is for steady flow, even though the problem involves an oscillating structure. Actual drag coefficients will differ from this estimate since the flow pattern around the structure will be affected of the motion of the structure itself.

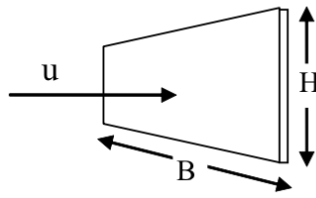
<b>Table B-2</b>		
Drag coefficient on three-dimensional objects for steady flow $C_{DS}$ .		
Drag force is defined as $F_D = \frac{1}{2}\rho C_{DS}Su^2$ .		
S = projected area normal to flow direction [ $m^2$ ].		
$Re = uD/\nu =$ Reynolds number where D = characteristic dimension.		
<i>Geometry</i>	<i>Dimensions</i>	<i><math>C_{DS}</math></i>
Rectangular plate normal to flow direction 	B/H	
	1 5 10 ∞	1.16 1.20 1.50 1.90
		$Re > 10^3$

Figure 3.10: Drag coefficients for a rectangular plate (DNV, 2014b)

Using the dimensions of the top section of the manifold, the ratio B/H is in my case 2.6. This gives, using linear interpolation, a drag coefficient  $C_{DS} = 1.18$ . Now the drag force acting on the flat plate can be calculated by use of the formula included in figure 3.10.

$$\frac{F_D}{u^2} = \frac{1}{2}\rho C_{DS}S \quad (3.1)$$

Inserting values I get that  $\frac{F_D}{u^2} = 62.1 \text{ kN}/(\text{m}/\text{s})^2$ . This is the total drag force acting on the top plate of the manifold. In RIFLEX the damping is given either as dimensional or non-dimensional drag coefficient. I use the dimensional one, given as force per velocity squared per meter. Since I use a beam model to build my model in RIFLEX, the drag force has to be distributed over the top beams. Therefore I divide the total drag force on the combined length of the three beams going in longitudinal direction in my model. This gives a drag force equal to that of a flat plate.

For the bottom part the situation is however more complex. This part consists of a truss work enclosing piping, valves etc. Finding damping forces on such a structure is not straight forward. However, estimates may be done by looking at test results for similar structures. Øritsland (1989) has performed several model tests for idealized subsea structures. By choosing a 3-D framework enclosing a sphere – a buoyant type module as he calls it – as shown in figure 3.11, a drag coefficient of 1.2 for heave motion is found. The damping force can then be calculated as for the flat plate. See equation 3.1. I use a projected area equal to that of the a flat plate with dimensions equal to the bottom rectangle of the module. This will naturally give larger damping than if a smaller projected area is used. However, I have investigated the effect of change of damping on the responses calculated, and the effects are small. These results can be seen in section 5.8. In addition, Øritsland (1989) states that an additional damping should be added in addition to the quadratic damping, since this often underpredicts the damping forces acting on an oscillating, submerged structure.

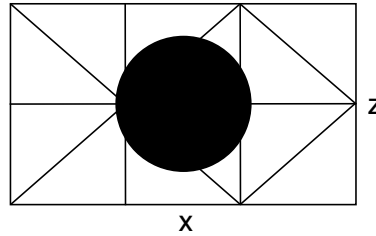


Figure 3.11: The idealized subsea structure used for estimation of hydrodynamic properties. (Reproduced from Øritsland, 1989).

### 3.4.2 Added mass

As for the damping, added mass is calculated for the top and bottom part of the module separately. Added mass for the flat plate can be calculated based on formulas in DNV-RP-H103. Figure 3.12 shows a table containing different added mass coefficients,  $C_A$  for rectangular plates with different length-width ratios. With the flat plate having a ratio of circa 2.5, an added mass coefficient of 0.801 will be applied. Knowing  $C_A$  the added mass is calculated from equation 3.2, where  $V_R$  is the reference volume, here shown in equation 3.3.  $a$  and  $b$  are shown in the figure below.

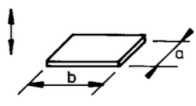
Rectangular plates 	Vertical	$b/a$	$C_A$	$b/a$	$C_A$	$\frac{\pi}{4} a^2 b$
		1.00	0.579	3.17	0.840	
1.25	0.642	4.00	0.872			
1.50	0.690	5.00	0.897			
1.59	0.704	6.25	0.917			
2.00	0.757	8.00	0.934			
2.50	0.801	10.00	0.947			
3.00	0.830	$\infty$	1.000			

Figure 3.12: Added mass coefficients for a rectangular plate (DNV, 2014b)

$$A_{33} = \rho C_A V_R \quad (3.2)$$

$$V_R = \frac{\pi}{4} a^2 b \quad (3.3)$$

Added mass for the bottom part is found from the same set of data where the damping coefficient was found. The added mass coefficient for heave is found to be 0.62 (Øritsland, 1989). The resulting added mass is found in the same way as for the flat plate, as shown in equation 3.2.  $V_R$  is set to the volume displacement of the manifold, i.e.  $55m^3$ .

Table 3.2 sums up the hydrodynamic coefficients for vertical motion of the manifold. The large added mass caused by the flat plate is worth noting. The added mass due to the flat plate alone contributes to more than twice the inertia from the structural mass.

	Added mass [tonnes]	Damping [ $\text{kN}/(\text{m}/\text{s})^2$ ]
Top part	416.7	62.1
Bottom part	35.0	73.2

Table 3.2: Hydrodynamic parameters for vertical motion

### 3.5 Crane and vessel

Modeling of the crane vessel is done by creating a support vessel in RIFLEX. The support vessel is given RAOs determining its motion characteristics. Depending on the direction of the incoming waves, the vessel response will differ. Therefore RAOs are given for different directions, and in my case for directions  $0^\circ$  to  $180^\circ$  with a step of  $15^\circ$ .  $0^\circ$  is often defined as head sea. However, a wave direction of  $0^\circ$  in RIFLEX is a wave traveling in positive x-direction. This is shown in figure 3.13 where the red arrow illustrates positive x-direction in RIFLEX. In RIFLEX it is possible to set the initial position of the vessel – both with regard to x-, y- and z-coordinates as well as rotations relative to the respective axes. By default the vessel's bow is pointing in positive x-direction as defined by RILFEX. But the RAO's definition of the bow is in negative x-direction. This is also shown in figure 3.13. Therefore, by leaving the vessel heading in positive x-direction as defined in RIFLEX, and letting incoming waves propagate along the same positive x-axis, the responses will be as if the vessel is in head sea.

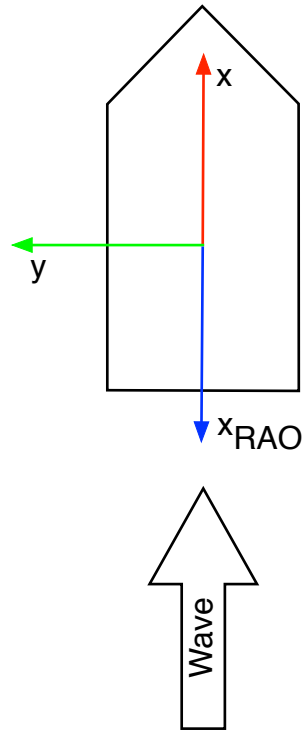


Figure 3.13: Illustration of RIFLEX coordinate system vs. RAO coordinate system.

I was provided with realistic RAOs by Subsea 7 for my model. The RAOs were given for another software called *Orcaflex*, but by use of a MATLAB script I managed to rewrite the Orcaflex format to that of RIFLEX. (See Appendix D for script)

The use of a support vessel allows me to define the motion of the crane tip point. The vessel has RAOs which transfers the incoming wave elevation into vessel motions. A supernode at the point where the crane tip is located is defined. If this point is fixed relative to the vessel, it will follow its motions rigidly. This implies that the crane is infinitely stiff, which it of course is not, but its vertical stiffness is much larger that of the lifting wire. In addition I assume that the motion characteristic of the vessel at the top of the crane is unaffected by the presence of the load. According to Nielsen (2007) this assumption require that the load is less than 1-2% of the vessel displacement and less than a few hundred tons. With the manifold in question weighing approximately 200 tons, plus the weight of the lifting wire, the crane vessel has to have a displacement of 5-10 000 tonnes. This seems reasonable and therefore also reasonable that the lift is considered as a light lift, and coupled dynamics are not needed.



# Chapter 4

## Matlab model

In addition to making a model in RIFLEX I have made a model using the programming language MATLAB. The model is based on the theory presented in the previous chapters, and can be seen in its entirety in appendix E. It is based on solving the equation of motion for a simple system as shown in figure 2.1. While the RIFLEX model includes both lifting wire and slings, motion in six degrees of freedom and irregular sea, my MATLAB model is based on a single lifting wire, one degree of freedom and regular waves. The wire stiffness is calculated based on slings in parallel and series as described in section 2.5.1. Clearly this model is a simplification, but it is meant as a verification model, rather than a substitute. What the MATLAB script does, is that it solves equation 2.6 for different wire lengths and wave periods and heights. The equation of motion is solved by use of the Newmark  $\beta$ -family.

For calculation purposes I use linear damping with an equivalent damping coefficient. An equivalent linear damping coefficient gives approximately the same damping force as when using quadratic damping. The coefficient is obtained by requiring the same amount of energy dissipation per cycle when using a linear model as when using a non-linear model. Langen and Sigbjørnsen (1979) show how this is found:

Mathematically an equivalent damping coefficient can be expressed as in equation 4.1.

$$c_{eq} = \frac{W_d}{\pi \omega u_0^2} \quad (4.1)$$

Where  $W_d$  is work or energy per cycle.  $\pi\omega u_0^2$  represent the ratio between energy per cycle and damping for a linear viscous damper.  $u_0$  is the response amplitude.

If the damping force is quadratically dependent on the response velocity,  $\dot{u}$

$$F_D = c|\dot{u}|\dot{u} \quad (4.2)$$

the energy dissipation per cycle is

$$W_d = \frac{8}{3} c\omega^2 u_0^3 \quad (4.3)$$

and the equivalent damping coefficient becomes

$$c_{eq} = \frac{8}{3\pi} c \omega u_0 \quad (4.4)$$

As seen from equation 4.4, the damping coefficient is a function of both the response frequency and amplitude of motion. If the load is harmonic with frequency  $\omega$ , so is the response (see section 2.4). Hence the response amplitude is the only parameter in the expression for the equivalent damping coefficient that is unknown. This has to be found by iteration. For each iteration a new response amplitude is found. This amplitude will give a new damping coefficient and hence a new response amplitude. This process is repeated until equilibrium is reached.

## 4.1 Numerical solution of the equation of motion

The method for solving the equation of motion presented here is taken from Langen and Sigbjørnsen (1979). I have chosen to use Newmark- $\beta$  when writing my MATLAB code. How expressions for  $\ddot{u}$ ,  $\dot{u}$  and  $u$  are achieved will be presented here.  $\ddot{u}$ ,  $\dot{u}$  and  $u$  are acceleration, velocity and displacement respectively. Time steps are denoted  $k$ , i.e.  $u_k$  is the displacement at time step  $k$  etc. Successive time steps,  $k$  and  $k+1$ , are separated with a time increment of  $h$ .

Firstly the basic relations between  $\ddot{u}$ ,  $\dot{u}$  and  $u$  are used to obtain expressions for the velocity and

displacement:

$$\dot{u}_{k+1} = \dot{u}_k + \int_0^h \ddot{u}(t) dt \quad (4.5)$$

$$u_{k+1} = u_k + \int_0^h \dot{u}(t) dt \quad (4.6)$$

Based on the equation of motion (eq. 2.19), with load  $Q(t)$  on the right hand side, the expression for the acceleration at time  $t$  will be

$$\ddot{u}(t) = \frac{1}{m} (Q(t) - c\dot{u}(t) - ku(t)) \quad (4.7)$$

Different methods for stepwise integration of the integrals in equations 4.5 and 4.6 exist. Depending on which assumptions are made on the acceleration during the time interval  $h$ , the integrations will differ. Newmark (1959) gives a general set of equations with parameters  $\gamma$  and  $\beta$  determining which assumptions are made on the acceleration. These equations are as follows:

$$\dot{u}_{k+1} = \dot{u}_k + (1 - \gamma)h\ddot{u}_k + \gamma h\ddot{u}_{k+1} \quad (4.8)$$

$$u_{k+1} = u_k + h\dot{u}_k + \left(\frac{1}{2} - \beta\right)h^2\ddot{u}_k + \beta h^2\ddot{u}_{k+1} \quad (4.9)$$

Whether the method is stable or not depends on the choice of  $\gamma$  and  $\beta$  as well as the step size  $h$ . However, it is independent of the time step  $h$ , and hence unconditionally stable, if

$$\gamma \geq \frac{1}{2}$$

$$\beta \geq \frac{1}{4} \left( \gamma + \frac{1}{2} \right)$$

The choice of  $\gamma$  also affects the damping of the system. If  $\gamma$  is greater than  $\frac{1}{2}$  the method introduces positive numerical damping. Is it less than  $\frac{1}{2}$  it will lead to negative numerical damping. Hence, the obvious choice is  $\gamma = \frac{1}{2}$ . The only exception is if one wants to damp out false high-

frequency components in the numerical solution; then one might want to use  $\gamma > \frac{1}{2}$ .

I have chosen  $\gamma = \frac{1}{2}$  and  $\beta = \frac{1}{4}$ . The choice of  $\gamma$  will give no numerical damping and the choice of  $\beta$  corresponds to constant average acceleration. I.e. the acceleration between  $\ddot{u}_k$  and  $\ddot{u}_{k+1}$  is assumed to be

$$\ddot{u}(t) = \frac{1}{2}(\ddot{u}_{k+1} - \ddot{u}_k) \quad (4.10)$$

This method is implicit which means it cannot be solved directly. It can however be rewritten to an explicit form. Langen and Sigbjørnsen (1979) have shown this as well. Starting with equations 4.8 and 4.9 the velocity and acceleration for step  $k+1$  can be written by use of  $u_{k+1}$ :

$$\ddot{u}_{k+1} = \frac{1}{\beta h^2} u_{k+1} - a_k \quad (4.11)$$

$$\dot{u}_{k+1} = \frac{\gamma}{\beta h} u_{k+1} - b_k \quad (4.12)$$

where

$$a_k = \frac{1}{\beta h^2} u_k + \frac{1}{\beta h} \dot{u}_k + \left( \frac{1}{2\beta} - 1 \right) \ddot{u}_k \quad (4.13)$$

$$b_k = \frac{\gamma}{\beta h} u_k + \left( \frac{\gamma}{\beta} - 1 \right) \dot{u}_k + \left( \frac{\gamma}{2\beta} - 1 \right) h \ddot{u}_k \quad (4.14)$$

By inserting equations 4.11 and 4.12 into the equation of motion for time  $t_{k+1}$ , and solving for  $u_{k+1}$  the following expression is obtained:

$$u_{k+1} = \frac{Q_{k+1} + c b_k + M a_k}{k + \frac{\gamma}{\beta h} c + \frac{1}{\beta h^2} M} \quad (4.15)$$

This is an explicit expression where the only thing needed from time step  $k+1$  is the load which is known. For time step 1 I need to assume the initial displacement and velocity. The acceleration for time step 1 is then determined from equation 4.7.

# Chapter 5

## Results from simulations

This chapter presents the results from simulations – both static and dynamic analyses. The dynamic analyses are from RIFLEX as well as my MATLAB model. Comparisons of dynamic responses from the two models are made for different depths and wave periods. Dynamic load responses are presented as a fraction of static load. This static load is the submerged weight of the module, including wire and slings and equals 1.39MN.

### 5.1 Static offset due to current

Ocean currents will exert forces on submerged bodies. Depending on the body's area, roughness and geometry these forces will vary. I have run static analyses based on the findings in 3.4. RIFLEX' way of calculating static offset due to current is by static analysis. I apply current forces during static analysis and read the static configuration of the lift wire in the xz-plane as static equilibrium is achieved. For each vertical position from -100m to -1287m, with a step of 100m, I take out the maximum horizontal offset in x-direction. The choice of current velocities and the maximum depth of 1287m is based on the field metocean<sup>1</sup> design basis from Statoil (Gaches and Bruserud, 2012). The report states that the water depth at the site is 1290m and that measurements of current velocities are performed for depths from 10m to three meters above sea bed.

---

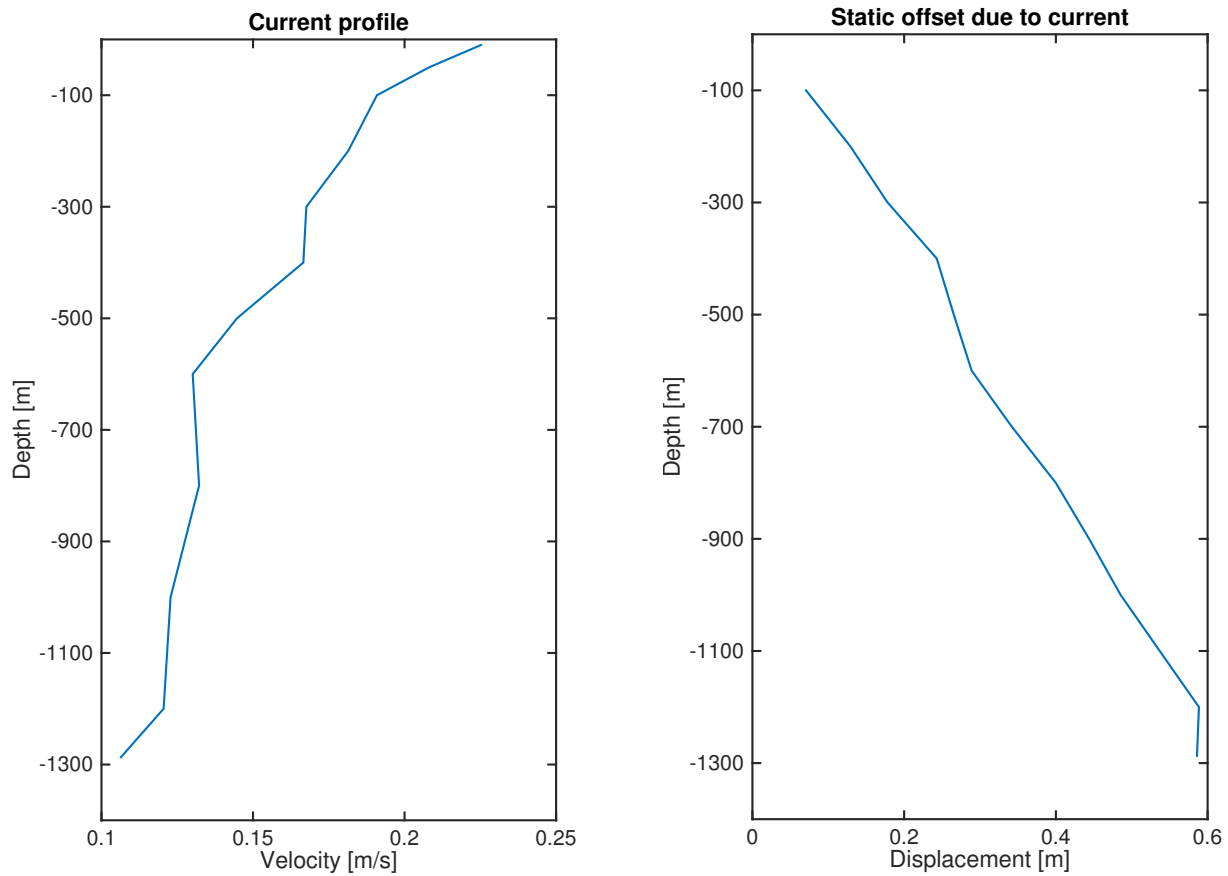
<sup>1</sup>Metocean is an abbreviation of the two words *meteorology* and *oceanography*

Measurements presented in the report by Gaches and Bruserud (2012) are done over approximately 3.5 years with a sample interval of 10 minutes. The results of these measurements are presented in table 5.1. The values are irrespective of direction, although the majority of current velocities are seen for a direction of  $270-300^\circ$ , i.e. West to Northwest by west. Current is applied in positive x-direction, i.e. in the longitudinal direction of the manifold.

<b>Depth</b>	<b>Current speed</b>	
	<b>Max</b>	<b>Mean</b>
<b>m</b>	<b>cm/s</b>	<b>cm/s</b>
10	131	22.52
50	99	20.81
100	93	19.09
200	86	18.14
300	67	16.76
400	80	16.66
500	59	14.47
600	46	13.01
800	52	13.22
1000	53	12.28
1200	48	12.05
1287	45	10.64

Table 5.1: Current velocities for the Aasta Hansteen field (Gaches and Bruserud, 2012).

In RIFLEX I have performed static analyses with the two current profiles presented in table 5.1. The results for mean current velocity is seen in figure 5.1. The horizontal offset is 7cm at 100m depth and increases almost linearly to 59cm at 1200m. The drop in current velocity seen between 1200m and 1300m leads to a reduction in offset from 1200m to 1300m.

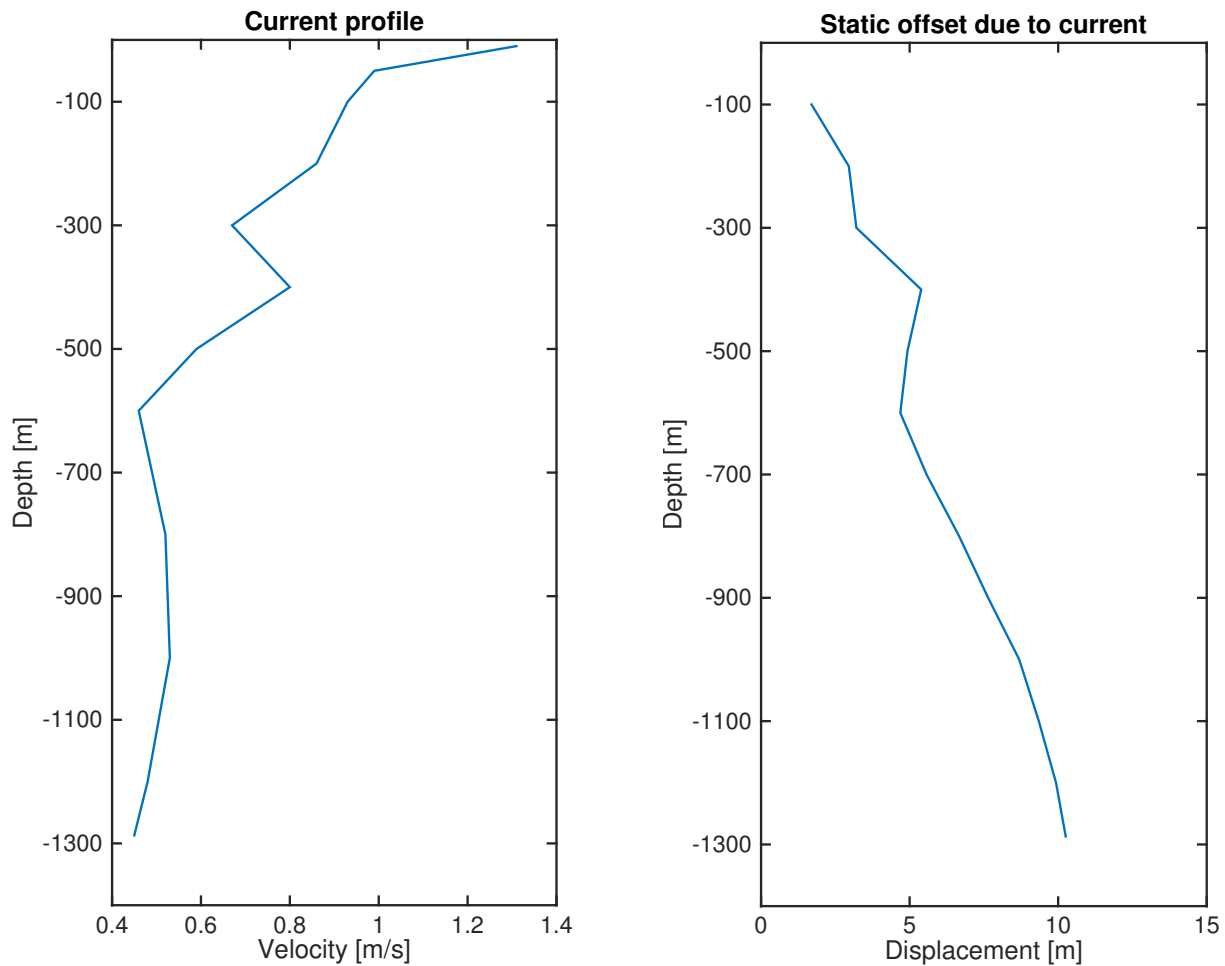


(a) Current velocity vs. depth

(b) Static offset due to current

Figure 5.1: Static offset of module for mean current velocity.

For the current profile with maximum current velocities the displacements are significantly larger. They range from 1.7m at 100m depth to over 10m at 1200m depth. This is in the order of 17-18 times as large displacements. See figure 5.2. Drag forces are proportional to velocity squared. Since the increase in current velocity is approximately 4-5 times larger for maximum velocity, an increase in the order of 17-18 times seems reasonable.



(a) Current velocity vs. depth

(b) Static offset due to current

Figure 5.2: Static offset of module for max current velocity.

## 5.2 Static elongation due to own weight

Dynamic loads will induce oscillating motions stretching the lifting wire, but static loads will elongate the lifting wire as well. Here I briefly show how the static elongation varies with wire length. In accordance with the inverse relationship between axial stiffness and length the static elongation increases with wire length. Table 5.2 shows how the values vary with depth. The axial stiffness ( $EA$ ) of the lifting wire is set to 852MN, while the slings are given a stiffness of 246MN.



Depth [m]	Static elongation [m]
100	0.27
200	0.44
300	0.61
400	0.79
500	0.97
600	1.16
700	1.35
800	1.54
900	1.74
1000	1.94
1100	2.14
1200	2.35
1287	2.54

Table 5.2: Static elongation of lifting wire due to weight of manifold and wire.

### 5.3 RAO for crane tip motion

RAOs presented here are obtained by simulations in RIFLEX with regular waves with wave height 0.2m. The reason for the low amplitudes is to avoid large responses due to resonance at certain periods. Simulations terminate if slack occurs in the slings attaching the module to the lifting wire. If using such small waves is to be correct, the relation between wave height and response has to be fully linear. This is not necessarily the case, but the results presented here will give a fairly good estimate of the RAOs. The crane tip is located at  $(x, y, z) = (-38.15, 27.5, 50.5)m$  relative to the vessel's position in RIFLEX. Values obtained for these RAOs are a result of the RAOs for the vessel, given a value of the metacentric height, GM.

In head sea the induced motions will come from a combination of heave and pitch. Figure 5.3 shows the RAO for crane tip motion in head sea.

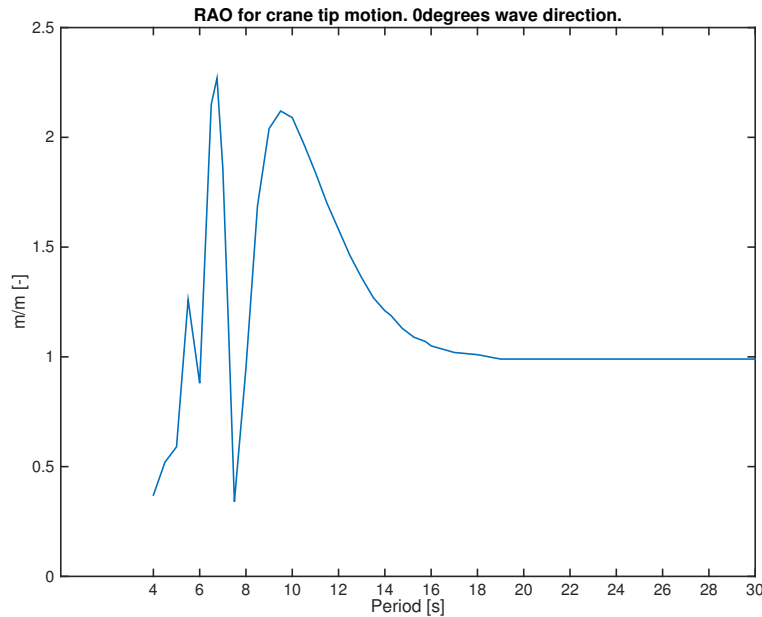


Figure 5.3: RAO for vertical crane tip motion at heading  $0^\circ$ .

When the wave direction deviates from  $0^\circ$ , roll motion will affect the vertical motion of the crane tip. The RAOs for wave direction  $\pm 15^\circ$  can be seen in figures 5.4 and 5.5 respectively. For the vessel's centre of motion the response will be equal for the two wave directions. But when calculating motions outside this point, depending on where in space this point is located, results will vary due to phase differences. In this case the contribution from roll motion will affect the vertical motion of the crane tip differently for the two headings. Looking at the vertical component of equation 2.29 this effect is clear. Incoming waves with  $+15^\circ$  heading with the crane on starboard side corresponds to a wave direction of  $-15^\circ$  and the crane on port side. This is the case since the vessel is symmetric. Hence, keeping the wave heading constant and changing the crane position from starboard to port, gives the same results as changing wave heading. The vertical component of equation 2.29 reads  $(\eta_3 + y\eta_4 - x\eta_5)\mathbf{k}$ . Changing from  $+15^\circ$  to  $-15^\circ$  heading will thus equal a sign change on the y-component, giving different responses for the two headings.

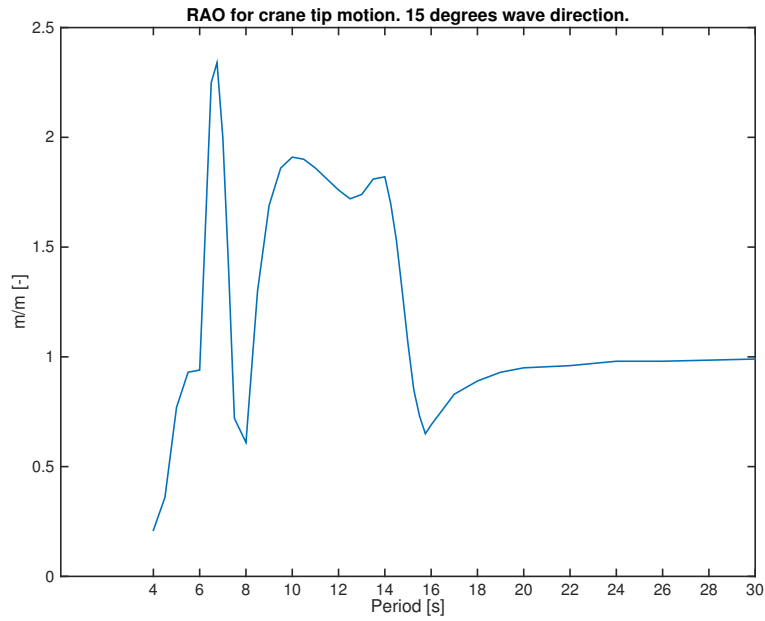


Figure 5.4: RAO for vertical crane tip motion at heading  $15^\circ$ .

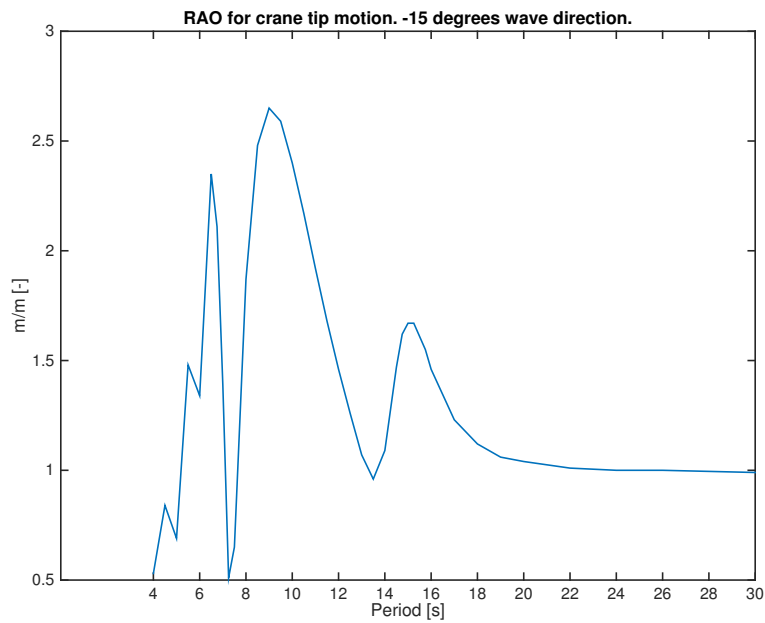


Figure 5.5: RAO for vertical crane tip motion at heading  $-15^\circ$ .

Changing from  $0^\circ$  to  $15^\circ$  heading causes an extension of the secondary peak seen for a wave

heading of  $0^\circ$ . The peak now stretches as far as to  $T=13s$ . Otherwise the results are similar to head sea. As for the case with  $-15^\circ$  wave heading, what was the second largest peak for head sea is now the largest. An additional peak is also seen at  $T=15s$ . Otherwise this is also similar to the result for head sea.

## 5.4 Eigenperiods from hand calculations

By use of formula 2.10 I have calculated the eigenperiods for the wire-mass-system. The adjustment factor for wire mass,  $\Theta$  is set to  $\frac{1}{3}$ . According to DNV (2014b) this is the value to be used if the crane is stiff, and the wire is the dominating soft spring – which is the case here. Vertical stiffness of the lifting wire and slings is calculated as shown in section 2.5.1. The result is presented in table 5.3.

Position [-m]	Eigenperiod [s]
0	1.56
100	2.30
200	2.85
300	3.32
400	3.73
500	4.10
600	4.44
700	4.76
800	5.06
900	5.34
1000	5.61
1100	5.87
1200	6.11
1300	6.35

Table 5.3: Eigenperiods for manifold motion.

## 5.5 Results from MATLAB model

By use of the RAOs from section 5.3 I have calculated dynamic responses in MATLAB (see app. E for code). For given wave heights the equation of motion is solved for different wave periods and depths. The depth  $d$  is defined as the length of the lifting wire. The RAOs from section 5.3 defines the crane tip motion which excites the system. Depending on the length of the lifting wire, responses will vary. Dynamic effects will give amplifications in loads, which will lead to greater maximum forces, but also lower minimum forces. Due to danger of snap loads in the wire and slings, it is crucial that there is always tension in the wires, and thus avoiding slack.

For each wave height the equation of motion is solved for 39 wave periods and 13 vertical positions of the module. This gives 507 solutions to the dynamic problem per wave height. A regular wave with height  $H$  and period  $T$  is used, and for every solution the axial force amplitude in the lifting wire is extracted and plotted. Values are divided by the static load from the weight of the module, adjusted for buoyancy.

### 5.5.1 Wire tension in head sea

Analyses are run for two wave heights, 1 and 2 meters. In figure 5.6 the maximum axial force responses for the lifting wire can be seen for a wave heading of  $0^\circ$ . The results show that peaks occur around three periods. The largest peak is seen at a wave period of 6.5s. This is recognized from figure 5.3 as a period where large dynamic amplifications are present for crane tip motion. This will lead to large amplitudes of motion and hence larger forces compared to say a period of 7.5s where there is cancellation. The second largest peak is found at a period of 5.5s. This is also a peak in the RAO for crane tip motion. Although smaller, it is close to the eigenperiods of the mass-spring-damper system that the manifold and wires make. Table 5.3 shows the eigenperiods I have calculated. The closer the excitation period is to the eigenperiod, the larger the responses will be. For depths from 500m and above eigenperiods are greater than 4s. 4s is the smallest period for which I have values for the vessel's RAO, and thus the smallest value for which I run simulations.

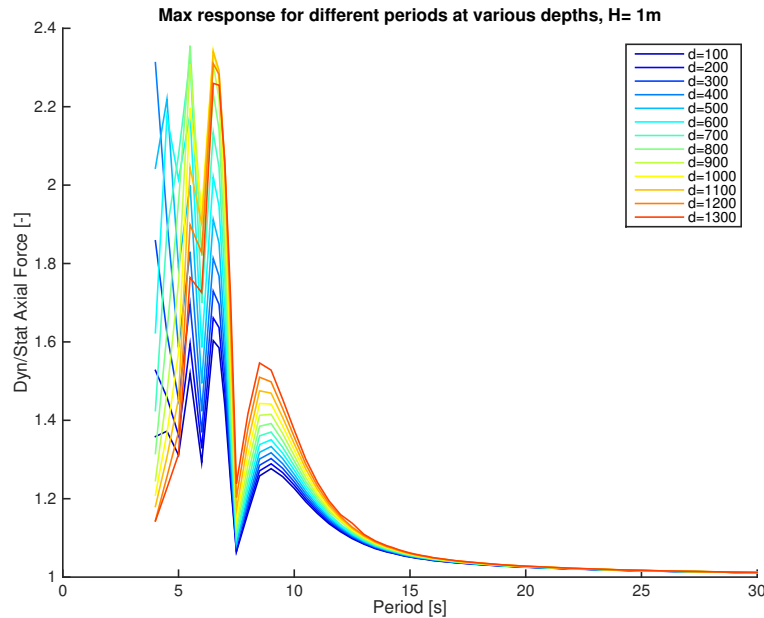


Figure 5.6: Dynamic amplification in axial force in lifting wire as a fraction of static load. Wave height 1m.

Just as important, if not more, is the minimum forces in the lifting wire. It is critical that neither the lifting wire nor the slings are slack. If so, wires may snap due to the yank that will take place. With my analyses in MATLAB being regular, the axial force in the lifting wire oscillates around the axial force from the static loading. This means that a dynamic amplification factor of 2 or greater will mean zero or negative axial force in the wire respectively.

A regular analysis with wave height of 2m is also performed. This allows me to express the relationship between amplitude in axial force and wave amplitude – the RAO. This is later compared to equivalent results from RIFLEX. Figure 5.7 shows the results of this analysis. Results are presented in one plot. This shows the major trends in responses, but makes it challenging to pick out values for each depth. A single plot for each depth is shown in appendix I.

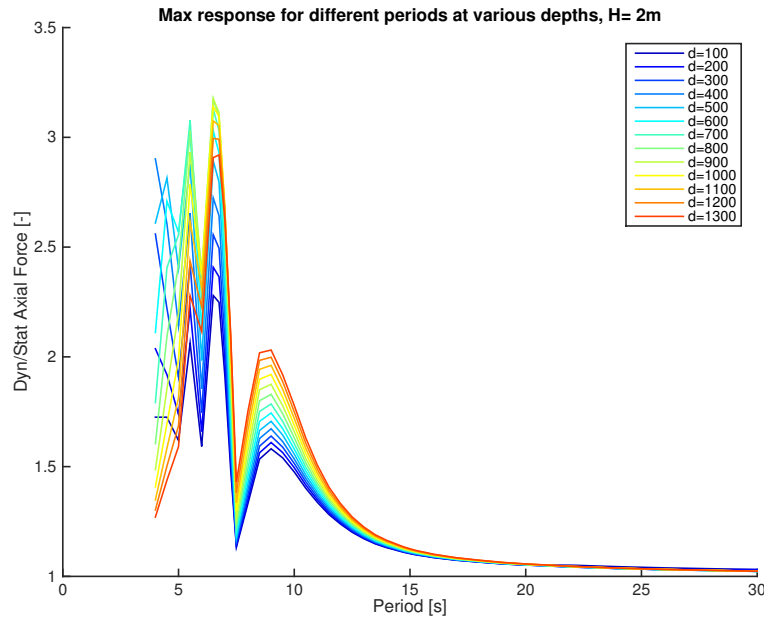


Figure 5.7: RAO for axial force in lifting wire.

### 5.5.2 Wire tension for $\pm 15^\circ$ wave direction.

During marine operations, waves will not necessarily hit the vessel directly at the bow. Both wave heights, periods, phases and directions will vary. In order to investigate the effect of waves coming in with an angle, and not directly at the vessel's bow, I have gathered crane responses from RIFLEX when waves are coming in with an angle of  $\pm 15^\circ$ . As seen in figures 5.4 and 5.5 crane responses vary with the two incoming angles. Hence the module responses will vary as well.

The major changes are in the period range 8-18s. This is an area where responses are relatively small, hence it affects the resulting module response and wire forces to a small extent.

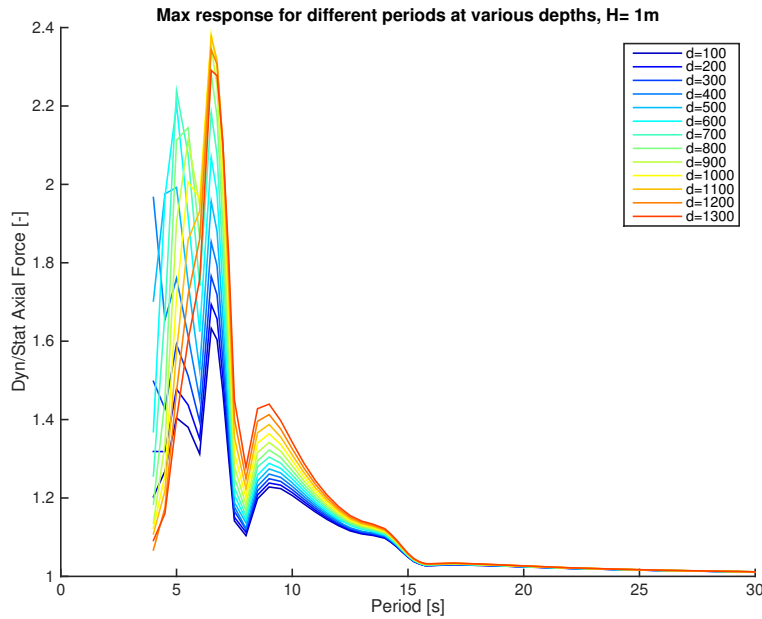


Figure 5.8: Maximum axial force in lifting wire as a fraction of static load. Wave height 1m,  $15^\circ$  incoming angle.

As for the case with  $+15^\circ$  wave direction the changes are at periods where responses are small. With a wave direction of  $-15^\circ$  an extra peak on the RAO for crane tip motion is seen at 15s. This shows as an extra peak in the axial force response. But as figure 5.9 shows, this is not of significance. There is however a shift from a maximum at  $T=6.75$ s for  $0^\circ$  to 9s for  $-15^\circ$ . The responses are larger for a heading of  $-15^\circ$  compared to head sea. Maximum dynamic amplification rises from approximately 2.4 to 2.6.



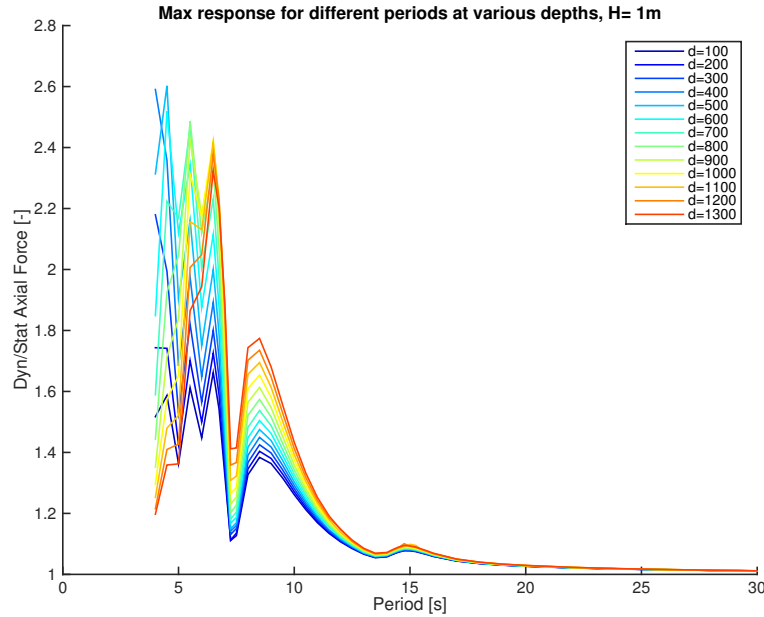


Figure 5.9: Maximum axial force in lifting wire as a fraction of static load. Wave height 1m,  $-15^\circ$  incoming angle.

## 5.6 RIFLEX results

### 5.6.1 Identification of eigenperiods

Simulations in RIFLEX are run with an irregular sea state for module positions ranging from -100m to -1300m. The sea state used is generated from a three parameter JONSWAP spectrum. The three parameters are peak period, significant wave height and peakedness parameter. I have specified two of them; peak period and significant wave height with values 15s and 1.5m respectively. The last parameter, gamma is set to a default value of 3.3.

After running simulations for the given depths, I use a built in function in RIFLEX where a fast fourier transform (FFT) is performed on the time series. The time series I have chosen is the axial force in the lifting wire. The FFT gives a spectrum showing how responses are distributed among response periods. By inspecting these spectra I am able to determine at which periods most of the response occur. The peak period of the wave spectrum tells which wave period con-

tains the most energy in the sea state. This is however not necessarily the peak period for the response spectrum. The distribution of energy in the response spectrum is determined by the eigenfrequencies of the system – both the eigenfrequencies of the vessel, but also of the mass-spring-damper system made by the wire, slings and manifold.

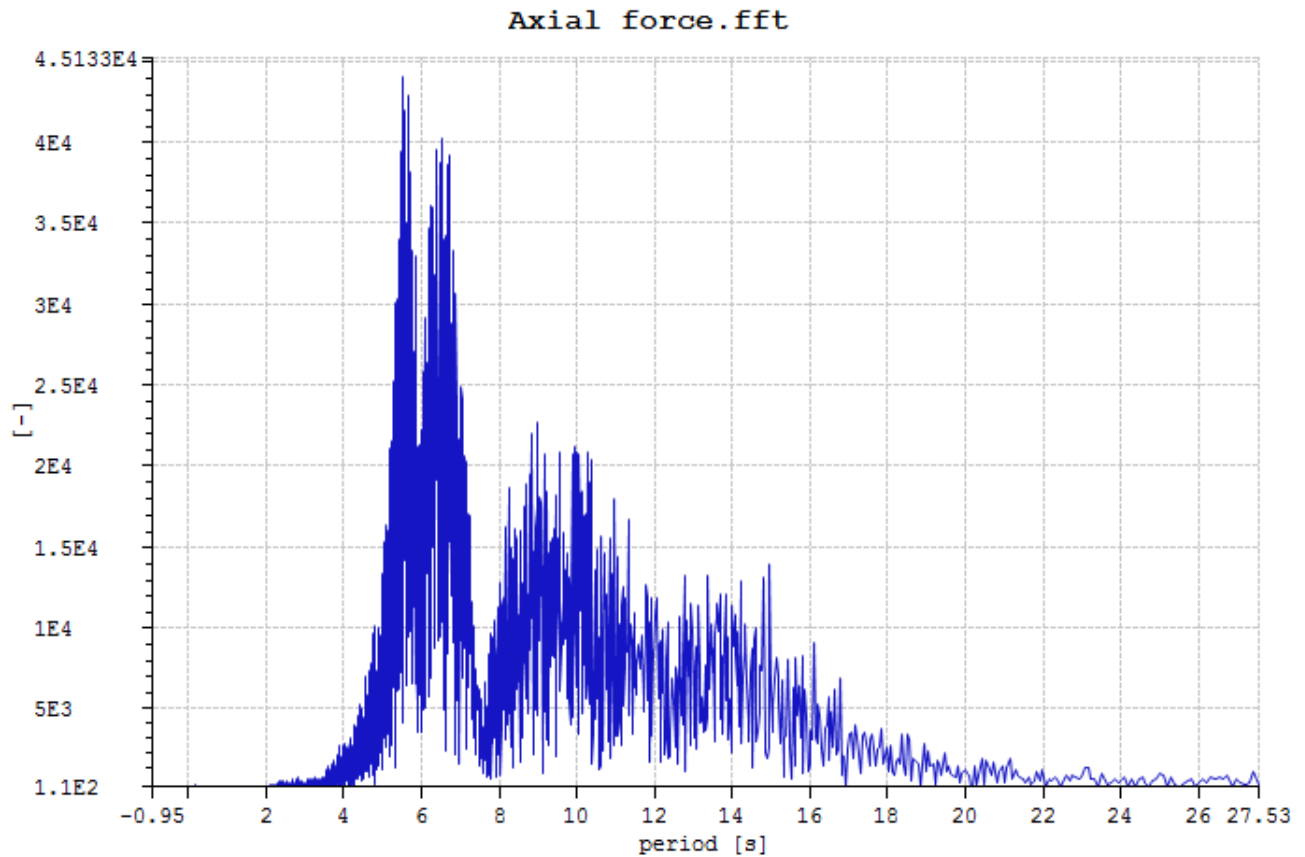


Figure 5.10: Response spectrum for axial force in the lifting wire.  $T_p=15s$ ,  $H_s=1.5m$ ,  $d=900m$ .

Eigenfrequencies will show as peaks in the response spectrum if excited. The eigenfrequency of the vertical crane tip motion will be present for each depth. This can easily be excluded by realizing that this is the peak value in the RAO for vertical crane tip motion. As seen from figure 5.3 this is 6.5-6.75s. Peaks for periods lower than this are due to resonant motion in the wire. These are quite easily found for peaks occurring at periods lower than 6.5s. But as the eigenfrequency for wire forces approaches the one for crane tip motion, they are not as easily separated from one and another. However, I have tried extracting values for each depth, and present them in

table 5.4. An example of a response spectrum from such an irregular analysis is shown in figure 5.10. The figure show three peaks: one at 5.5s, one at 6.5s and one at 9-10s. This trend is seen for all depths. The peak occurring at the lowest period is due to the eigenperiod of the wire and mass. The two peaks at 6.5s and 10s are due to the crane tip motions. As previously mentioned figure 5.3 shows the RAO for crane tip motion. This has one peak at 6.5s and one at 10s approximately. Response spectra for depths of 100m to 1300m are enclosed in appendix H.

<b>Depth [m]</b>	<b>Eigenperiod [s]</b>
100	2.27
200	2.89
300	3.37
400	3.89
500	4.33
600	4.63
700	4.88
800	5.41
900	5.53
1000	5.66
1100	5.88
1200	Indistinguishable
1300	Indistinguishable

Table 5.4: Eigenperiods from RIFLEX simulations

Comparing with the eigenperiods from hand calculations, shown in table 5.3, I see that they are within a range of  $\pm 0.3s$ , with an average of 0.1s error. All except the eigenperiods for depths 100m and 200m are underestimated compared to what RIFLEX gives. Figure 5.10 shows a situation where the eigenperiod for the wire and mass is distinguishable from the one of the crane tip motion. For 1200m and 1300m depth, the eigenperiods are too close to separate. As figure 5.11 clearly shows, a single distinguishable peak does not appear.

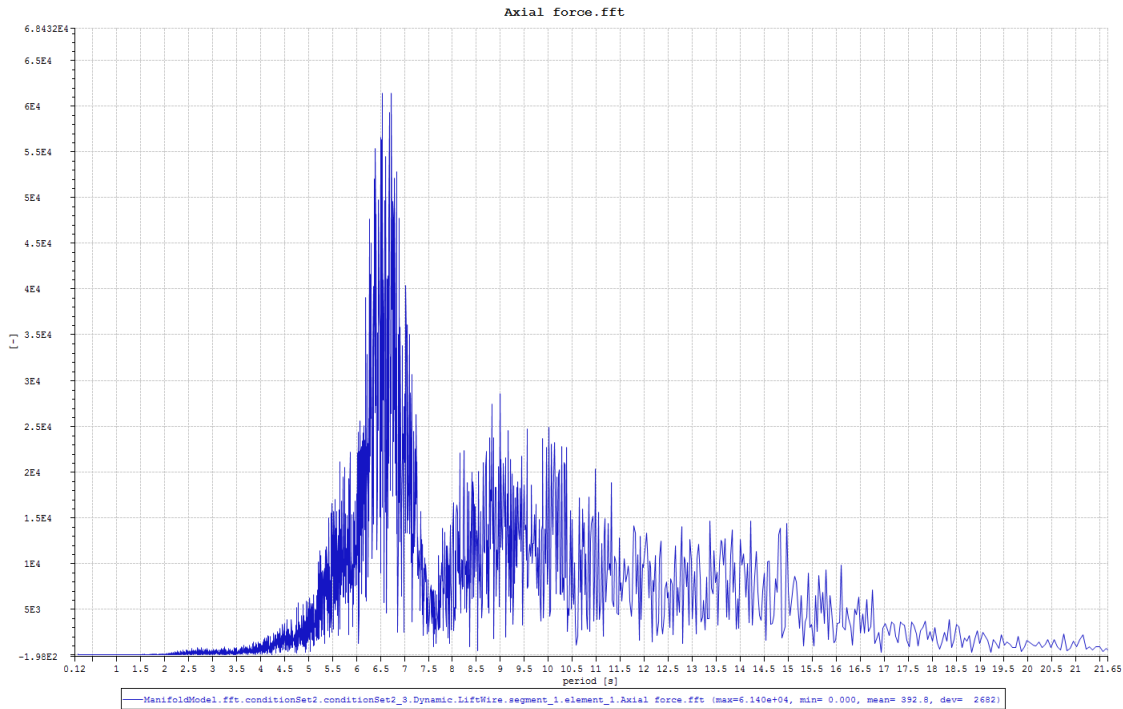


Figure 5.11: Response spectrum for axial force in the lifting wire.  $T_p=15s$ ,  $H_s=1.5m$ ,  $d=1200m$ .

The dynamic effects is noticeable when the eigenperiod of the module motion gets closer to the peak in the RAO for crane tip motion. Figure 5.12 shows the spectrum for vertical crane tip motion in a sea state with a peak period of 13s. Besides the peak at 13s a peak occurs at 6.75s. This peak is recognized in figure 5.13 and 5.14 as well. The two figures show response spectra for vertical module motion for a vertical position of 600m and 200m respectively. The eigenperiod at 200m depth is 2.9s and 4.6s at 600m. Responses are increased for periods around the peak in crane tip motions for a depth of 600m compared to what is seen for a depth of 200m. Going from a depth of 200m to a depth of 600m reduces the difference in eigenperiods of module and crane tip motion. Consequently dynamic effects increase as shown figure 2.2. The eigenperiod for 200m depth is low enough for it not to cause significant dynamic effects. It only causes a minor peak in the response specter.

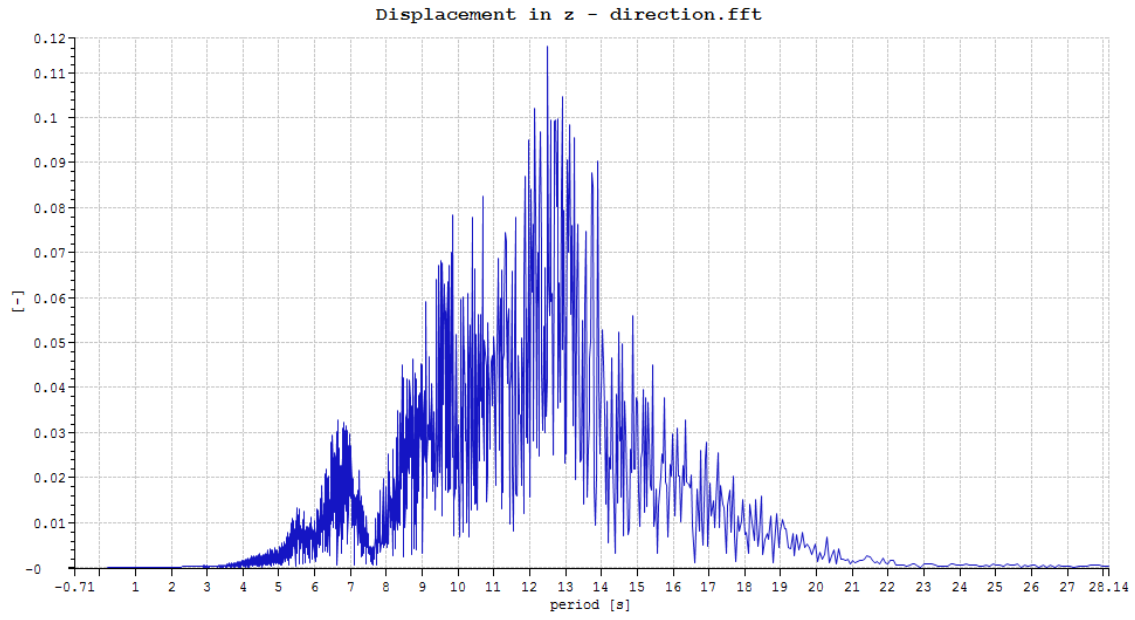


Figure 5.12: Spectrum for vertical crane tip motion

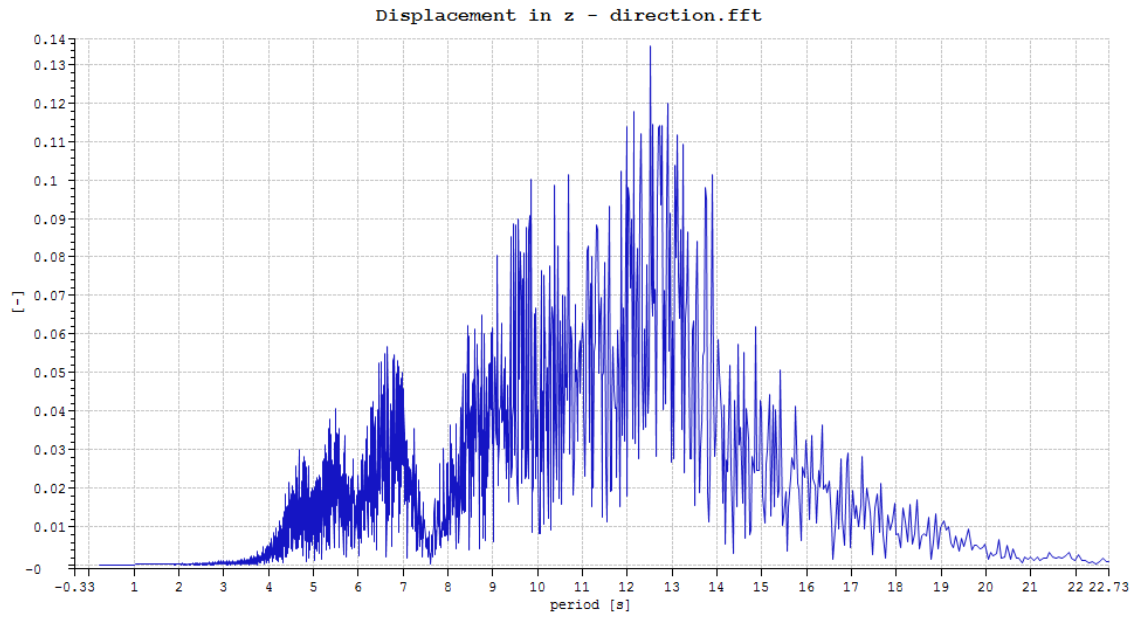


Figure 5.13: Spectrum for vertical module motion at a depth of 600m

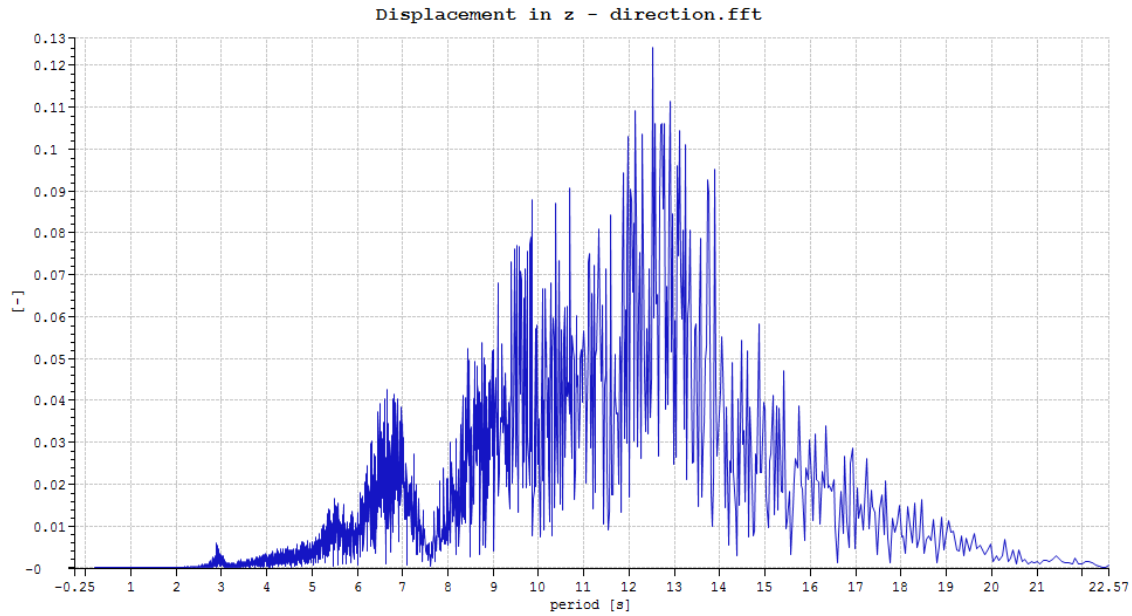


Figure 5.14: Spectrum for vertical module motion at a depth of 200m

### 5.6.2 RAO for wire tension

Forces in the lifting wire will vary with wave height and period. In RIFLEX I have run analyses with regular waves with 1m wave height and periods from 4s to 20s. For the cases where responses are large, and slack occurs, I have run for 0.5m wave height and performed a linear extrapolation to obtain results for 1m wave height. For this to be correct, the relation between increase in wave height and increase in axial force has to be linear. This is for most periods *almost* the case. For other cases the relation is perfectly linear. However, for periods close to the eigenperiods the relation is non-linear. This is the periods where I extrapolate the results, and hence a linear extrapolation of the results will not give 100% accurate results. On the other hand, the non-linearity is such that a linear extrapolation gives a conservative estimate for the cases I have checked.

For a given vertical position of the manifold and wave period, 10 regular waves with heights from 0.1m to 1m are used to check if responses increase linearly. The axial force amplitude in the lifting wire is then registered. The dynamic amplification factor is calculated for each wave height. As figure 5.15 shows, the relation is perfectly linear for that specific combination of depth and

wave period. In figure 5.16 on the other hand, the increase in response is slightly non-linear. The non-linearity is however such that the slope is negative. Note that only six wave heights are used in figure 5.16, since a higher wave height will give slack.

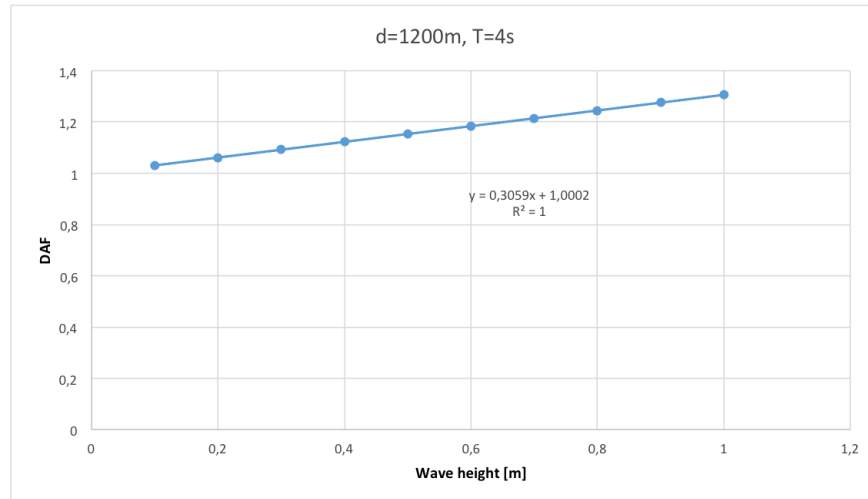


Figure 5.15: Linearity check for a depth of 1200m and wave period 4s.  $R^2$  value and interpolated equation included.

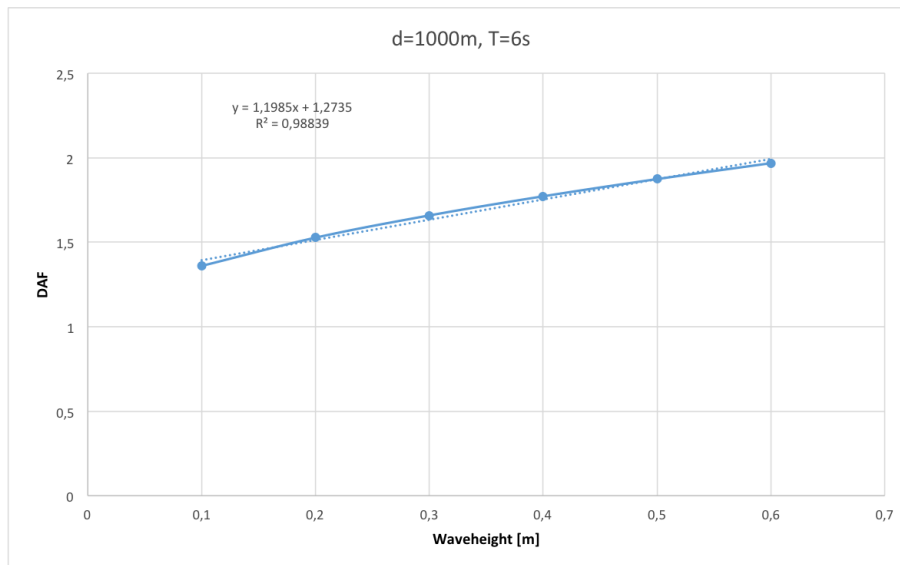


Figure 5.16: Linearity check for a depth of 1000m and wave period 6s.  $R^2$  value and interpolated equation included.

The results from RIFLEX for head sea have been gathered in figure 5.17. The y-axis shows the

ratio between dynamic and static load, where the static load is in submerged condition measuring 1.39MN. As for the results from MATLAB, there are large responses for periods below 7s and a minor peak at around 9-10s. The graphs for each single depth is enclosed in appendix J.

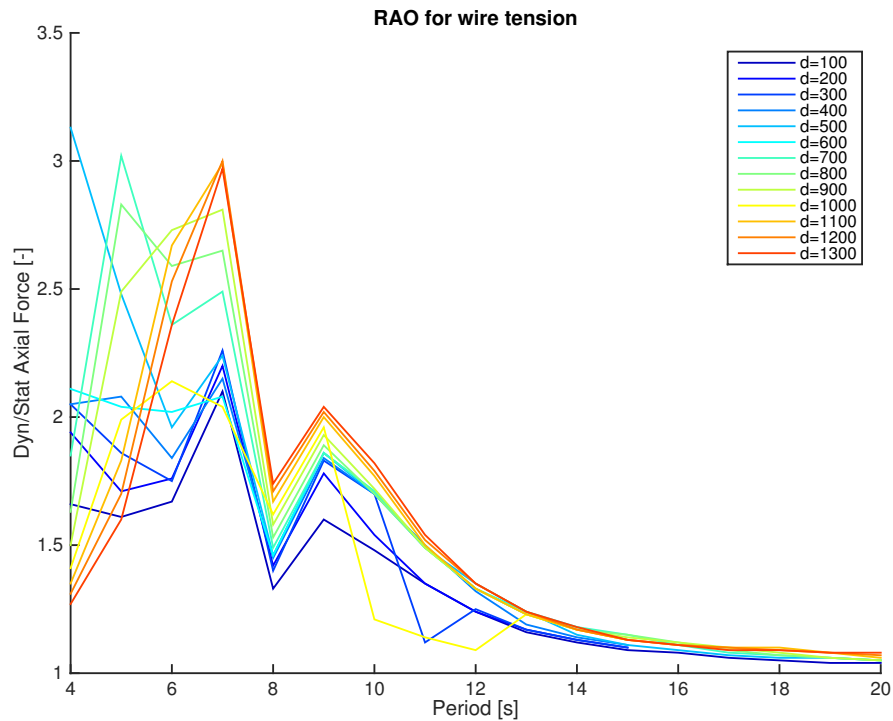


Figure 5.17: Wire tension amplitude per meter wave amplitude for wire tension in head sea.

## 5.7 Comparison of MATLAB and RIFLEX results for wire tension RAOs

When comparing results from my MATLAB model and the results I obtained from RIFLEX simulations, I wanted to choose a wave height for which my RIFLEX model does not crash due to slack. The reason for this is that I want to run both models with the same wave height, and not scale the results for different wave heights. The wave height at which I chose to run the simulations was 0.6m. This wave height is used in both RIFLEX and MATLAB. I have compared the dynamic amplification of the axial force in the lifting wire. First I present the results for each



model. Wave periods range from 4s to 20s with a step of 1s. I have done the same for 1m wave amplitude, but then with extrapolated results for dynamic amplifications greater than 2.

Table 5.5 presents the dynamic amplifications obtained from my MATLAB model, while table 5.6 shows corresponding results from RIFLEX. A selection of depths are chosen, both in the upper half of the ocean as well as near the bottom.

<b><i>Depth [m]</i></b> <b><i>T[s]</i></b>	<b>400</b>	<b>600</b>	<b>800</b>	<b>1200</b>	<b>1300</b>
<b>4</b>	1.69	1.45	1.21	1.10	1.08
<b>5</b>	1.30	1.52	1.60	1.25	1.21
<b>6</b>	1.23	1.30	1.42	1.51	1.47
<b>7</b>	1.30	1.36	1.44	1.59	1.60
<b>8</b>	1.11	1.12	1.14	1.19	1.21
<b>9</b>	1.17	1.19	1.21	1.26	1.28
<b>10</b>	1.14	1.15	1.16	1.19	1.20
<b>11</b>	1.10	1.10	1.11	1.13	1.13
<b>12</b>	1.07	1.07	1.08	1.08	1.09
<b>13</b>	1.05	1.05	1.05	1.06	1.06
<b>14</b>	1.04	1.04	1.04	1.04	1.04
<b>15</b>	1.03	1.03	1.03	1.03	1.03
<b>16</b>	1.02	1.03	1.03	1.03	1.03
<b>17</b>	1.02	1.02	1.02	1.02	1.02
<b>18</b>	1.02	1.02	1.02	1.02	1.02
<b>19</b>	1.02	1.02	1.02	1.02	1.02
<b>20</b>	1.01	1.01	1.01	1.02	1.02

Table 5.5: MATLAB results showing wire tension responses, expressed as ratio between dynamic and static force.

<b><i>Depth [m]</i></b> <b><i>T[s]</i></b>	<b>400</b>	<b>600</b>	<b>800</b>	<b>1200</b>	<b>1300</b>
<b>4</b>	1.88	1.43	1.19	1.09	1.08
<b>5</b>	1.32	1.66	1.68	1.22	1.19
<b>6</b>	1.23	1.34	1.52	1.56	1.48
<b>7</b>	1.31	1.38	1.50	1.71	1.72
<b>8</b>	1.12	1.13	1.15	1.23	1.26
<b>9</b>	1.19	1.21	1.22	1.29	1.32
<b>10</b>	1.16	1.17	1.17	1.21	1.22
<b>11</b>	1.12	1.11	1.13	1.13	1.14
<b>12</b>	1.08	1.08	1.08	1.08	1.09
<b>13</b>	1.05	1.06	1.06	1.06	1.06
<b>14</b>	1.04	1.05	1.04	1.05	1.05
<b>15</b>	1.03	1.03	1.04	1.04	1.04
<b>16</b>	1.03	1.03	1.03	1.03	1.03
<b>17</b>	1.02	1.02	1.02	1.02	1.02
<b>18</b>	1.02	1.02	1.02	1.02	1.02
<b>19</b>	1.02	1.02	1.02	1.00	1.02
<b>20</b>	1.01	1.02	1.02	1.02	1.00

Table 5.6: RIFLEX results showing wire tension responses, expressed as ratio between dynamic and static force.

Comparison of results are done by calculating the absolute value of the difference in percent for each combination of depth and wave period. The difference is calculated according to equation 5.1.

$$|(1 - RAO_{MATLAB}/RAO_{RIFLEX})| \cdot 100 \quad (5.1)$$

Table 5.7 shows the absolute value of the difference in percent. The average difference is 1.3%, with a standard deviation of 2 percentage points. The greatest differences are found for the lower region of the period range (4-7s). In this region the average difference is 3.35% with a standard deviation of 3 percentage points. In the region for higher periods (8-20s), the mean and standard deviation are 0.68% and 0.8 percentage points respectively. This corresponds well to the period ranges where the responses differ as well. The responses are greatest for the lower period range and more modest for the higher period range.

<b><i>Depth [m]</i></b> <b><i>T[s]</i></b>	<b>400</b>	<b>600</b>	<b>800</b>	<b>1200</b>	<b>1300</b>
<b>4</b>	10.37	1.29	1.39	0.66	0.14
<b>5</b>	1.71	8.52	4.94	2.09	1.65
<b>6</b>	0.68	2.52	6.49	3.66	1.09
<b>7</b>	0.23	1.37	3.69	7.47	7.10
<b>8</b>	0.96	0.44	0.80	2.78	3.65
<b>9</b>	1.59	1.86	0.52	2.31	2.83
<b>10</b>	1.61	1.81	0.53	1.25	1.55
<b>11</b>	2.32	0.96	1.42	0.53	0.73
<b>12</b>	1.01	0.66	0.61	0.02	0.24
<b>13</b>	0.16	0.79	0.36	0.28	0.08
<b>14</b>	0.10	1.06	0.31	0.27	0.27
<b>15</b>	0.07	0.16	0.53	0.20	0.21
<b>16</b>	0.05	0.05	0.66	0.13	0.14
<b>17</b>	0.04	0.05	0.12	0.15	0.14
<b>18</b>	0.02	0.03	0.05	0.23	0.14
<b>19</b>	0.13	0.04	0.03	1.65	0.28
<b>20</b>	0.01	0.03	0.04	0.17	1.85

Table 5.7: Comparison of MATLAB and RIFLEX results. Table values are difference in percent.

Increased response means that non-linearities are more present. Hence the differences between my MATLAB results and the results from RIFLEX will differ to a greater extent when increasing the wave amplitude to 1m. From an average difference (in absolute values) of 1.3% for 0.3m wave amplitude, the average absolute difference is 6.7% for 1m wave amplitude. As seen from table 5.8 differences are in general larger than for a wave amplitude of 0.3m. Equation 5.1 is used here as well, but without taking the absolute value. Hence negative values means larger values for MATLAB than for RIFLEX. Comparisons are made for periods up to 15s, since responses are moderate for greater periods.

$T$ [s] Depth [m]	4	5	6	7	8	9	10	11	12	13	14	15
100	-0.27	-2.80	-8.06	-13.35	-1.67	-3.66	-2.40	-2.63	-1.44	0.04	0.16	0.60
200	-2.72	-2.75	-9.75	-14.76	-7.19	-13.46	-5.30	-1.89	-0.99	-0.55	-0.56	-0.19
300	10.72	-3.33	-4.51	-13.49	-4.24	-14.77	-14.87	16.09	-1.34	-0.27	-0.37	-0.06
400	23.77	-4.94	-4.41	-3.56	-6.34	-13.43	-13.54	-11.53	-6.52	-1.67	-1.06	-0.84
500	-20.10	-12.81	-4.95	-3.25	-5.35	-12.54	-12.15	-9.95	-8.43	-5.64	-1.74	-0.70
600	4.47	14.26	-1.81	8.32	-3.44	-10.43	-11.28	-9.10	-6.30	-5.32	-4.19	-2.37
700	0.97	-24.43	-12.25	-5.53	-3.44	-8.20	-9.83	-8.14	-5.77	-4.14	-3.97	-4.03
800	1.32	-19.62	-17.83	-8.75	-3.88	-7.62	-7.62	-7.20	-5.20	-3.81	-2.88	-3.88
900	1.31	-11.96	-21.21	-12.57	-4.77	-7.57	-7.27	-6.27	-4.60	-3.46	-2.66	-2.83
1000	1.36	2.35	5.30	19.42	-4.83	-6.91	25.70	19.47	14.74	-3.08	-2.43	-1.77
1100	1.27	2.12	-19.54	-17.50	-5.43	-6.95	-7.03	-4.91	-3.44	-2.71	-2.19	-1.61
1200	0.55	1.80	-16.04	-18.26	-5.33	-6.14	-6.54	-5.21	-4.34	-3.16	-1.93	-1.45
1300	0.74	1.67	-12.05	-18.19	-4.79	-5.55	-6.72	-5.47	-3.67	-2.79	-2.56	-1.28

Table 5.8: Difference in percent between RAOs from RIFLEX and MATLAB for 1m wave amplitude.

As table 5.8 clearly shows, there are significant differences between results from the two models for certain combinations wave amplitudes and periods.

## 5.8 Effect of changing damping

As mentioned in section 3.4.1, I have investigated the effect of varying damping force. That is, I wanted to see if a precise projected area had to be found for the manifold. This is difficult, at least with few technical drawings and lack of experience on the subject. Therefore I chose to run analyses with half the projected area originally used. Reducing damping for the lower part by reducing the area by 50% gave changes in axial force responses. How they change is shown in figure 5.18, where several combinations of periods and depths are checked. The figure shows if the response is reduced or increased, and the color codes show where the differences are greatest. Red means an increase in response, green a reduction. While yellow is close to 1, i.e. practically no change. The greatest increase is 8.8% and the greatest reduction is 1%. The average change is 0.5% with a standard deviation of 1.7%.

This check is performed in MATLAB using my model. Similar tests have been performed in RIFLEX showing the same trend. The reason for using MATLAB is that it is more efficient and easier to run such a large number of simulations. With the differences being so small as they

are, I continue using the original assumption where the damping force is calculated based on a full area equal to that of the bottom part of the manifold.

Depth [m] T [s]	100	200	300	400	500	600	700	800	900	1000	1100	1200	1300
4	0,999	1,010	1,009	1,086	1,053	1,011	1,009	1,003	0,998	1,003	1,004	0,990	1,007
4,5	1,009	1,000	0,998	1,016	1,072	1,088	1,040	1,015	1,010	1,002	1,006	0,998	1,003
5	1,003	0,993	0,997	1,002	1,015	1,053	1,082	1,070	1,036	1,017	1,012	1,005	1,004
5,5	0,998	0,998	0,998	1,001	1,008	1,029	1,060	1,085	1,087	1,080	1,060	1,041	1,030
6	0,998	1,003	1,000	0,999	1,001	1,003	1,012	1,030	1,057	1,074	1,074	1,065	1,045
6,5	0,997	0,996	0,995	0,995	0,996	1,001	1,011	1,027	1,047	1,064	1,076	1,080	1,080
6,75	0,996	0,996	0,995	0,995	0,995	0,998	1,005	1,017	1,032	1,050	1,064	1,074	1,078
7	0,998	0,997	0,998	0,997	0,997	0,998	1,001	1,006	1,016	1,030	1,046	1,061	1,069
7,25	1,000	0,998	1,001	1,001	0,999	0,999	1,000	1,001	1,003	1,009	1,018	1,031	1,045
7,5	1,000	0,999	1,003	1,003	0,996	1,002	0,998	1,002	1,001	0,998	0,999	1,004	1,004
8	0,999	1,001	1,001	0,998	1,001	1,000	0,999	0,999	0,999	1,000	1,002	1,005	1,009
8,5	0,999	1,001	0,999	0,998	0,998	0,998	0,998	0,998	0,998	0,999	1,001	1,003	1,007
9	0,998	0,998	0,998	0,998	0,998	0,997	0,997	0,997	0,997	0,997	0,997	1,000	1,003
9,5	0,998	0,998	0,998	0,998	0,998	0,997	0,997	0,997	0,997	0,997	0,997	0,998	0,999
10	0,999	0,998	0,998	0,998	0,998	0,998	0,998	0,997	0,997	0,997	0,997	0,997	0,998
10,5	0,999	0,999	0,999	0,999	0,999	0,998	0,998	0,998	0,998	0,998	0,998	0,998	0,998
11	0,999	0,999	0,999	0,999	0,999	0,999	0,999	0,999	0,998	0,998	0,998	0,998	0,998
11,5	0,999	0,999	0,999	0,999	0,999	0,999	0,999	0,999	0,999	0,999	0,999	0,999	0,999
12	0,999	0,999	1,000	1,000	0,999	0,999	0,999	0,993	0,999	0,999	0,999	0,999	0,999
12,5	1,000	1,000	1,000	1,000	1,000	1,000	1,000	1,000	1,000	0,999	0,999	0,999	0,997
13	1,000	1,000	1,000	0,999	0,999	0,999	1,000	1,000	0,999	1,000	0,999	0,999	0,999
13,5	1,000	1,000	1,000	1,000	1,000	1,000	0,999	1,000	0,999	1,000	1,000	0,999	0,999
14	1,000	1,000	1,000	1,000	1,000	0,999	1,000	0,999	1,000	1,000	1,000	0,999	0,999
14,25	1,000	1,000	1,000	1,000	0,999	1,000	0,999	1,000	1,000	1,000	1,000	1,000	1,000
14,5	1,000	1,000	1,000	1,000	1,000	1,000	1,000	1,000	1,000	1,000	1,000	1,000	0,999
14,75	1,000	1,000	1,000	1,000	1,000	1,000	0,999	0,999	1,000	0,999	1,000	1,000	1,000
15	1,000	1,000	1,000	1,000	1,000	1,000	0,999	1,000	1,000	0,999	1,000	1,000	0,999
15,25	1,000	1,000	1,000	1,000	1,000	1,000	1,000	1,000	1,000	1,000	0,999	1,000	1,000
15,5	1,000	1,000	1,000	1,000	1,000	1,000	1,000	1,000	1,000	1,000	1,000	1,000	0,999
15,75	1,000	1,000	1,000	1,000	1,000	1,000	0,999	1,000	1,000	1,000	1,000	1,000	1,000
16	1,000	1,000	1,000	1,000	1,000	1,000	1,000	1,000	1,000	1,000	1,000	1,000	0,999
17	1,000	1,000	1,000	1,000	1,000	1,000	1,000	1,000	1,000	1,000	1,000	1,000	1,000
18	1,000	1,000	1,000	1,000	1,000	1,000	1,000	1,000	1,000	1,000	1,000	1,000	1,000
19	1,000	1,000	1,000	1,000	1,000	1,000	1,000	1,000	1,000	1,000	1,000	1,000	1,000
20	1,000	1,000	1,000	1,000	1,000	1,000	1,000	1,000	1,000	1,000	1,000	1,000	1,000
22	1,000	1,000	1,000	1,000	1,000	1,000	1,000	1,000	1,000	1,000	1,000	1,000	1,000
24	1,000	1,000	1,000	1,000	1,000	1,000	1,000	1,000	1,000	1,000	1,000	1,000	1,000
26	1,000	1,000	1,000	1,000	1,000	1,000	1,000	1,000	1,000	1,000	1,000	1,000	1,000
30	1,000	1,000	1,000	1,000	1,000	1,000	1,000	1,000	1,000	1,000	1,000	1,000	1,000

Figure 5.18: Ratio between maximum responses for reduced and full damping. Period to the left, depth at the top.

# Chapter 6

## Discussion and Recommendations for Further Work

### 6.1 Discussion

#### 6.1.1 Identification of eigenperiods

The results from my RIFLEX simulations regarding eigenperiods are very close to the results I achieved from calculating the periods by use of DNV's formula (equation 2.10). The results from my MATLAB model is however not suited for finding eigenperiods. The same trend as RIFLEX and the DNV formula shows is seen, but the resolution in periods is not good enough to separate the eigenperiods. Where the response is largest, for wave periods from 4 to 7s, I calculate response for each 0.5s. As table 6.1 shows, all eigenperiods are within this range or below.

	<b>RIFLEX</b>	<b>Calculated</b>
<b>Depth [m]</b>	$T_0$ [s]	$T_0$ [s]
100	2.27	2.30
200	2.89	2.85
300	3.37	3.32
400	3.89	3.73
500	4.33	4.10
600	4.63	4.44
700	4.88	4.76
800	5.41	5.06
900	5.53	5.34
1000	5.66	5.61
1100	5.88	5.87
1200	-	6.11
1300	-	6.35

Table 6.1: Comparison of eigenperiod results from RIFLEX and DNV's formula.

## 6.2 Calculation of damping

When calculating the damping force for the manifold I have chosen to use projected area equal to that of the bottom part of the module. This is an overestimate of the damping force. But, as my results when reducing the projected area by 50% show, this does not affect the results significantly. It is however difficult to predict how the water flow around the module will behave when oscillating in the water. The module consists of a truss work with a flat plate on top. The flat plate will stop water from flowing straight through the structure. The model used in the model tests performed by Øritsland (1989) does not have such a flat plate on top, and results are hence not directly comparable with the manifold in this thesis. Superimposing drag forces for a flat plate and the structure used by Øritsland (1989) is therefore questionable. A better alternative would have been using computational fluid dynamics (CFD) to obtain a drag coefficient for the entire structure. Even better would have been a model test, but this is much more costly.

### 6.3 Force responses

Studying the RAOs for axial forces in the lifting wire shows that results from RIFLEX and MATLAB are roughly the same. But when responses increase, so do the non-linearities. My MATLAB model does not take into account non-linear effects, a part from non-linear damping. When the manifold oscillates, it does not necessarily oscillate in phase with the crane tip motion. In-phase-oscillation is most likely to happen for very high periods and low dynamic effects. When the motions are out of phase, the wire will stretch and give rise to axial forces. The change in vertical distance between crane tip and manifold will cause the angles between slings and the horizontal plane to change. This gives change in vertical stiffness of the system, and hence change in both forces and response. This I have not taken into consideration in my MATLAB model.

The RAO values for axial force in the lifting wire are found by use of a regular wave with height of 1m. The RAOs are presented as a fraction of static load when submerged. In other words it represents the dynamic amplification for a given wave period per meter wave height. The results show dynamic amplifications of approximately 1.5 and above for periods below 10s. With my values being relative to submerged weight, they will automatically be larger than one with reference to dry weight. The manifold has a displacement of  $55m^3$ , equivalent to approximately 55.6 tonnes buoyancy. This is 30% of the mass, meaning that a DAF with reference to dry weight equals 70% of a DAF with reference to submerged weight. A DAF of 1.5 then becomes 1.05.

Jacobsen and Næss (2014) present findings from 9 template installations. They present DAFs for each operation as well as the environmental conditions on site. DAFs are related to weight in air. During the lowering phase where the templates installed were submerged, six DAFs are recorded. Values range from 0.9 to 1.32. Such operations are, as one would expect, dependent on weather conditions. As stated by the authors: "overboarding operations are done in significant seastates ( $H_s$ ) lower than 2m". This is also seen from the recorded data. One of the installations mentioned is the installation of a manifold on Skuld, near Norne outside the coast of Northern Norway. Although the water depth there is "only" 340m, the manifold is similar to the one to



be installed on Aasta Hansteen both in shape and weight (Jacobsen, 2015). During installation a sea state with  $H_s=1.7\text{m}$  and  $T_p=13\text{s}$  a maximum DAF of 0.9 relative to dry weight was registered. I have run simulations with 3 hour sea states using a JONSWAP spectrum with the same significant wave height and peak period. Maximum registered DAF in my simulations are 1.45, 1.39 and 1.28 for depths of 1300m, 600m and 200m respectively. All DAFs are relative to dry weight. Clearly the manifold will not be situated at a single depth for 3 hours, but it seems that my RIFLEX model gives somewhat large force responses compared to what is experienced in real life operations.

It is worth mentioning that my analysis does not include heave compensation, which is common when installing objects at the sea bed nowadays. This may be why larger dynamic amplifications are registered in the analyses performed in this thesis, since heave compensating systems reduce load responses.

## **6.4 Recommendations for Further Work**

In stead of using a combination of experimental data and DNV formulae, use of CFD analysis could have given an estimate of drag coefficients to be used in this analysis. In addition an evaluation of the weather aspect of the operation. Determination of the likelihood for a successful operation through statistical analysis and defining limiting parameters through e.g. module velocities when approaching the seabed. This is possible to do with an already finished hydrodynamic and structural model of the system, and thereafter run multiple irregular sea-states. This proved to laborious for me to complete during this work.

In addition implementation of a heave compensating system would have given a more realistic picture of the operation. In addition the real limitations of the operation could have been found if such a system was implemented in the model. PS: On the day of delivery, June 10 2015, I received an e-mail from Tore Jacobsen with a picture of the ongoing installation. The manifold is installed, and as far as I know everything has gone as planned.

# Bibliography

DNV (2014a). *DNV-RP-C205 - Environmental Conditions and Environmental Loads*. Det Norske Veritas.

DNV (2014b). *DNV-RP-H103 - Modelling and Analysis of Marine Operations*. Det Norske Veritas.

Faltinsen, O. M. (1990). *Sea Loads on Ships and Offshore Structures*. Cambridge Ocean Technology Series. Cambridge University Press.

Gaches, R. and Bruserud, K. (2012). Aasta hansteen field metocean design basis. Technical Report C134-AHA-V-FD-00001, Statoil.

Hasselmann, K., Barnett, T. P., and Bouws, E. (1973). Measurement of wind-wave growth and swell decay during the joint north sea wave project (jonswap). *Ergänzungsheft zur Deutschen Hydrographischen Zeitschrift*, (12).

Jacobsen, T. (2014-2015). Mail correspondence, subsea 7.

Jacobsen, T. and Næss, T.-B. (2014). Installation of subsea structures using mid-size construction vessels in harsh environments.

Langen, I. and Sigbjørnsen, R. (1979). *Dynamisk analyse av konstruksjoner: Dynamic Analysis of Structures*. Tapir.

Larsen, C. M. (2012). *Kompendium, Marin Dynamikk*. Institutt for marin teknikk.

Larsen, C. M. (2014). Handbook on design and operation of flexible pipes. Joint Industry Project, "Safe and Cost Effective Operation of Flexible Pipes" Vol. 1, MARINTEK, NTNU, 4subsea.

Larsen, C. M. (2015). Personal communication.

MARINTEK (2011). *RIFLEX Theory manual*, 3.6v2 edition.

Newland, D. (1993). *An introduction to random vibrations, spectral and wavelet analysis*. Longman, 3rd edition edition.

Newmark, N. M. (1959). A method of computation for structural dynamics. *Journal of the Engineering Mechanics Divisions*, 85(3):67–94.

Nielsen, F. G. (2007). *Lecture Notes in Marine Operations*. Department of Marine Hydrodynamics, Trondheim.

Øritsland, O. (1989). A summary of subsea module hydrodynamic data. Technical Report 511110.05, MARINTEK, Trondheim.

Pettersen, B. (2007). *Marin Teknikk 3, Hydrodynamikk*. Institutt for marin teknikk.

Pierson, W. J. and Moskowitz, L. (1964). A proposed spectral form for fully developed wind seas based on the similarity theory of s.a. kitaigorodskii. *Journal of Geophysical Research*, 69(24):5181–5190.

Statoil (2015). Statoil news and media. [http://www.statoil.com/en/NewsAndMedia/News/2013/Pages/05Mar\\_AastaHansteen.aspx](http://www.statoil.com/en/NewsAndMedia/News/2013/Pages/05Mar_AastaHansteen.aspx).

Technip (2015). Technip media center. <http://www.technip.com/en/press/technip-received-letter-intent-world>



# Appendices

## A Sling configuration

Rev	Date	Level	Annotations	Cr.By	Ap.By
		As Built			
		Issued for Approval			
		Issued for Approval			

Design Factors		
W (Weight of lifted objekt)	(Ton)	250
RW (Weight of rigging)	(Ton)	3
		253
DAF (Onshore)		1,7
Screw Load		1,1
CoG Shift		1,05
Weight consequence faktor		1,1
Sum		2,16
Safety factor	Sling	1,3
Load factor		1,3
Consequence factor		1,3
Material factor		2
Sum		3,4
		2,20
Total Safety factors		7,3
		4,75

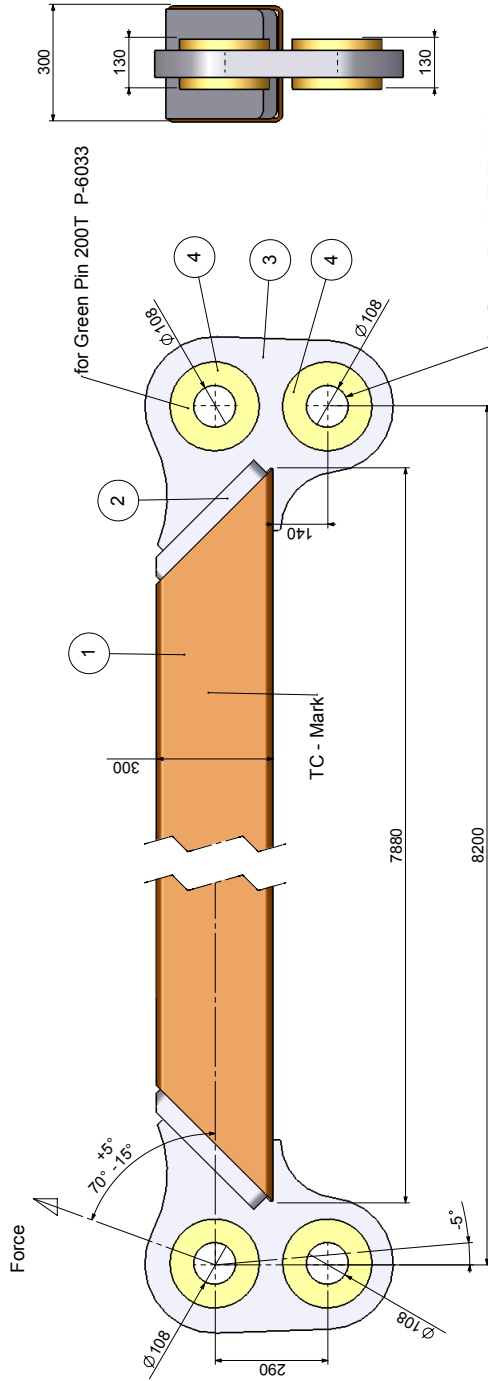
Notes:	
1	Standard Designed acc. to EN10004 for planning and execution of Marine Operation Pt 2 Cr. Lifting capacity 2500 and DNV 2.22 LIFTING OF PLATFORMS
2	Certificate Lifting Gear / Desl. Of conformity (F&E)
3	NET Material inspection certificate acc. to NS 10204.3.1 Magnetic particle inspection on all welds (MPT) acc. to NS-EN 1200 and NS-EN 5817 VT acc. to NS-EN 670 and NS-EN 6917
4	Welding Welding procedures: NS-EN 15614-1
5	Coating Painted with Color RAL 1004 (V-ellor)
6	Paint Eye Norwalk standard M-501 acc. 5. Coating System No.7
7	Marking on Product Contact area / Shackle bolts to be without paint and protected with grease
8	Proof Force Designed to R 2007to Green Pin P-6033
9	Weight FRAM CE = Proof Year Item No. 0000X TC Code SWL: 250 Ton 2097,7 kg

ITEM NO.	POS.	QTY.	PART NO.	DESCRIPTION	MATERIAL	NOTE
T6333007	1	1	633-3007	250 T Spreader bar		Sep.Drw
	2	4	111-1226	200 Te WB Shackle		P-6033
	3	2	633-3012	SD 957	HIMTEPE	L=15000
	4	4	633-3013	SD 553	HIMTEPE	L=14600

Date	Design	Drawing	Issue	Scale
15-05-2012	Gunbre			
Revision:	Approved:	N/A		
Lifting Arrangement SWL 250 Ton Item No: T6333005				
Reference:	Calculations:	File name:	Size:	Page
		V:\Drawings\633-3005	A3	1 of 1

# B Spreader bar

Rev	Date	Level	Annotations	Cr.By	Ap.By



**NOTES:**

- Standard: Designed acc. to DIN 220 LIFTING APPLIANCES
- Material: Steel, C45 according to EN 10025 (Material inspection certificate to 3.1 according to EN 10204)
- NDT: Magnetic particle inspection according to EN 15817 (VT acc. to NB EN 979 and NB EN 9817)
- Welding: Welding procedure: NB-EN 15614-1
- Coating: Powdered epoxy paint, RAL 19005 (1 black) (Norex standard A10521 and 5' Coating System No. 7 Contact area: (Shackle bolt) to be without paint and protected with grease)
- Part Eye: Designed to fit: 200 Tls Green Pin P-6033
- Marking on Product: FRAM OE - Prod Year: T6333007 SWL 250 Ton
- Proof Force: 2597,7 kN
- Weight: 1050 kg

ITEM NO.	POS.	QTY.	PART NO.	DESCRIPTION	MATERIAL	CNC FILE	NOTE
1	1	1	633-3008	HUP 300x300x10	S355NH		L=
R2009	2	2	633-3009	PL50	S690DL/Weldox 700E	6333009	
R2011	3	2	633-3010	PL70	S690DL/Weldox 700E	6333010	
R2007	4	8	633-3011	PL30	S690DL/Weldox 700E	6333011	

15-05-2012  
 Drawn by: Gunhild  
 Approved: [Signature]  
 Scale: 1:10  
**FRAM**  
 KJÆTTINGFABRIKEN AS

Replaced by:  
 Drawing nr.: 633-3007  
 Reference: V:\Drawings\633-3007  
 Size: A3  
 Page 1 of 3

# C Excel spreadsheet from Tore Jacobsen

## Mass, volume and hydrodynamic properties

Project: SKULD R&P manifold  
 Structure: MANIFOLD  
 Client: Statoil  
 Date initiated: 28.10.11  
 Date for last change:  
 Date concluded:  
 Originator: TJA50

- References**
- [1] DNV-RP-H103, April 2010
  - [2] DNV-RP-C205, April 2007
  - [3] O. Ørnsland "A summary of Subsea Module hydrodynamic data" MARINTEK Report No. 5.11110.05
  - [4] Email from AkerSolutions

### Typical flow parameters

Wave height: 5,000 m  
 Wave period: 10,000 s  
 Wave length: 156,000 m  
 Max velocity: 1,571 m/s

Ref. [2]  
 Ref. [2]

**General input**

Material density (steel)	ρ <sub>steel</sub>	7,85
Water density	ρ <sub>sw</sub>	1,025
GRP density	ρ <sub>REG</sub>	2,124
Kinematic viscosity of water	ν	0,00001188
Acceleration of gravity	g	9,81

**General**  
 In this sheet the basic SIMO model is modelled. The object is modelled by using the "slender" elements and fixed body elements in SIMO. The model and the co-ordinate system used in the SIMO model is illustrated in the figures below.

### Main dimensions

Length: 18,9 m  
 Breadth: 6,3 m  
 Height: 5,5 m

### The mass and volume properties of the ITS:

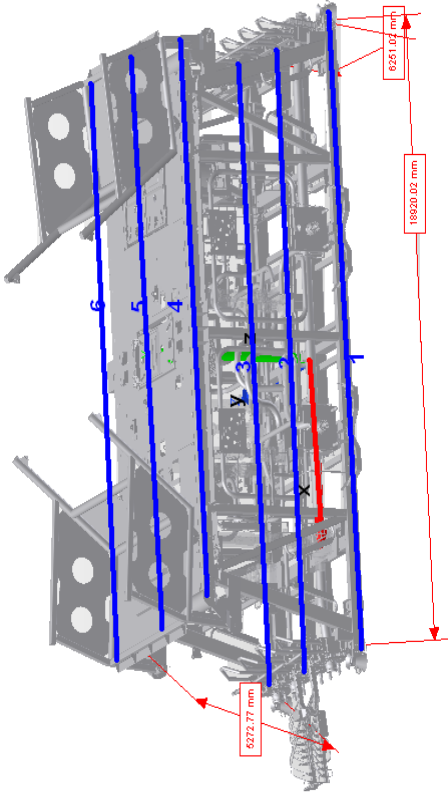
Mass of steel:	191 Te	Ref [4]
Mass of misc:	Te	rigger
<b>Total mass:</b>	<b>191 Te</b>	

ref Aker weight rapport

Displaced volume of steel:	23,00 m <sup>3</sup>
Displaced volume of misc:	32,00 m <sup>3</sup>
<b>Total displaced volume:</b>	<b>55,00 m<sup>3</sup></b>
Buoyancy force from steel:	23,58 Te
Buoyancy force from misc:	32,80 Te
<b>Total buoyancy force:</b>	<b>56,38 Te</b>
Submerged weight of structure:	167,4 Te
Submerged weight of misc:	-32,8 Te
<b>Total submerged weight:</b>	<b>134,63 Te</b>

### Position of CoG:

Source	X	Y	Z
SIMO			



**Mass Matrix Te\*m2 (about origin shown in figure above) provided by Petter Stabel @ Aker Ref [4]**

Mass	Ixx	Iyy	Izz	Ixy	Ixz	Iyz
------	-----	-----	-----	-----	-----	-----

## Distributed element forces

Reference is made to the figure above.

### Bottom assembly

#### Slender elements 1 2 3

Length of manifold	L	m	18,9		
Steel cross-sectional area	Asteel	m <sup>2</sup>	0		
Total cross-section area	A	m <sup>2</sup>	0		
Displaced volume of beams	V	m <sup>3</sup>	10,00		
Mass of beams	M	ton	0,00		
Additional volume	Vadd	m <sup>3</sup>	0		
Additional mass	Madd	ton	0		
Number of elements	n	m	3		
Length of elements	L	m	18,9		
Volume per element per meter	Vol	m <sup>2</sup>	0,340	45 % of volume	
Mass per element per meter	Mas	ton/m	1,28		0 Mass will be given as separate mass matrix

#### Hydrodynamic properties

			x	y	z
KC-number	KC	-	0,8	0,8	0,8
2D Added mass coeff	Ca	-	0,50	0,62	0,620 ref øristland page 5.9
Added mass	AdMass	ton	11,79	14,62	14,62
Additional added mass	AdMasadd	ton	5,00	6,20	6,20 assumed entrapped water from trusswork
2D Linear damping coeff	b1	-			
Linear damping	LinDamp	kN/(m/s)			
Additional Linear damping	LinDampadd	kN/(m/s)			
2D Quadratic damping coeff	b2 (Cdd)	-	1,00	1,20	1,20 ref øristland page 5.9
Quadratic damping	QuadDamp	kN/(m/s) <sup>2</sup>	17,76	73,23	73,23
Additional Quadratic damping	QDampadd	kN/(m/s) <sup>2</sup>	0,00	0,00	0,00
Cross sectional added mass coeff.	Am	ton/m	0,30	1,10	1,10
Cross sectional linear damping	C1	(kN/(m/s))/m	0,00	0,00	0,00
Cross sectional quadratic damping	C2	(kN/(m/s) <sup>2</sup> )/m	0,31	1,29	1,29

### Top assembly (flat plate)

#### Slender elements 4 5 6

Length of beams	L	m	16,3		
width of plate	B	m	6,3		
Steel cross-sectional area	Asteel	m <sup>2</sup>	2		
Total cross-section area	A	m <sup>2</sup>	0		
Displaced volume of beams	V	m <sup>3</sup>	0		
Additional volume	Vadd	m <sup>3</sup>	0		
Additional mass	Madd	ton	0		
Number of elements	n	m	3		
Length of elements	L	m	16,3		
Volume per element per meter	Vol	m <sup>2</sup>	0,731083845	55 % of volume	
Mass per element per meter	Mas	ton/m	2,421676892		0 Mass will be given as separate mass matrix

#### Hydrodynamic properties

			x	y	z
KC-number	KC	-	2,5	1,0	1,0
2D Added mass coeff	Ca	-	0,00	0,00	0,80 Appendix A in Ref. [1]
Added mass	AdMass	ton	0,00	0,00	417,17
Additional added mass	AdMasadd	ton	0,00	0,00	0,00
2D Linear damping coeff	b1	-	0,00	0,00	0,00
Linear damping	LinDamp	kN/(m/s)	0,00	0,00	0,00
Additional Linear damping	LinDampadd	kN/(m/s)	0,00	0,00	0,00
2D Quadratic damping coeff	b2 (Cdd)	-	0,00	0,00	1,20 Appendix B in Ref. [1]
Quadratic damping	QuadDamp	kN/(m/s) <sup>2</sup>	0,00	0,00	63,15
Additional Quadratic damping	QDampadd	kN/(m/s) <sup>2</sup>	0,00	0,00	0,00
Cross sectional added mass coeff.	Am	ton/m	0,00	0,00	8,53
Cross sectional linear damping	C1	(kN/(m/s))/m	0,00	0,00	0,00
Cross sectional quadratic damping	C2	(kN/(m/s) <sup>2</sup> )/m	0,00	0,00	1,29



## D Matlab script for RAO conversion

```
1 %RAO READ
2 clear,clc
3 fid = fopen('Subsea7_Orcaflex.txt','r');
4 %Skip 12 lines
5 linesToSkip = 12;
6 for i = 1:linesToSkip-1
7     fgetl(fid);
8 end
9 %Process all remaining lines
10 tline = fgetl(fid);
11 raw_data = [];
12 while (~isempty(tline) )
13     tline = fgetl(fid);
14     %Getting rid of non-numbers
15     tline = regexp(tline, '[^0-9\s+-.eE]', '');
16     raw_data = [raw_data; str2num(tline)];
17 end
18 fclose(fid);
19
20 dir=0:15:180;
21
22 for j=1:39
23     freq(j)=1/raw_data(j,1)*2*pi;
24 end
25 freq=freq';
26 %Separating response amplitudes and phases
27     XA=raw_data(:,2);
28     XP=raw_data(:,3);
29     YA=raw_data(:,4);
30     YP=raw_data(:,5);
31     ZA=raw_data(:,6);
32     ZP=raw_data(:,7);
33     RXA=raw_data(:,8);
```

```

34   RXP=raw_data(:,9);
35   RYA=raw_data(:,10);
36   RYP=raw_data(:,11);
37   RZA=raw_data(:,12);
38   RZP=raw_data(:,13);
39
40   for n=0:12
41       for i=1:39
42
43           %Surge
44           su(i+39*n,:)= [1+n i XA(i+39*n) XP(i+39*n)];
45
46           %Sway
47           sw(i+39*n,:)= [1+n i YA(i+39*n) YP(i+39*n)];
48
49           %Heave
50           h(i+39*n,:)= [1+n i ZA(i+39*n) ZP(i+39*n)];
51
52           %Roll
53           r(i+39*n,:)= [1+n i RXA(i+39*n) RXP(i+39*n)];
54
55           %Pitch
56           p(i+39*n,:)= [1+n i RYA(i+39*n) RYP(i+39*n)];
57
58           %Yaw
59           y(i+39*n,:)= [1+n i RZA(i+39*n) RZP(i+39*n)];
60
61       end
62   end
63
64   %Transposing matrices
65   su=su';
66   sw=sw';
67   h=h';
68   r=r';
69   p=p';
70   y=y';

```

```

70
71 %Opening file
72 RAO = fopen('RAO_CONV.txt','w');
73
74 fprintf(RAO,'%7s\r\n','idhftr');
75 fprintf(RAO,'%6s\r\n','VESSEL');
76
77 fprintf(RAO,'%25s\r\n','-----',...
78 '-----');
79 fprintf(RAO,'%30s\r\n','HFTRANSFER REFERENCE POSITION');
80 fprintf(RAO,'%25s\r\n','-----',...
81 '-----');
82
83 fprintf(RAO,'%2s\r\n','zg');
84 fprintf(RAO,'%10s\r\n','0.000000');
85
86 fprintf(RAO,'%25s\r\n','-----',...
87 '-----');
88 fprintf(RAO,'%24s\r\n','HFTRANSFER CONTROL DATA');
89 fprintf(RAO,'%25s\r\n','-----',...
90 '-----');
91
92 fprintf(RAO,'%25s\r\n','ndhftr nwhftr isymhf itypin');
93 fprintf(RAO,'%23s\r\n','13      39      2      2');
94
95 fprintf(RAO,'%25s\r\n','-----',...
96 '-----');
97 fprintf(RAO,'%16s\r\n','WAVE DIRECTIONS');
98 fprintf(RAO,'%25s\r\n','-----',...
99 '-----');
100 fprintf(RAO,'%11s\r\n','ihead head');
101 for i=1:9
102 fprintf(RAO,'%s %1g %3s %1f\r\n',i,dir(i));
103 end
104 for i=10:13
105 fprintf(RAO,'%s %1g %2s %1f\r\n',i,dir(i));

```

```

106     end
107
108
109
110     fprintf(RAO, '%25s\r\n', ''-----', ...
111             '-----');
112     fprintf(RAO, '%17s\r\n', ' WAVE FREQUENCIES');
113     fprintf(RAO, '%25s\r\n', ''-----', ...
114             '-----');
115     fprintf(RAO, '%12s\r\n', ''ifreq whftr');
116     for i=1:9
117         fprintf(RAO, '%s %1g %3s %1f\r\n', '', i, '', freq(i));
118     end
119     for i=10:39
120         fprintf(RAO, '%s %1g %2s %1f\r\n', '', i, '', freq(i));
121     end
122
123
124     fprintf(RAO, '%25s\r\n', ''-----', ...
125             '-----');
126     fprintf(RAO, '%25s\r\n', ' HFTRANSFER FUNCTION SURGE');
127     fprintf(RAO, '%25s\r\n', ''-----', ...
128             '-----');
129     fprintf(RAO, '%25s\r\n', ''idir ifreq amplitude phase[deg]');
130
131     for i=0:8
132         for j=1:9
133             fprintf(RAO, '%2g %1s %2g %3s %5.7f %5f\r\n', su(1, j+i*39), '', ...
134                     su(2, j+i*39), '', su(3, j+i*39), su(4, j+i*39));
135         end
136         for k=10:39
137             fprintf(RAO, '%2g %2s %2g %2s %5.7f %5f\r\n', su(1, k+i*39), '', ...
138                     su(2, k+i*39), '', su(3, k+i*39), su(4, k+i*39));
139         end
140     end
141     for i=9:12

```

```

142     for j=1:9
143 fprintf(RAO, '%s %2g %s %2g %3s %5f %s %5f\r\n', '', su(1, j+i*39), ...
144     '', su(2, j+i*39), '', su(3, j+i*39), '', su(4, j+i*39));
145     end
146     for k=10:39
147 fprintf(RAO, '%s %2g %1s %2g %2s %5f %s %5f\r\n', '', su(1, k+i*39), ...
148     '', su(2, k+i*39), '', su(3, k+i*39), '', su(4, k+i*39));
149     end
150 end
151
152 fprintf(RAO, '%25s\r\n', '-----', ...
153     '-----');
154 fprintf(RAO, '%25s\r\n', ' HFTRANSFER FUNCTION SWAY');
155 fprintf(RAO, '%25s\r\n', '-----', ...
156     '-----');
157 fprintf(RAO, '%25s\r\n', 'idir ifreq amplitude phase[deg]');
158     for i=0:8
159     for j=1:9
160 fprintf(RAO, '%2g %1s %2g %3s %5.7f %5f\r\n', sw(1, j+i*39), '', ...
161     sw(2, j+i*39), '', sw(3, j+i*39), sw(4, j+i*39));
162     end
163     for k=10:39
164 fprintf(RAO, '%2g %2s %2g %2s %5.7f %5f\r\n', sw(1, k+i*39), '', ...
165     sw(2, k+i*39), '', sw(3, k+i*39), sw(4, k+i*39));
166     end
167 end
168 for i=9:12
169     for j=1:9
170 fprintf(RAO, '%s %2g %s %2g %3s %5f %s %5f\r\n', '', sw(1, j+i*39), ...
171     '', sw(2, j+i*39), '', sw(3, j+i*39), '', sw(4, j+i*39));
172     end
173     for k=10:39
174 fprintf(RAO, '%s %2g %1s %2g %2s %5f %s %5f\r\n', '', sw(1, k+i*39), '', ...
175     sw(2, k+i*39), '', sw(3, k+i*39), '', sw(4, k+i*39));
176     end
177 end

```

```

178
179 fprintf(RAO, '%25s\r\n', ' '-----', ...
180     '-----');
181 fprintf(RAO, '%25s\r\n', ' HFTRANSFER FUNCTION HEAVE');
182 fprintf(RAO, '%25s\r\n', ' '-----', ...
183     '-----');
184 fprintf(RAO, '%25s\r\n', ' 'idir ifreq amplitude phase[deg]');
185     for i=0:8
186     for j=1:9
187 fprintf(RAO, '%2g %1s %2g %3s %5.7f %5f\r\n', h(1, j+i*39), ' ', ...
188     h(2, j+i*39), ' ', h(3, j+i*39), h(4, j+i*39));
189     end
190     for k=10:39
191 fprintf(RAO, '%2g %2s %2g %2s %5.7f %5f\r\n', h(1, k+i*39), ' ', ...
192     h(2, k+i*39), ' ', h(3, k+i*39), h(4, k+i*39));
193     end
194 end
195 for i=9:12
196     for j=1:9
197 fprintf(RAO, '%s %2g %s %2g %3s %5.7f %5f\r\n', ' ', h(1, j+i*39), ...
198     ' ', h(2, j+i*39), ' ', h(3, j+i*39), h(4, j+i*39));
199     end
200     for k=10:39
201 fprintf(RAO, '%s %2g %1s %2g %2s %5.7f %5f\r\n', ' ', h(1, k+i*39), ...
202     ' ', h(2, k+i*39), ' ', h(3, k+i*39), h(4, k+i*39));
203     end
204 end
205
206 fprintf(RAO, '%25s\r\n', ' '-----', ...
207     '-----');
208 fprintf(RAO, '%25s\r\n', ' HFTRANSFER FUNCTION ROLL');
209 fprintf(RAO, '%25s\r\n', ' '-----', ...
210     '-----');
211 fprintf(RAO, '%25s\r\n', ' 'idir ifreq amplitude phase[deg]');
212     for i=0:8
213     for j=1:9

```

```

214 fprintf(RAO, '%2g %1s %2g %3s %5.7f %5f\r\n', r(1, j+i*39), '', ...
215         r(2, j+i*39), '', r(3, j+i*39), r(4, j+i*39));
216     end
217     for k=10:39
218 fprintf(RAO, '%2g %2s %2g %2s %5.7f %5f\r\n', r(1, k+i*39), '', ...
219         r(2, k+i*39), '', r(3, k+i*39), r(4, k+i*39));
220     end
221 end
222 for i=9:12
223     for j=1:9
224 fprintf(RAO, '%s %2g %s %2g %3s %5.7f %5f\r\n', '', r(1, j+i*39), ...
225         '', r(2, j+i*39), '', r(3, j+i*39), r(4, j+i*39));
226     end
227     for k=10:39
228 fprintf(RAO, '%s %2g %1s %2g %2s %5.7f %5f\r\n', '', r(1, k+i*39), ...
229         '', r(2, k+i*39), '', r(3, k+i*39), r(4, k+i*39));
230     end
231 end
232
233 fprintf(RAO, '%25s\r\n', '-----', ...
234         '-----');
235 fprintf(RAO, '%25s\r\n', ' HFTRANSFER FUNCTION PITCH');
236 fprintf(RAO, '%25s\r\n', '-----', ...
237         '-----');
238 fprintf(RAO, '%25s\r\n', ''idir ifreq amplitude phase[deg]');
239     for i=0:8
240     for j=1:9
241 fprintf(RAO, '%2g %1s %2g %3s %5.7f %5f\r\n', p(1, j+i*39), '', ...
242         p(2, j+i*39), '', p(3, j+i*39), p(4, j+i*39));
243     end
244     for k=10:39
245 fprintf(RAO, '%2g %2s %2g %2s %5.7f %5f\r\n', p(1, k+i*39), '', ...
246         p(2, k+i*39), '', p(3, k+i*39), p(4, k+i*39));
247     end
248 end
249 for i=9:12

```

```

250     for j=1:9
251 fprintf(RAO, '%s %2g %s %2g %3s %5.7f %5f\r\n', '', p(1, j+i*39), ...
252     '', p(2, j+i*39), '', p(3, j+i*39), p(4, j+i*39));
253     end
254     for k=10:39
255 fprintf(RAO, '%s %2g %1s %2g %2s %5.7f %5f\r\n', '', p(1, k+i*39), ...
256     '', p(2, k+i*39), '', p(3, k+i*39), p(4, k+i*39));
257     end
258 end
259
260 fprintf(RAO, '%25s\r\n', ''-----'); ...
261     '-----');
262 fprintf(RAO, '%25s\r\n', ' HFTRANSFER FUNCTION YAW');
263 fprintf(RAO, '%25s\r\n', ''-----'); ...
264     '-----');
265 fprintf(RAO, '%25s\r\n', ''idir ifreq amplitude phase[deg]');
266 for i=0:8
267     for j=1:9
268 fprintf(RAO, '%2g %1s %2g %3s %5.7f %5f\r\n', y(1, j+i*39), '', ...
269     y(2, j+i*39), '', y(3, j+i*39), y(4, j+i*39));
270     end
271     for k=10:39
272 fprintf(RAO, '%2g %2s %2g %2s %5.7f %5f\r\n', y(1, k+i*39), '', ...
273     y(2, k+i*39), '', y(3, k+i*39), y(4, k+i*39));
274     end
275 end
276 for i=9:12
277     for j=1:9
278 fprintf(RAO, '%s %2g %s %2g %3s %5.7f %5f\r\n', '', y(1, j+i*39), '', ...
279     y(2, j+i*39), '', y(3, j+i*39), y(4, j+i*39));
280     end
281     for k=10:39
282 fprintf(RAO, '%s %2g %1s %2g %2s %5.7f %5f\r\n', '', y(1, k+i*39), '', ...
283     y(2, k+i*39), '', y(3, k+i*39), y(4, k+i*39));
284     end
285 end

```



286

287     fclose(RAO)

## E Matlab script for calculation of dynamic response

```
1 %Calculation of dynamic response in 1D
2 %Pure heave motion induced by crane tip motion
3 %Linear analysis
4 %
5 %   Joar Pedersen, NTNU, 2015
6
7 clear, clc, close all
8 %%
9 %Defining parameters
10
11 %Enviromental parameters
12 %Hmin, Hmax, wave height (double amplitude)
13 Hmin=0.5;
14 Hmax=1;
15 Hstep=.5;
16
17 %Physical constants
18 g=9.81;      %acc. of gravity
19 rho=1030;    %sea water density
20
21 %Module parameters
22 module_mass=191017;      %module mass in kg
23 added_mass=433949;      %added mass in kg
24 M=module_mass+added_mass; %combined structural and added mass
25 V=55.133;                %submerged volume [m^3]
26 Cd_top=1.2;              %Drag coefficient [-], area dependent
27 Cd_bottom=1.2;
28 Cd_mid=1.2;
29
30 L_top=16.3;              %length of top part
```

```

31 L_bottom=18.9;           %length of bottom part
32 B=6.3;                  %width of module
33 A_top=B*L_top;         %top area
34 A_bottom=B*L_bottom;   %bottom area
35 A_mid=B*0.5*(L_top+L_bottom)*0;
36 c=0.5*rho*(Cd_top*A_top+Cd_bottom*A_bottom+Cd_mid*A_mid); %Damping coeff. N/(m/s)^2
37
38 %Wire data
39 minlength=100;         %minimum wire length
40 maxlength=1300;       %maximum wire length
41 length_step=100;      %difference in wire length for each run
42 EA_liftwire=8.52e+08; %EA [N]
43 static_load=(module_mass-rho*V)*g; %static force acting on wire [N]
44
45 %RAO for crane tip motion. From RIFLEX simulations. For [-15, 0, 15]
46 %degrees wave heading.
47 T=[4 4.5 5 5.5 6 6.5 6.75 7 7.25 7.5 8 8.5 9.0...
48     9.5 10 10.5 11 11.5 12 12.5 13 13.5 14 14.25 ...
49     14.5 14.75 15 15.25 15.5 15.75 16 17 18 19 20 22 24 26 30];
50
51 %RAOs from RIFLEX. 0, 15 and 15 (345) degrees vessel heading.
52 RAO_0=[T;...
53     0.37 0.52 0.59 1.26 0.88 2.15 2.27 1.86 1.12 0.34 0.95 1.69 2.04...
54     2.12 2.09 1.97 1.84 1.70 1.58 1.46 1.36 1.27 1.21 1.19 1.16 1.13...
55     1.11 1.09 1.08 1.07 1.05 1.02 1.01 0.99 0.99 0.99 0.99 0.99 0.99];
56
57 RAO_15=[T;...
58     0.21 0.36 0.77 0.93 0.94 2.25 2.34 2.00 1.40 0.72 0.61 1.30 1.69...
59     1.86 1.91 1.90 1.86 1.81 1.76 1.72 1.74 1.81 1.82 1.70 1.53 1.30...
60     1.06 0.85 0.73 0.65 0.69 0.83 0.89 0.93 0.95 0.96 0.98 0.98 0.99];
61
62 RAO_345=[T;...
63     .53 0.84 0.69 1.48 1.34 2.35 2.11 1.39 0.51 0.65 1.87 2.48 2.65...
64     2.59 2.40 2.17 1.92 1.68 1.46 1.26 1.07 0.96 1.09 1.28 1.47 1.62...
65     1.67 1.67 1.61 1.55 1.46 1.23 1.12 1.06 1.04 1.01 1.00 1.00 0.99];
66

```

```

67 %Newmark beta parameters for solution of eq. of motion
68 gamma=0.5;
69 beta=0.25*(gamma+0.5)^2;
70
71 nP=15; %number of periods to run simulation
72
73 %%
74
75 figcount1=1; %Dummy counter variable
76 figcount2=2; %Dummy counter variable
77
78 pcount=0;
79 ptot=length(T)*2*13;
80 progress=waitbar(0,'Please wait...');
81
82 for H=Hmin:Hstep:Hmax
83     count1=1; %Dummy counter variable, period
84     for T=T
85         count2=1; %Dummy counter variable, depth
86         for length_liftwire=minlength:length_step:maxlength
87             %% Calculations
88             k_tot=...
89             1/(1/(EA_liftwire/(length_liftwire+16))+1/(4.97E+07)+1/(1.63E+07)); %Total vertical stif
90
91 %Steplength and duration
92 simulation_length=nP*T;
93 h=0.05; %Step size, time
94
95 %Calculating wave elevation
96 wave_elevation=...
97     0.5*H*sin(2*pi/T*linspace(0,simulation_length,1/h*simulation_length+1));
98
99 t=0:h:nP*T-2*h;
100
101 I=find(RAO_0(1,:)==T); %Finding the correct value of RAO to match T
102 crane_disp=RAO_0(2,I)*wave_elevation; %Crane displacement

```

```

103 crane_vel=diff(crane_disp)/h;           %Crane velocity
104 crane_acc=diff(crane_vel)/h;           %Crane acceleration
105 %Crop vectors to same length due to loss of 1 step per differentiation
106 crane_vel(end)=[];
107 crane_disp(end-1:end)=[];
108
109 %%
110 %Solving differential equation by use of explicit Newmark-beta
111 rel_disp=[];
112 rel_vel=[];
113 rel_acc=[];
114 %Initial conditions
115 %System at rest at t=0, define zero at initial position, i.e.:
116 rel_disp(1)=0;
117 rel_vel(1)=0;
118 rel_acc(1)=...
119     1/M*(-M*crane_acc(1)-c*crane_vel(1)-c*rel_vel(1)-k_tot*rel_disp(1));
120
121 maxiterations=10^3; %If convergence is slow, a limit is set to avoid
122     %too long runs.
123 itercount=2;
124 disp_amp(1)=0;
125 disp_amp(2)=1;
126 c_eq=c;
127 limit=0.005; %Iteration limit, accepted difference in amplitudes before
128     %iteration stops. [m]
129 %Solving the equation of motion, with iteration on the damping.
130 while abs(disp_amp(itercount) - disp_amp(itercount-1))>limit && ...
131     itercount <= maxiterations
132     for n = 2:length(t)
133         load(n)=-M*crane_acc(n)-c_eq*crane_vel(n); %Load
134         a=1/beta/h^2*rel_disp(n-1)+1/beta/h*rel_vel(n-1)+...
135             (1/2/beta-1)*rel_acc(n-1);
136
137         b=gamma/beta/h*rel_disp(n-1)+(gamma/beta-1)*rel_vel(n-1)+...
138             (gamma/2/beta-1)*h*rel_acc(n-1);

```

```

139
140     rel_disp(n)=(load(n)+c_eq*b+M*a)/(k_tot+c_eq*gamma/beta/h+M/beta/h^2);
141     rel_vel(n)=gamma/beta/h*rel_disp(n)-b;
142     rel_acc(n)=1/beta/h^2*rel_disp(n)-a;
143
144     end
145     itercount=itercount+1;
146
147     module_disp=rel_disp+crane_disp;
148     [dispmax]=findpeaks(module_disp);
149     u0=max(dispmax); %only using positive maxima, i.e.
150     disp_amp(itercount)=u0;
151
152     c_eq=8/3/pi*c*2*pi/T*u0;
153
154     end
155
156     AxialForce=k_tot*rel_disp+static_load;
157     AxialForce=AxialForce/static_load;
158     %Locating maxima and minima
159     [pks,locs]=findpeaks(AxialForce);
160     minDummy=1.001*max(AxialForce)-AxialForce;
161     [min,minlocs]=findpeaks(minDummy);
162     minima=AxialForce(minlocs);
163     ForceMax(count1,count2)=pks(end-1);
164     ForceMin(count1,count2)=minima(end-1);
165
166     count2=count2+1;
167     pcount=pcount+1;
168     progress=waitbar(pcount/ptot);
169     end
170
171     count1=count1+1;
172     end
173     %%
174     %%PLOTS%%

```

```

175 c_col=jet(15); %create color array for plotting
176 T=[4 4.5 5 5.5 6 6.5 6.75 7 7.25 7.5 8 8.5 9.0...
177     9.5 10 10.5 11 11.5 12 12.5 13 13.5 14 14.25 ...
178     14.5 14.75 15 15.25 15.5 15.75 16 17 18 19 20 22 24 26 30];
179
180 figure(1)
181 L=minlength:length_step:maxlength;
182 for i=1:length(L)
183     figure(figcount1)
184     hold all
185     plot(T,ForceMax(:,i), 'color', c_col(i,:))
186     figure(figcount2)
187     hold all
188     plot(T,ForceMin(:,i), 'color', c_col(i,:))
189 end
190 figure(figcount1)
191 title(['Max response for different periods at various depths, H= '...
192     num2str(H) 'm'])
193 xlabel('Period [s]')
194 ylabel('Dyn/Stat Axial Force [-]')
195 legend('d=100','d=200','d=300','d=400','d=500','d=600','d=700','d=800' ...
196     , 'd=900','d=1000','d=1100','d=1200', 'd=1300','Location','northeast')
197
198 figure(figcount2)
199 title(['Min response for different periods at various depths, H= '...
200     num2str(H) 'm'])
201 xlabel('Period [s]')
202 ylabel('Dyn/Stat Axial Force [-]')
203 legend('d=100','d=200','d=300','d=400','d=500','d=600','d=700','d=800' ...
204     , 'd=900','d=1000','d=1100','d=1200','d=1300','Location','northeast')
205 figcount1=figcount1+2;
206 figcount2=figcount2+2;
207
208 end
209 close(progress)

```

## F Matlab script for computing RAO

```

1 %Read data from condition set, and compare data
2 close all
3 clear all
4 clc
5
6 T=[4 4.5 5 5.5 6 6.5 6.75 7 7.25 7.5 8 8.5 9 9.5 10 10.5 11 11.5 12 12.5...
7 13 13.5 14 14.25 14.5 14.75 15 15.25 15.5 15.75 16 17 18 19 20 22 24 26 30];
8
9 %d=input('What is the depth? (Absolute value) ');
10 d=500;
11 w_amp=input('What is the wave amplitude? ');
12
13 %Opening and reading values from RIFLEX results
14 fid = fopen('ConditionSpaceRIFLEX.txt','r');
15 C = textscan(fid, '%f', 'Delimiter', '\n', 'CommentStyle', '#');
16 C = C{:};
17 fclose(fid);
18
19 %Difference between time and displacement value causing program to
20 %swap between collecting time and space values
21 limit=10;
22
23 j=1;
24 k=1;
25
26 for i=1:length(C)-1
27     %Creating a variable for each line of values in text file
28     eval(['dummy' num2str(j) '(k) =' num2str(C(i)) ';' ])
29     k=k+1;
30     if abs(C(i+1)-C(i)) > limit
31         j=j+1;
32         k=1;
33     end

```

```

34 end
35 %Adding the last value
36 eval(['dummy' num2str(j) '(k) =' num2str(C(i+1)) ';' ])
37
38 %Gathering time and displacement values in matrices
39 %One for each condition set (cs)
40 m=1;
41 c=jet(round(j/2)); %create color array for plotting
42 for n=1:j/2
43     eval(['cs' num2str(n) '(:,1)=' ' transpose(dummy' num2str(m) ');' ])
44     eval(['cs' num2str(n) '(:,2)=' ' transpose(dummy' num2str(m+1) ');' ])
45     m=m+2;
46     %Subtracting first value from displacement to ensure all plots start
47     %at zero.
48     eval(['cs' num2str(n) '(:,2)=cs' num2str(n) '(:,2)-cs' num2str(n) '(1,2);'])
49
50     %Finding peaks, amplitudes and period of oscillation
51     [pks,locs] = findpeaks(eval(['cs' num2str(n) '(:,2)']));
52
53     %Max response amplitude
54     amp_max(n)=max(pks);
55     %Average response amplitude
56     amp_ave(n)=mean(pks);
57     %Second to last peak (stabilized amplitude)
58     amp_stab(n)=pks(length(pks)-1);
59     %Average response period
60     T_ave(n)=mean(diff(eval(['cs' num2str(n) '(locs,1)'))));
61
62     hold all
63
64     leg{n} = ['T= ' num2str(T_ave(n)) 's, A= ' num2str(amp_ave(n)) 'm'];
65 end
66
67 figure(2)
68 plot(T,amp_stab/w_amp)
69 title(['RAO for crane tip motion, head sea.' ])

```



```

70 xlabel('Period [s]')
71 ylabel('m/m [-]')
72 set(gca,'xtick',4:2:30);

```

## G Matlab script for plot of RAOs.

```

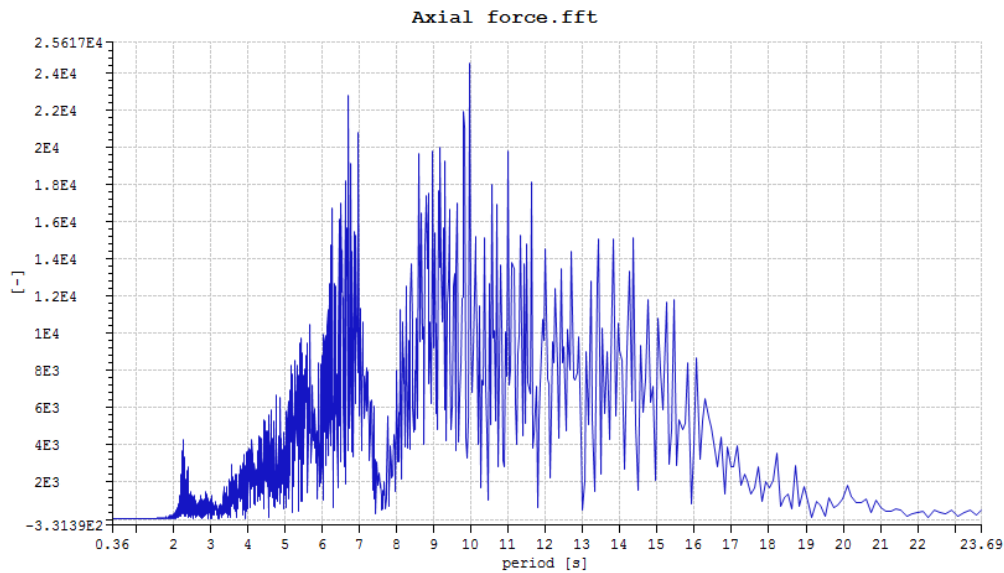
1 %RAO for crane tip motion. From RIFLEX simulations.
2 T=[4 4.5 5 5.5 6 6.5 6.75 7 7.25 7.5 8 8.5 9.0...
3     9.5 10 10.5 11 11.5 12 12.5 13 13.5 14 14.25 ...
4     14.5 14.75 15 15.25 15.5 15.75 16 17 18 19 20 22 24 26 30];
5
6 RAO_0=[0.37 0.52 0.59 1.26 0.88 2.15 2.27 1.86 1.12 0.34 0.95 1.69 2.04...
7         2.12 2.09 1.97 1.84 1.70 1.58 1.46 1.36 1.27 1.21 1.19 1.16 1.13...
8         1.11 1.09 1.08 1.07 1.05 1.02 1.01 0.99 0.99 0.99 0.99 0.99 0.99];
9
10 RAO_15=[0.21 0.36 0.77 0.93 0.94 2.25 2.34 2.00 1.40 0.72 0.61 1.30 1.69...
11          1.86 1.91 1.90 1.86 1.81 1.76 1.72 1.74 1.81 1.82 1.70 1.53 1.30...
12          1.06 0.85 0.73 0.65 0.69 0.83 0.89 0.93 0.95 0.96 0.98 0.98 0.99];
13
14 RAO_345=[.53 0.84 0.69 1.48 1.34 2.35 2.11 1.39 0.51 0.65 1.87 2.48 2.65...
15           2.59 2.40 2.17 1.92 1.68 1.46 1.26 1.07 0.96 1.09 1.28 1.47 1.62...
16           1.67 1.67 1.61 1.55 1.46 1.23 1.12 1.06 1.04 1.01 1.00 1.00 0.99];
17
18 figure(101)
19 plot(T,RAO_0)
20 title(['RAO for crane tip motion. 0degrees wave direction.' ])
21 xlabel('Period [s]')
22 ylabel('m/m [-]')
23 set(gca,'xtick',4:2:30);
24
25 figure(102)
26 plot(T,RAO_15)
27 title(['RAO for crane tip motion. 15 degrees wave direction.' ])
28 xlabel('Period [s]')
29 ylabel('m/m [-]')

```

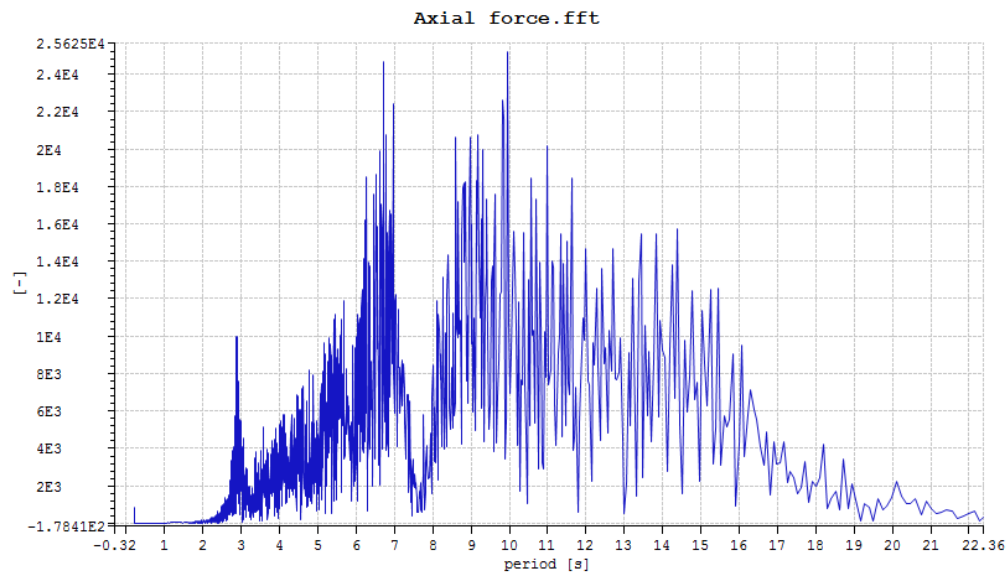
```
30 set(gca,'xtick',4:2:30);
31
32 figure(103)
33 plot(T,RAO_345)
34 title(['RAO for crane tip motion. -15 degrees wave direction.' ])
35 xlabel('Period [s]')
36 ylabel('m/m [-]')
37 set(gca,'xtick',4:2:30);
```

## H Response spectra for lifting wire tension from RIFLEX.

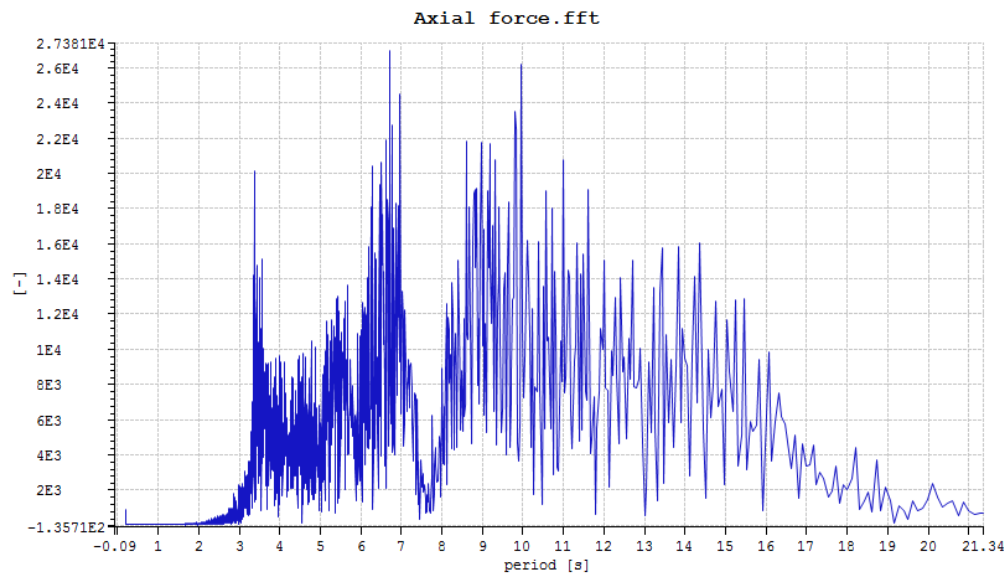
### 100m depth



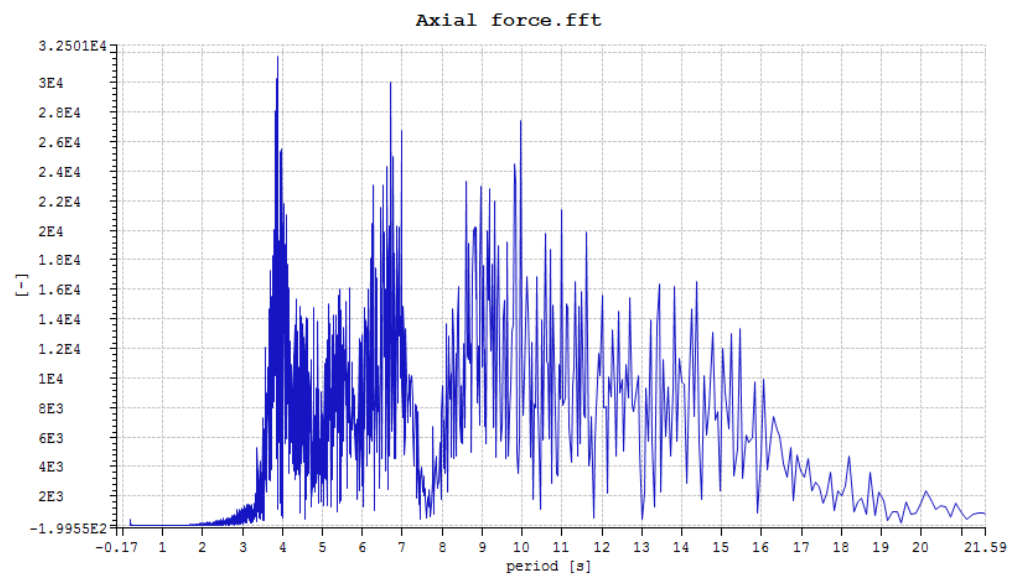
## 200m depth



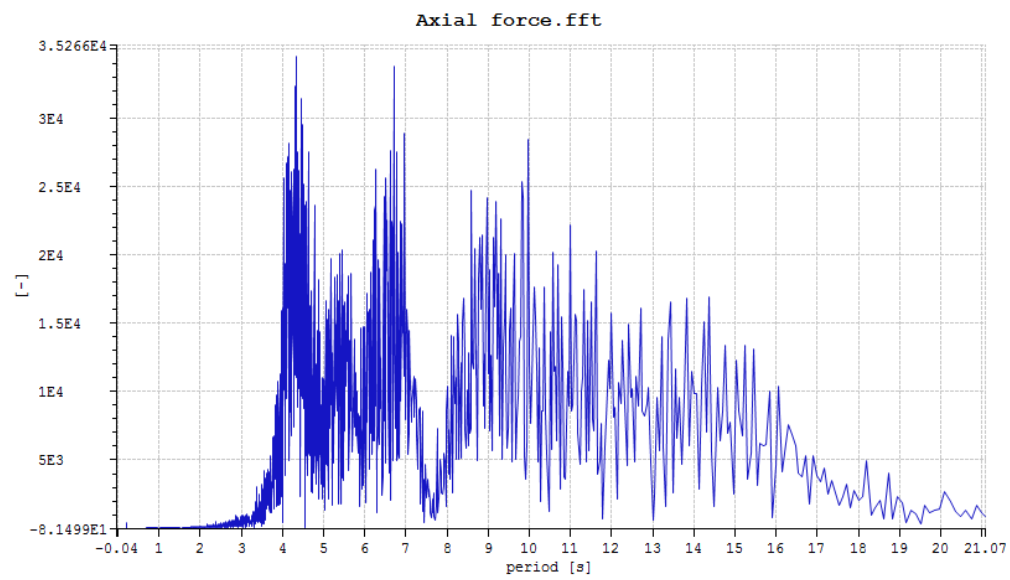
## 300m depth



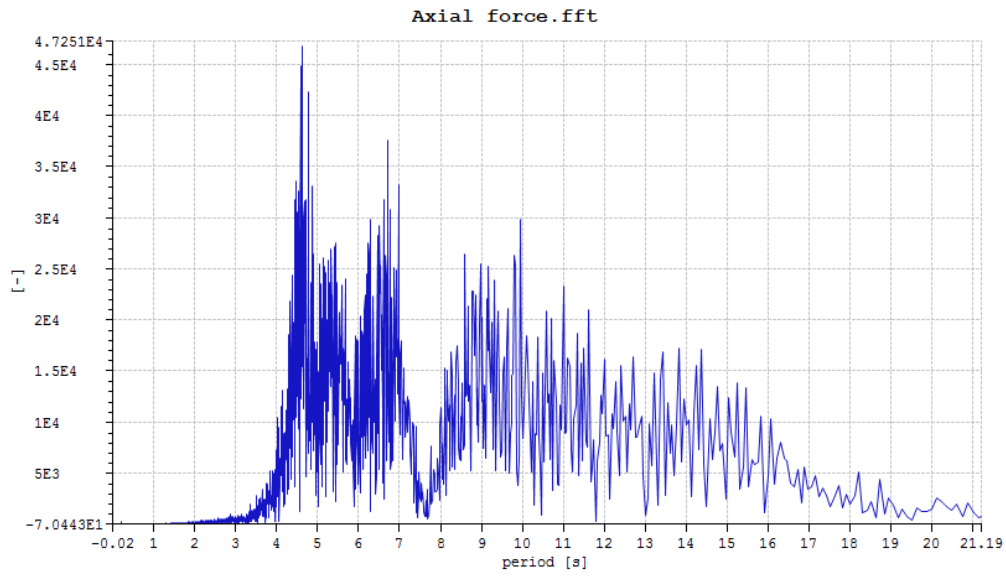
## 400m depth



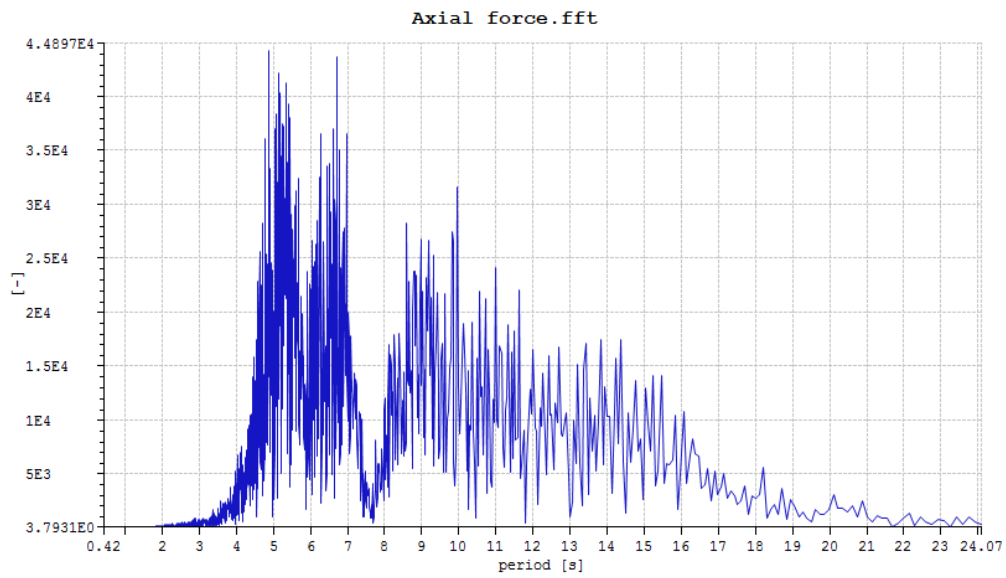
## 500m depth



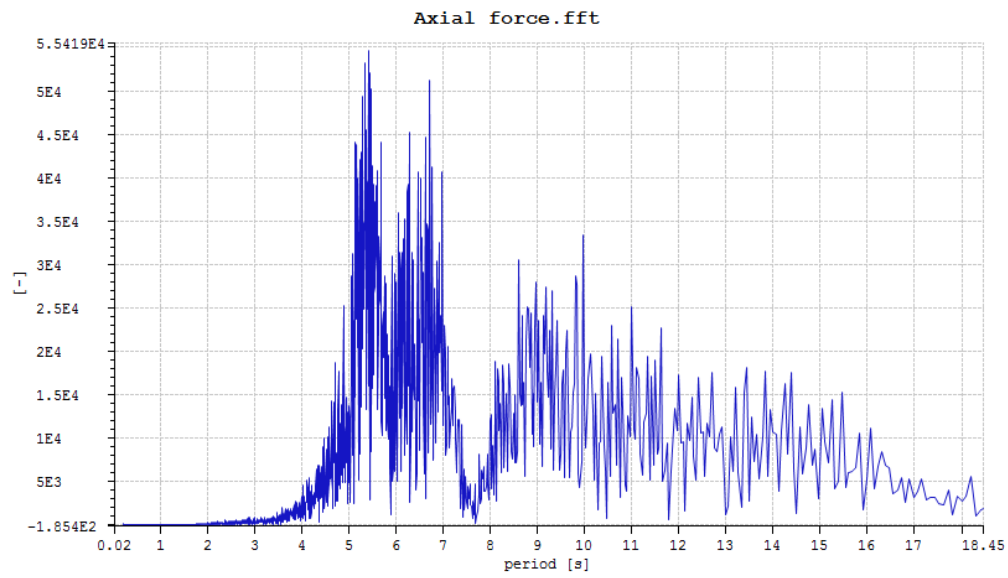
## 600m depth



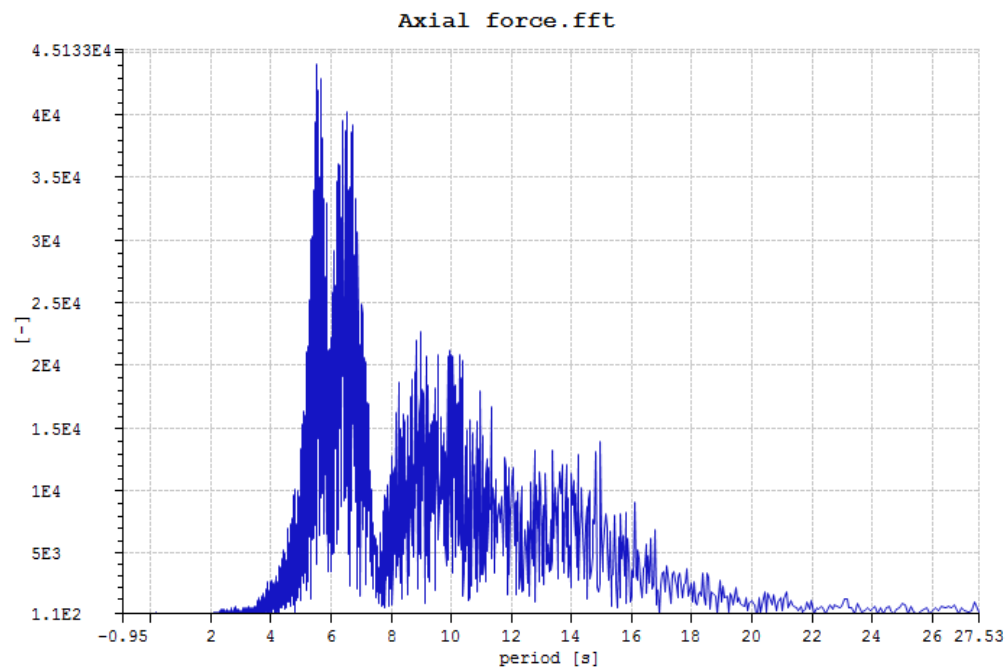
## 700m depth



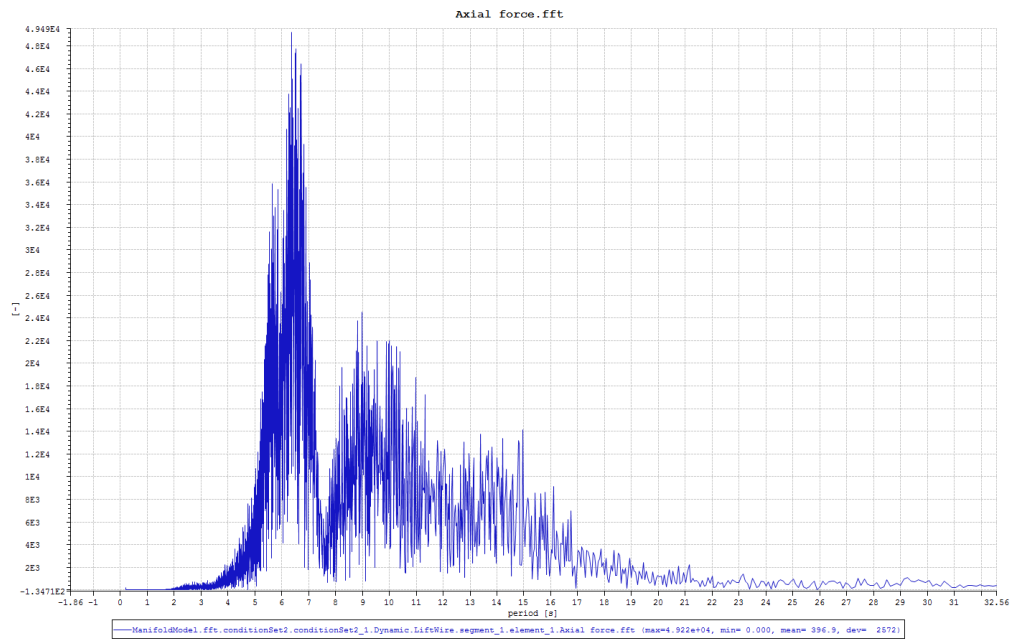
## 800m depth



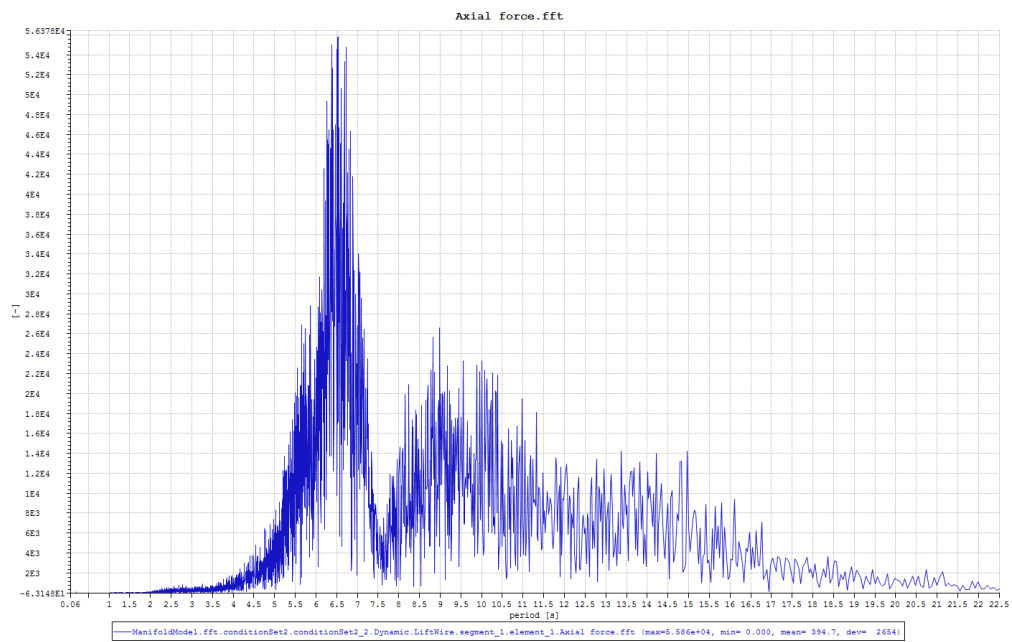
## 900m depth



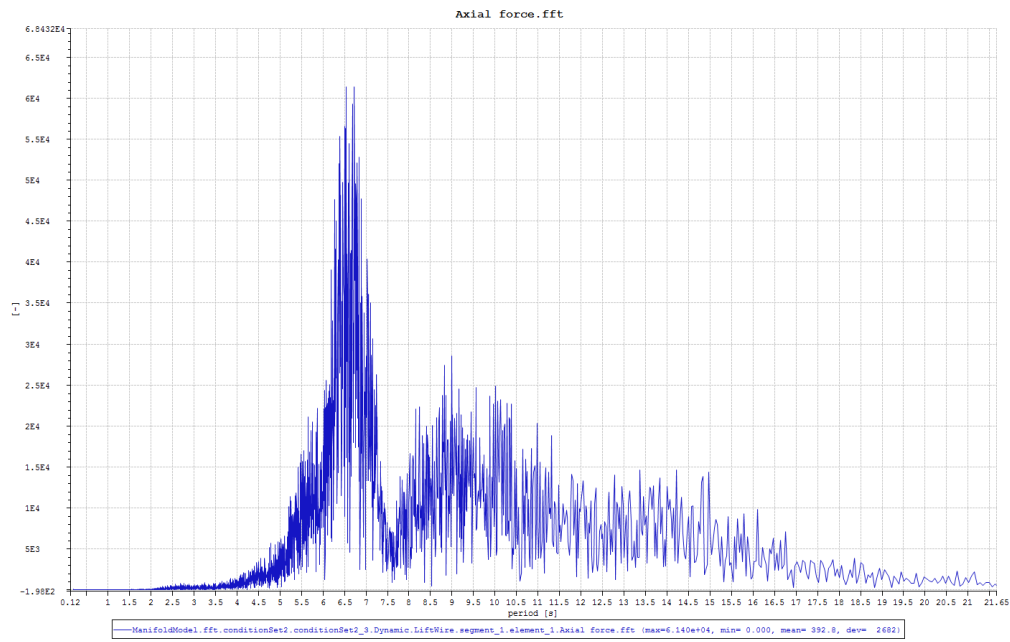
## 1000m depth



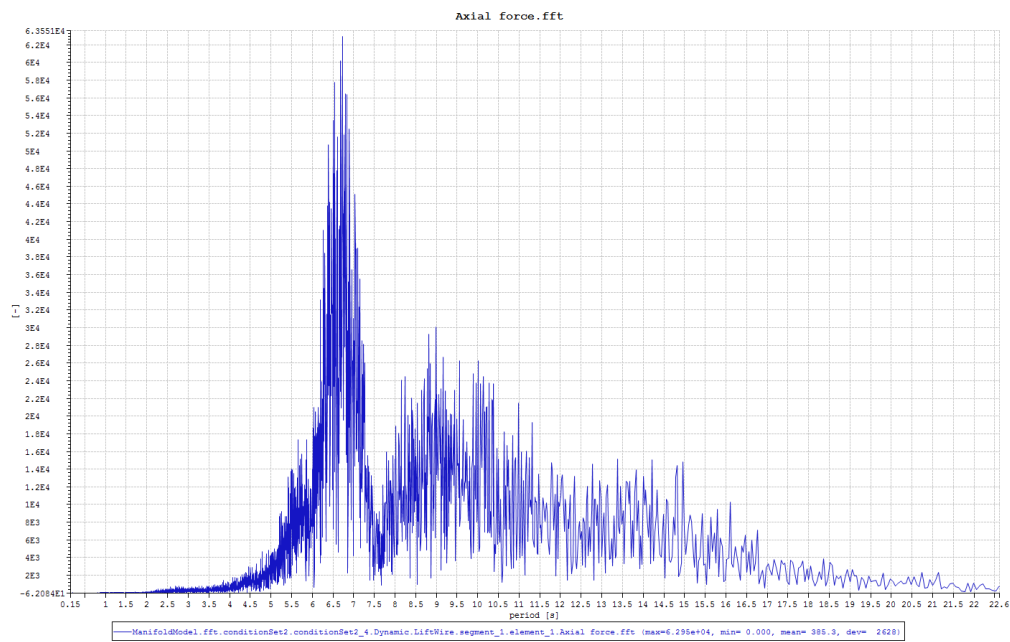
## 1100m depth



## 1200m depth

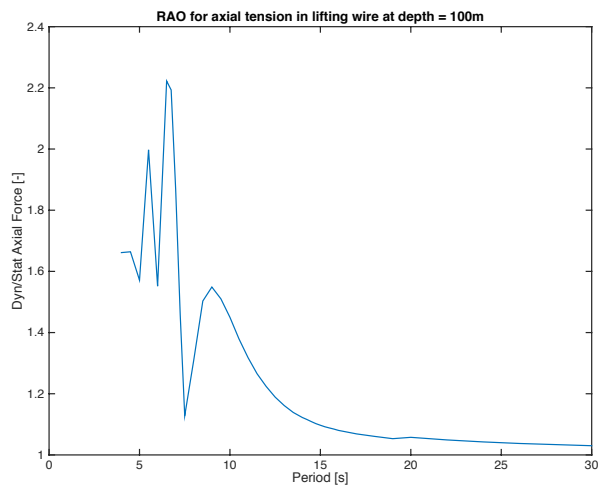
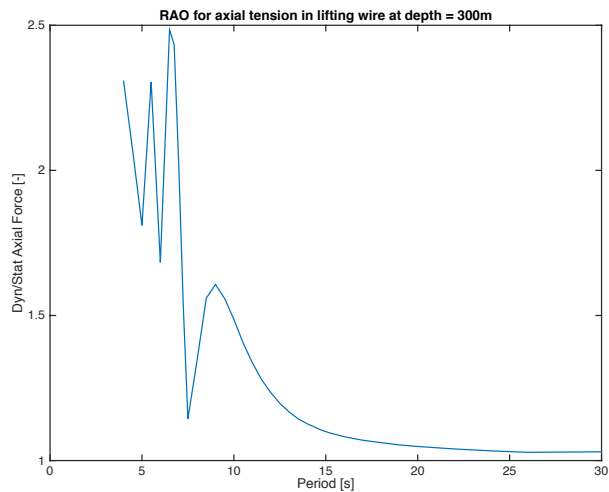
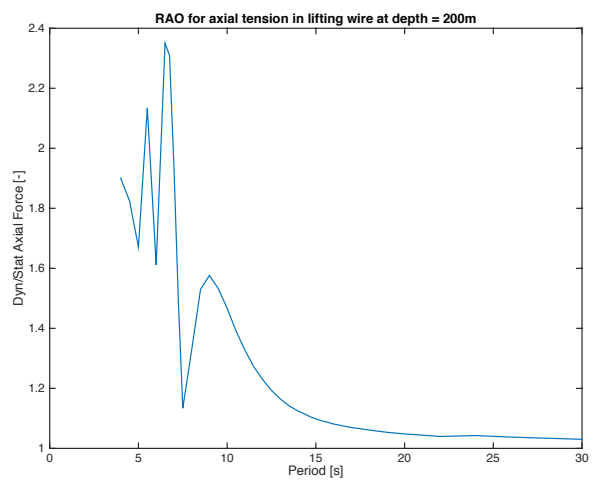
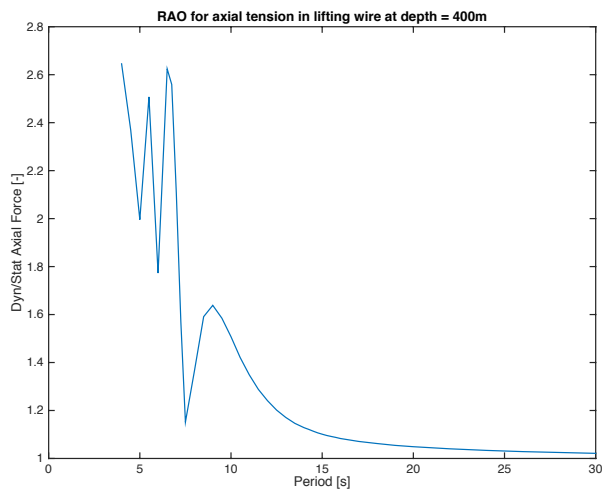


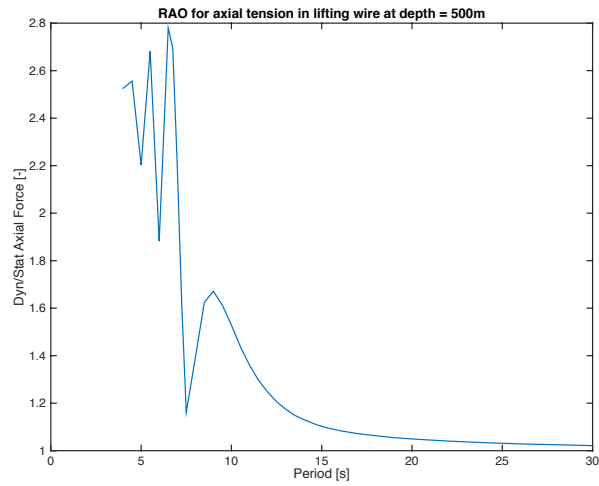
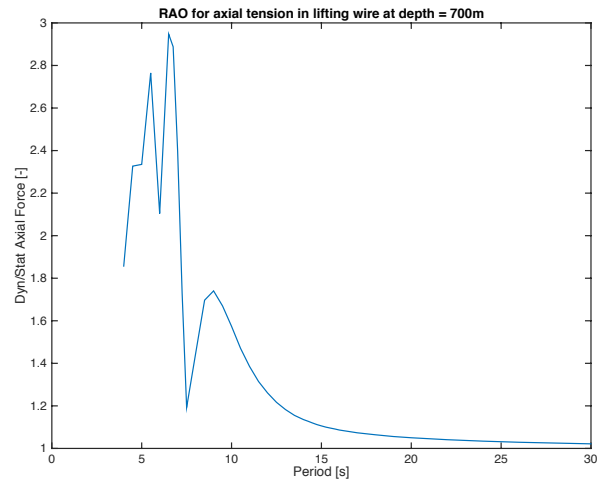
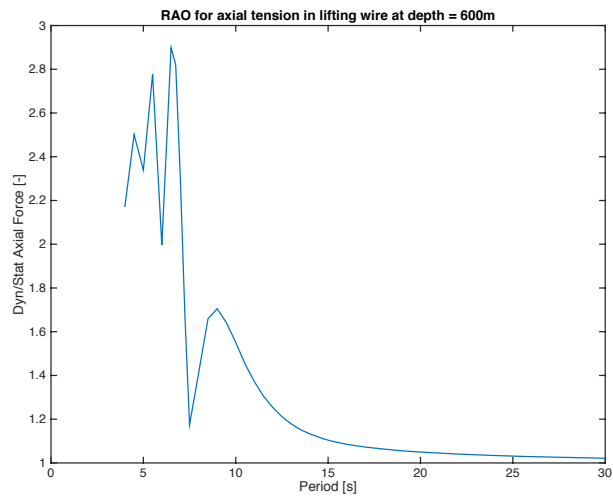
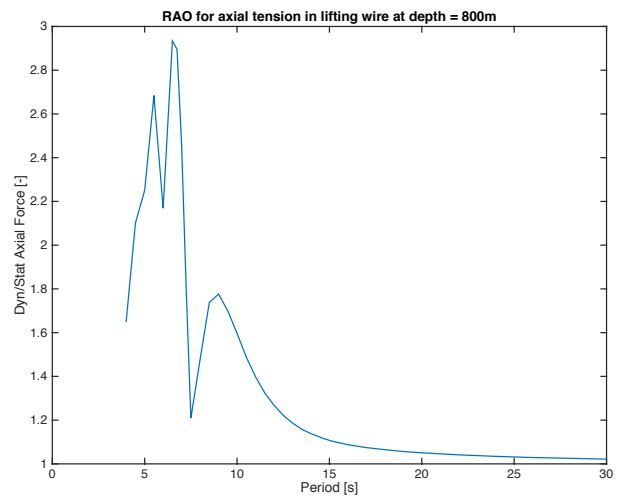
## 1300m depth

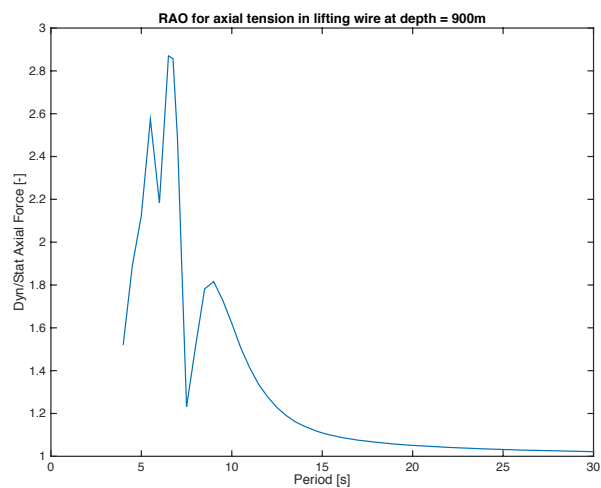
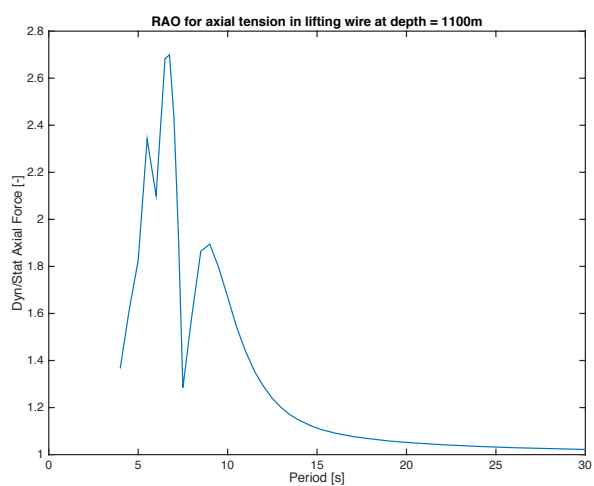
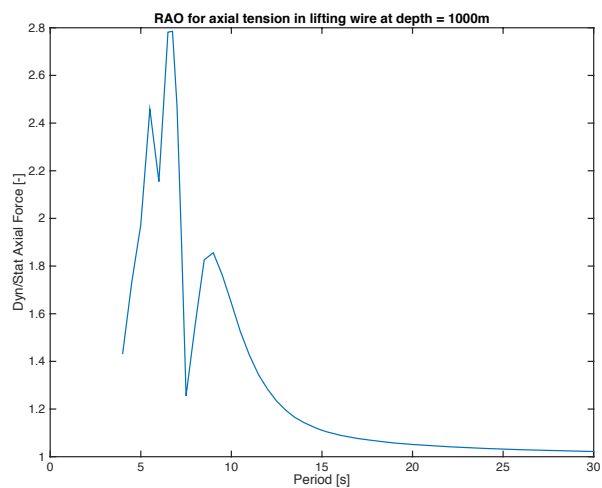
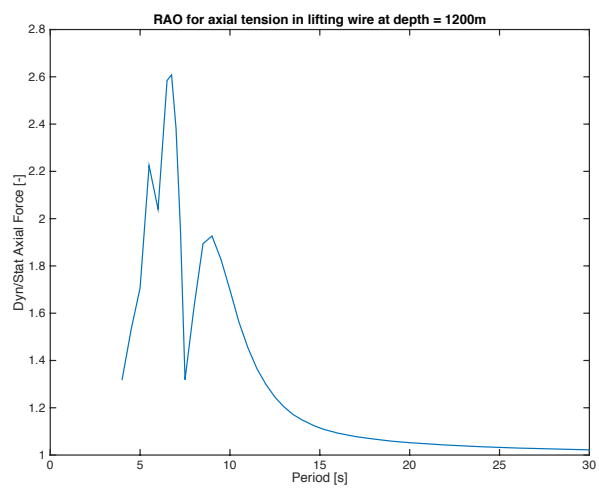


## I RAOs from MATLAB for different vertical positions.

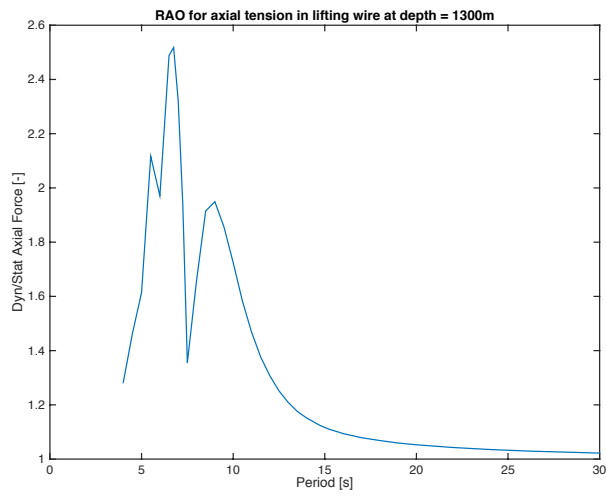


**100m depth****300m depth****200m depth****400m depth**

**500m depth****700m depth****600m depth****800m depth**

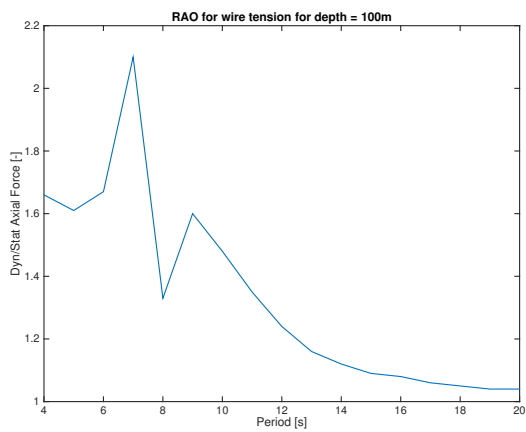
**900m depth****1100m depth****1000m depth****1200m depth**

### 1300m depth

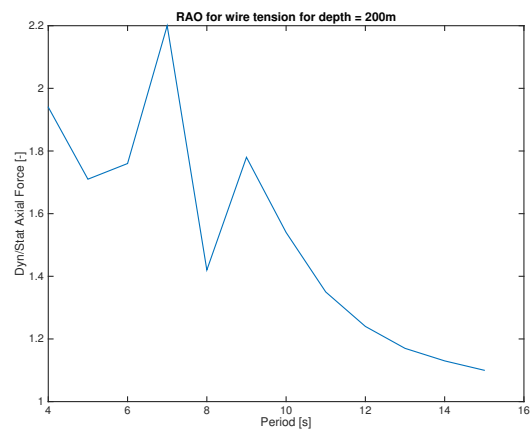


## J RAOs from RIFLEX for different vertical positions.

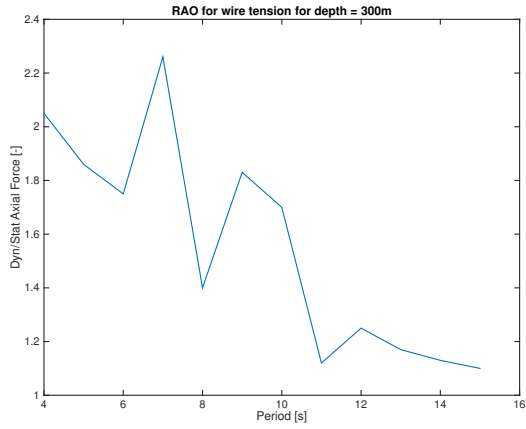
### 100m depth



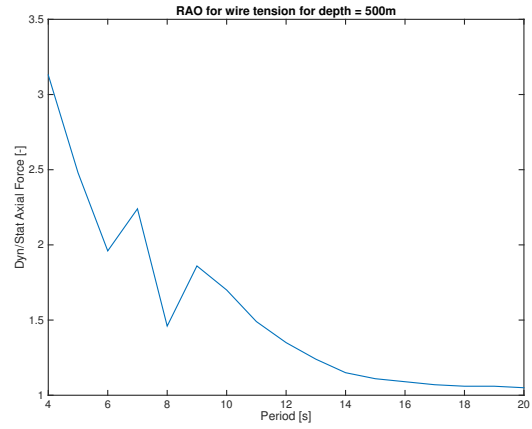
### 200m depth



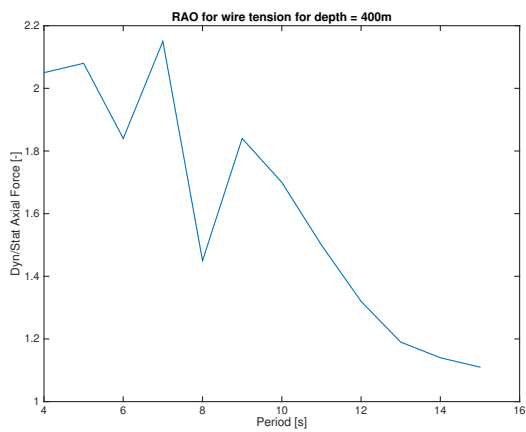
### 300m depth



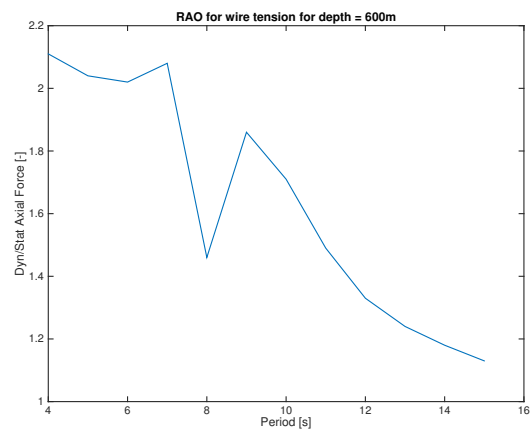
### 500m depth

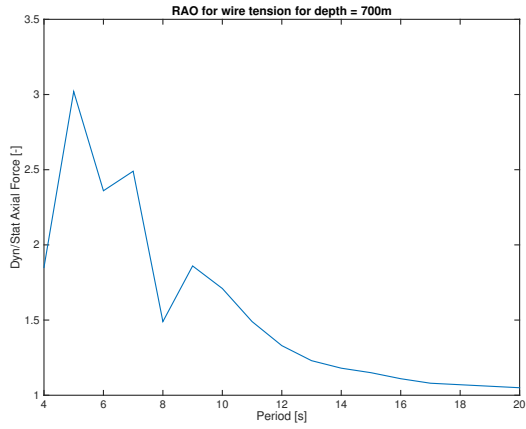
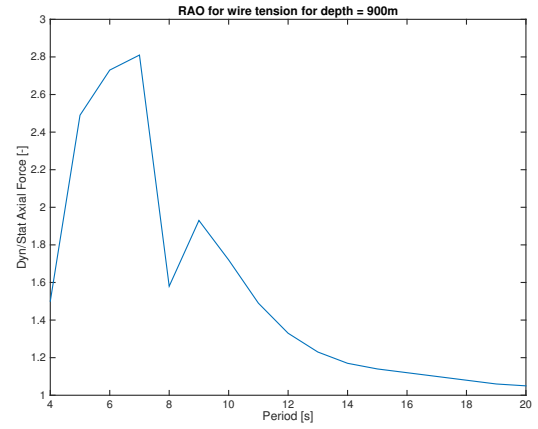
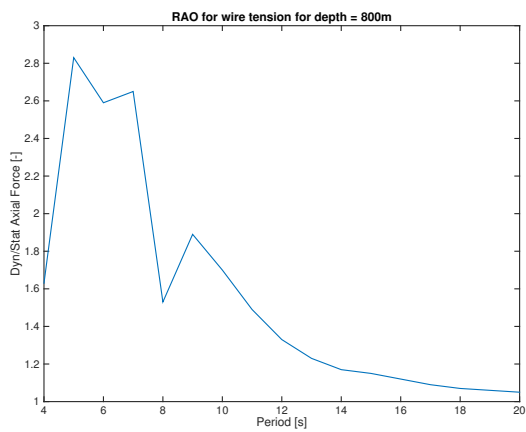
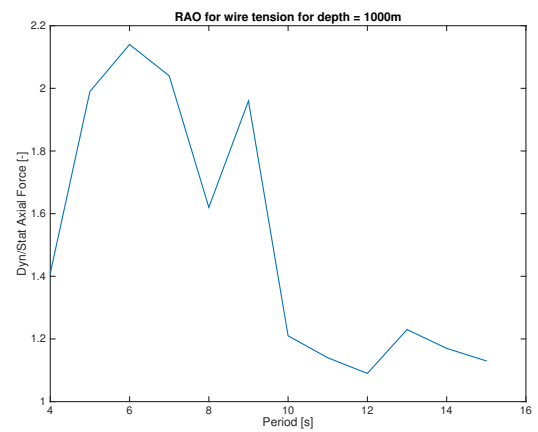


### 400m depth

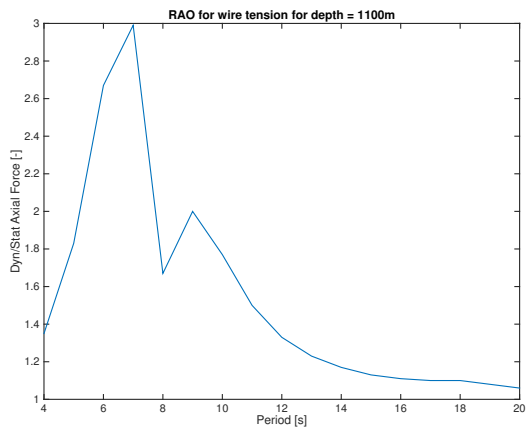


### 600m depth

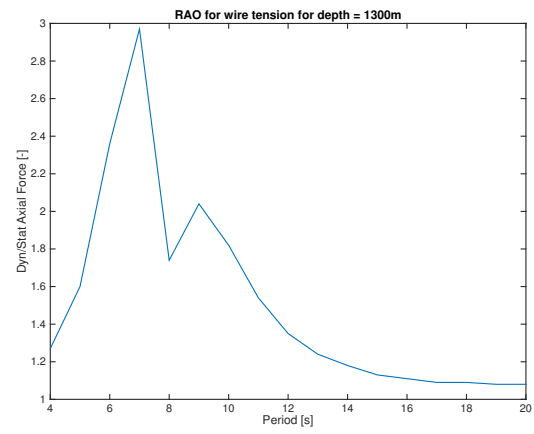


**700m depth****900m depth****800m depth****1000m depth**

## 1100m depth



## 1300m depth



## 1200m depth

